Acceleration-Based Bilateral Teleoperation System under Time Delay Based on Modal Space Analysis

September 2013

A thesis submitted in partial fulfilment of the requirements for the degree of
Doctor of Philosophy in Engineering

Keio University

Graduate School of Science and Technology
School of Integrated Design Engineering

Suzuki, Atsushi

Acknowledgements

I joined Professor Ohnishi's laboratory in 2008 when I was an undergraduate student, and I had been with the laboratory for three years. After receiving the M.E. degree in 2011, I joined TOSHIBA MITSUBISHI-ELECTRIC INDUSTRIAL SYSTEMS CORPORATION (TMEIC) where I have been engaged in application engineering of cold rolling mills metals process systems and industrial automation systems. In 2012, I decided to join Professor Ohnishi's laboratory again in order to complete my work and to acquire Ph.D. in engineering for confidence and pride in myself as an application engineer . This dissertation is the result of four years of work at Keio University whereby I have been accompanied and supported by many people.

I would like to express my gratitude to all those who gave me the possibility to complete this dissertation here. First of all, I would like to express my deep and sincere gratitude and respect to my supervisor Professor Dr. Kouhei Ohnishi. His detailed and constructive comments and his important support throughout this work are a great help to me. Without his help, I could not have accomplished this dissertation. The most impressive thing which I have learned from him is never give up to seek new successes in research. I am deeply grateful to Professor Dr. Toshiyuki Murakami, Professor Dr. Naoaki Yamanaka, Associate Professor Dr. Takahiro Yakoh, Associate Professor Dr. Seiichiro Katsura, Associate Professor Dr. Hiroaki Nishi, and Research Associate Dr. Ryogo Kubo for giving me instructive advices. I owe my warm gratitude to Research Associate Dr. Kenji Natori at Chiba University, Associate Professor Dr. Tomoyuki Shimono at Yokohama National University, and Assistant Professor Dr. Naoki Motoi at Yokohama National University for giving me a lot of helpful advices. When I was undergraduate and master student, Discussions with Assistant Professor Dr. Sho Sakaino at Saitama University, Assistant Professor Dr. Daisuke Yashiro at Mie University, Dr. Hiroyuki Tanaka, and Dr. Tomoya Sato polished up my research. When I was doctor student, Support of Mr. Takahiro Nozaki, Mr. Takahiro Mizoguchi, and Miss. Mariko Mizuochi deeply helped me advance my own research. Their kind support and guidance have been of great value in this study.

Finally, I really give my thanks to many people who supported me in my life.

September, 2013

Atsushi Suzuki

Table of Contents

List of Figures

List of Tables

Chapter 1

Introduction

1.1 Haptics and Its Possibility

"Haptics" is defined as the research field in tactile sensation. Human beings recognize the real world five senses: seeing, hearing, smelling, tasting and touching. Among these senses, the sense of touching has original property unlike the passive senses of seeing and hearing shown as Fig. 1-1. The sound and visual information are unilateral information. On the other hand, the tactile-informational handling is difficult beacuse it is bilateral information. The realization of the law of action and reaction is absolutely required to acquire tactile sensation from environment. For touching in long distance, the device system should be prepared to touch a remote environment. Up to now, haptics has been aimed at recognizing and reproducing virtual objects. It is assumed that the virtual objects exist in computers, and operators receive virtual impedance. However, in recent years, along with the development of force feedback technologies, haptic interfaces have attracted attention as instruments for teleoperation. Especially, bilateral control which consists of master and slave robot is expected as a future device system to realize tele-haptic communication over the world.

This dissertation deals with an acceleration-based bilateral teleoperation systems for "real-world haptics". Real-world haptics has been expected to bring some novel innovation. Firstly, it is expected to be a new advanced teleoperation system in ultimate environments such as deep water, nuclear reactors, or in space. Secondly, it realizes tactile communication over internet. Haptic communication systems have been attracting attention as the third communication media followed by visual and audio communication systems. Thirdly, it might achieve skill transfer and preservation of experienced workman as haptic

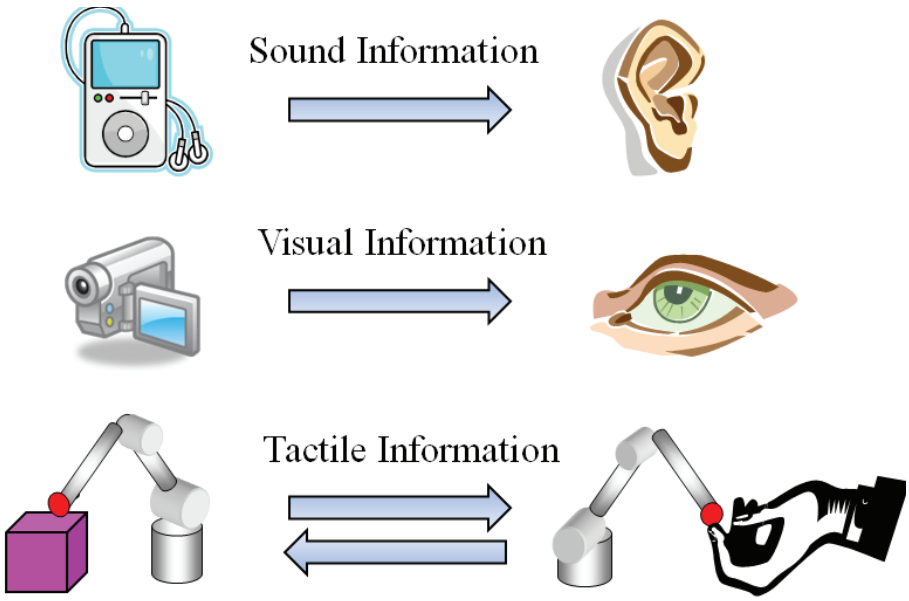

Fig. 1-1: Real world sound, visual, and tactile information

database.

Especilally, many people pay attention to telehaptics in medical fields. Minimally invasive surgery (MIS) has been developed in these days[1, 2]. Da Vinci is one of the surgical robots for MIS[3]. However, Da Vinci cannot provide force feedback. As a result, operators can not feel the impedance of patients' organs. To solve this issue, there are some haptic robots which recently have been developed[5, 6, 32]. Bilateral control systems using master-slave robots are applicable to these haptic robots.

1.2 Bilateral Teleoperation (Previous Research)

The bilateral control system which consists of master and slave robots enables the operator to feel the reaction force from a remote environment. As a result, the operator can perform dangerous operations safely such as in nuclear reactors and space through this control system[7] [8]. There are a lot of bilateral control architectures. The most known architecture is the four-channel (4ch) architecture which has four communication channels. The controller utilizes the information of the master/slave position and force. There are many studies about performance of bilateral control systems. One of the performance indices of bilateral control is "transparency". Hannaford applied two-port circuit model to bilateral systems and discussed ideal performance [9]. Then Lawrence formulated the concept as transparency[10]. Hashtrudi-

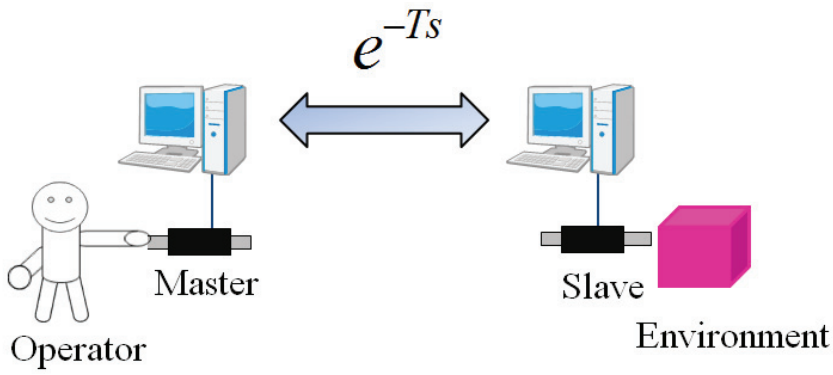

Fig. 1-2: Time delay in bilateral teleoperation

Zaad et al. studied local force feedback and discussed its effect of it on transparency[11]. Furthermore, there are two evaluation indices for bilateral control systems based on transparency, which are "reproducibility" and "operationality" [12]. Reproducibility shows how precisely the environmental impedance is reproduced in the master side. Operationality shows how smoothly the operator manipulates the master robot.

Some researchers utilize four-channel Acceleration-based Bilateral Control (4ch ABC) which is hybrid of position and force control in the acceleration dimension based on disturbance observer[13] [14]. 4ch ABC has high reproducibility and operationality, so that it is able to transfer vivid haptic sensation. There are some researchers who proposed abstraction and reproduction of force sensation from the real environment by using 4ch ABC[15–19], and multilateral control consisting of more than two robots to achieve a complicated task[20] [21].

However, there are some network constraints over real time network in teleoperation system: time delay, packet loss, bandwidth limitation, and transmission path block. This dissertation focuses on the effect of time delay. If there exists time delay on communication line, it seriously deteriorates the performance and possibly makes the system unstable. Fig. 1-2 shows the concept of time delay in bilateral teleoperation. Time delay in feedback loop is still one of the critical issues in any control systems[22–36]. Recently, time delay problem is mainly discussed in the research field of networked-based control system because of wide spread of network technology[37–41]. One of the major solutions of time-delayed bilateral control is passive bilateral control using wave variables[42, 43]. Advanced control methods such as H_∞ control have been tested on teleoperation systems with time delay[44–47]. Furthermore, time delay compensation such as Smith predictor is widely used[48–50]. Model predictive control approach is also utilized

in bilateral teleoperation including linear quadratic Gaussian (LQG) control[51, 52]. Some researchers proposed network-based bilateral teleoperation system using internet. Oboe and Fiorini proposed a design structure of internet-based telerobotics[53]. Oboe also presented a force-reflecting type Internet-based telerobotic systems[54, 55]. Uchimura and Yakoh described bilateral robot system on hard real-time networks[56]. Yashiro proposed multirate sampling method of packet-sending period and control period separately in bilateral teleoperation[57]. Network delays especially over Internet is time-varying and very specific[58, 59]. To solve this problem, Natori has proposed a novel time delay compensation method based on the concept of network disturbance (ND) and communication disturbance observer (CDOB)[60]. This compensation method shows almost the same effectiveness as Smith predictor. The specific feature of CDOB is that it does not require any time-delay models for compensation. The effectiveness of time-delay compensation on 4ch ABC was demonstrated by experimental results[61]. Furthermore, the effect of time delay compensation on transparency has been analyzed[62]. However the effect on stability has not been analyzed precisely. From the experimental results, time delay compensation by CDOB makes free motion stable, but other solution methods require much important on the stability of contact motion with hard environments.

1.3 Proposal of This Dissertation

This dissertation proposes several solution methods for time-delayed ABC system to improve performance and stability by frequency-domain loop-shaping of two modal space. There are three conditions to realize high performance and stability as follows.

1. Reproducibility
2. Operationality
3. Stability

Reproducibility shows how precisely environmental impedance is reproduced in master side. Op-

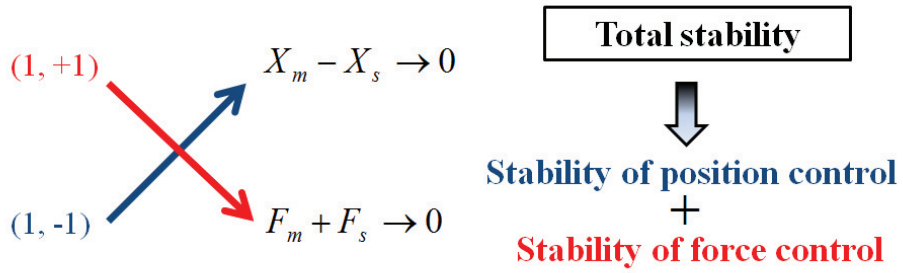

Fig. 1-3: Necessary and sufficient stability condition

erationality means how smoothly the operator manipulates master robot. Stability assures that stable teleoperation is achieved. Reproducibility and operationality are defined by using hybrid parameters.

However, the way to analyze the stability of ABC has not been well established. In this control system, force control and position control work simultaneously in the acceleration dimension, so that the structure is not so simple. As a result, it is difficult to analyze the stability of the system. Due to time delay, the analysis of stability based on pole allocation is impossible, so that the stability analysis gets more difficult. There are passivity-based approaches like scattering theory and wave variables. However, these strict stability conditions are too conservative to realize high performance teleoperation. To solve this problem, this dissertation conducts modal decomposition of ABC system under time delay, and analyzes the stability of each modal space under time delay. Satisfactions of stability conditions of two modal spaces assure the whole system such as Fig. 1-3. For realization of high performance and stability, this dissertation analyzes the stability of each modal space: common modal space (1, +1) and differential modal space (1, -1). According to modal decoupling, a position control and a force control is designed separately each other about one robot separately. This dissertation analyzes the stability of each modal space under time delay. Based on modal space analysis, this dissertation proposes several novel controller designs for time-delayed ABC to achieve high performance and stability.

The chapter organization is described in Fig. 1-4. The following Chapter 2 mentions robust acceleration motion control based on disturbance observer (DOB). Chapter 3 describes the principle of acceleration-based bilateral control (ABC), and explains the destabilization caused by time delay. Chapter 4 explains the performance indices of ABC system: reproducibility and operationality. Chapter 5 and 6 introduce conventional methods to improve the stability of time-delayed ABC, and describe the problems. Chapter 5 explains time delay compensation by communication disturbance observer (CDOB).

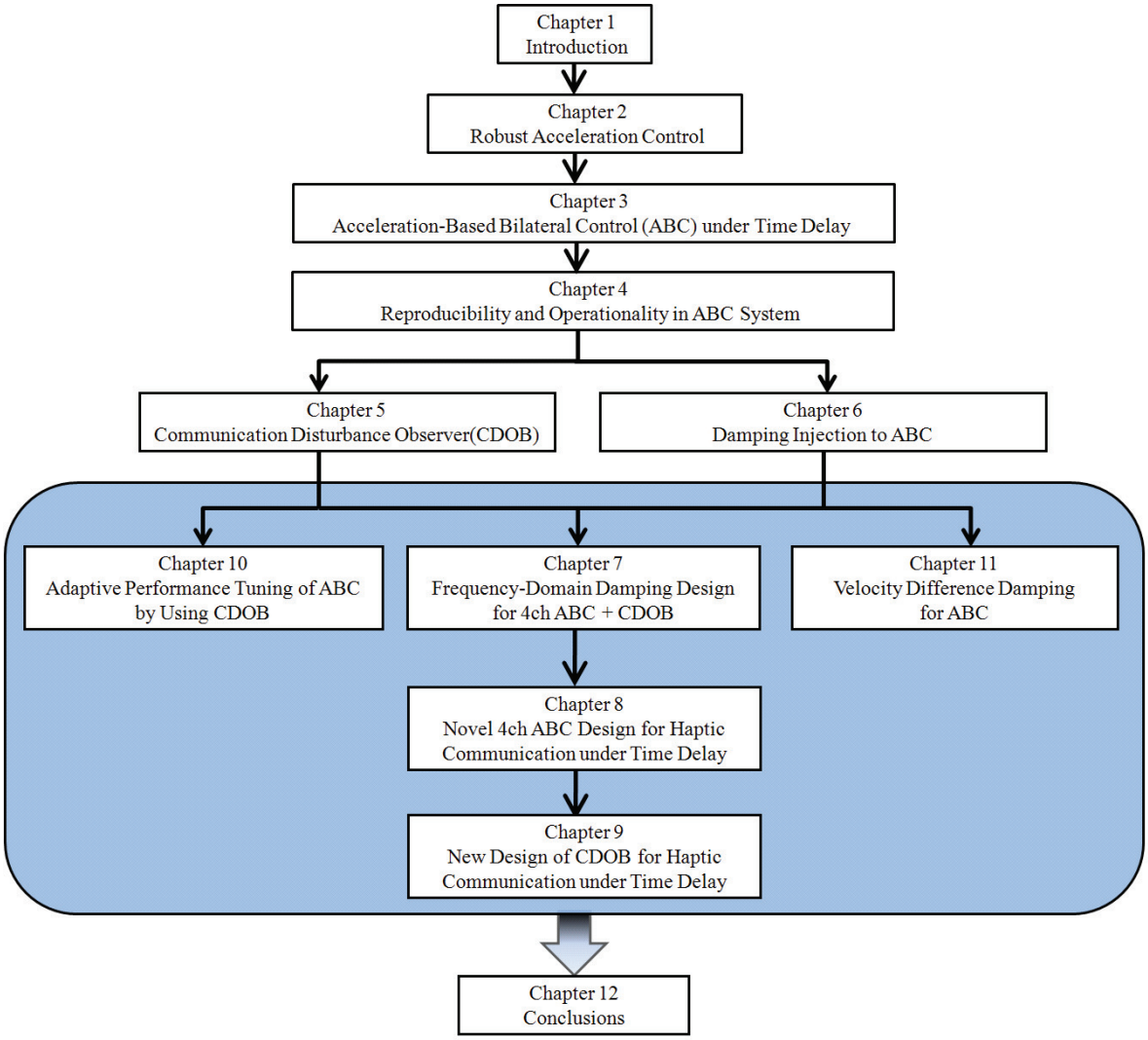

Fig. 1-4: Chapter Organization

Chapter 6 analyzes the effect of damping injection by velocity feedback on ABC system.

The proposed control systems are introduced in Chapters 7∼11. Chapter 7 proposes frequency-domain damping design (FDD) for ABC system. FDD changes the strength of damping injection depending on frequency area in order to realize both good operationality and stability. Time delay element lags the phase of the system. As a result, systems with time delay element tends to be unstable in high frequency area. FDD injects high damping only in high frequency area using HPF. The HPF is designed on robust H_∞ stability condition. Chapter 8 proposes a novel 4ch ABC design for haptic communication

under time delay. In conventional 4ch ABC, the difference of positions is controlled to be zero by PD control, and the sum of forces is controlled to be zero by force P control. On the other hand, in proposed 4ch ABC, the difference of position is controlled to be zero by P-D control (differential proactive PD control), and the sum of force is controlled to be zero by damping-injected force P control. Furthermore, the damping controller is designed based on FDD. Chapter 9 proposes a new design of communication disturbance observer (CDOB) for haptic communication with bilateral control. The proposed new CDOB is effective for time delay compensation only in high frequency area using loop-shaping HPF. Furthermore, the proposed ABC system with new CDOB compensates time delay on both master and slave robot. The proposed ABC system achieves more stable and higher performance haptic communication under time delay. Chapter 10 and 11 introduce event-based approaches only in contact motion. Chapter 10 explains an adaptive method of time-delayed ABC by using CDOB. Time delay compensation by CDOB improves operationality, but simultaneously deteriorates reproducibility. Therefore, chapter 10 proposes scaling down compensation value of CDOB only at contact. Reproducibility is improved in all frequency area by scaling down compensation value from 0 to 1.0. Chapter 11 introduces an event-based damping method only at contact. Chapter 11 proposes a method of velocity difference damping that utilizes the velocity difference between the robot and the robot model. This method improves the performance and the stability of force control in common modal space without deteriorating the position control. The proposed solutions are based on modal space analysis. By using them, high-performance and stable bilateral teleoperation are realized at the same time even under time delay. Finally conclusions are described in Chapter 12.

Chapter 2

Robust Acceleration Control

2.1 Introduction

This chapter describes robust acceleration control based on disturbance observer (DOB)[63]. This dissertation deals with linear motion of a one-degree-of-freedom (1 DOF) robot. Parameters are shown as Table 2-1.

2.2 Disturbance Observer (DOB)

In actual motion control, disturbance force F^{dis} is exerted on a robot. DOB estimates disturbance force F^{dis} and gives compensating current I^{cmp} for robust motion control. The block diagram of DOB is shown in Fig. 2-1. The components of F^{dis} are described as follows. The equivalent system of Fig. 2-1 is shown in Fig. 2-2. It shows that the disturbance force F^{dis} is input to the system through the high-pass filter (HPF) by the compensation of DOB. If g_{dis} is large enough, the disturbance force F^{dis} hardly affects the system such as Fig. 2-3.

$$F^{dis} = F^{ext} + F^{int} + F^{fric} + (M - M_n)s^2 X^{res} + (K_{tn} - K_t)I_a^{ref} \tag{2.1}$$

Disturbance force F^{dis} also includes the force caused by modeling error of nominal mass M_n and nominal thrust coefficient K_{tn}. Interactive force F^{int} includes Coriolis term, centrifugal term, and gravity term. As a result, the disturbance force F^{dis} is estimated through the LPF as follows.

Table 2-1: Parameters

Parameter	Meaning
M	Mass [kg]
K_t	Thrust coefficient [N/A]
I_a	Motor current [A]
F^{dis}	Disturbance force [N]
F^{ext}	External force [N]
F^{fric}	Frcition force [N]
F^{int}	Interactive force [N]
g_{dis}	Cut-off frequency of DOB(RFOB) [rad/s]]
$\hat{}$	Estimated value
$(superscript)cmd$	Command value
$(superscript)ref$	Reference value
$(superscript)res$	Response value
$(superscript)cmp$	Compensation value
$(subscript)n$	Nominal value
$(subscript)m$	Master system
$(subscript)s$	Slave system
$(subscript)sm$	Slave model system
$(subscript)mm$	Master model system

$$\hat{F}^{dis} = \frac{g_{dis}}{s + g_{dis}} F^{dis} \tag{2.2}$$

2.3 Position Control Based on Robust Acceleration Control

Robust motion control is achieved by using the DOB. The block diagram of a position control system based on acceleration control is shown in Fig. 2-4. $C_p(= K_p + sK_v)$ is a position PD controller. Fig. 2-5 is the equivalent system of Fig. 2-4. In Fig. 2-5, position response is described as follows.

$$x^{res} = \frac{C_p}{s^2}(x^{cmd} - x^{res}) \tag{2.3}$$

(2.3) is transformed as follows.

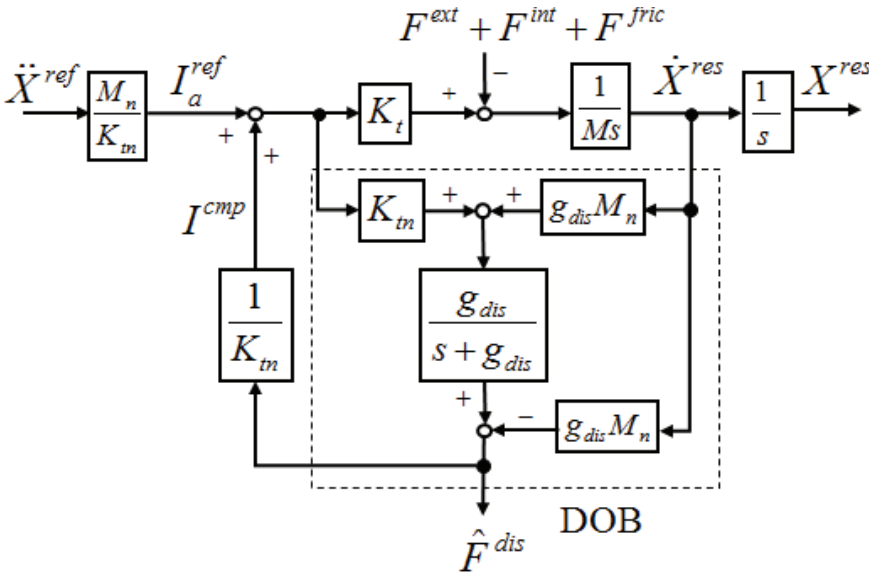

Fig. 2-1: Block diagram of DOB

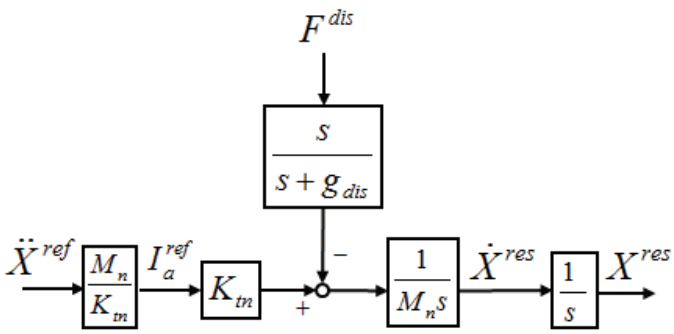

Fig. 2-2: Robust acceleration control

$$\begin{aligned}\frac{x^{res}}{x^{cmd}} &= \frac{C_p}{s^2 + C_p} \\ &= \frac{sK_v + K_p}{s^2 + sK_v + K_p} \\ &= \frac{2\zeta\omega_n s + {\omega_n}^2}{s^2 + 2\zeta\omega_n s + {\omega_n}^2}\end{aligned} \tag{2.4}$$

In this dissertation, damping ratio ζ is set at 1.0. Undamped natural frequency $w_n = \sqrt{K_p}$ is required

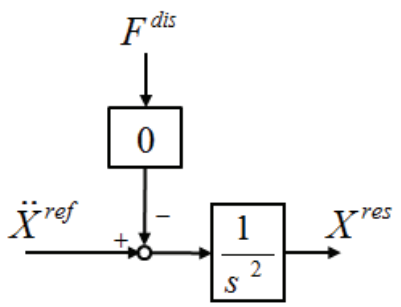

Fig. 2-3: Ideal robust acceleration control

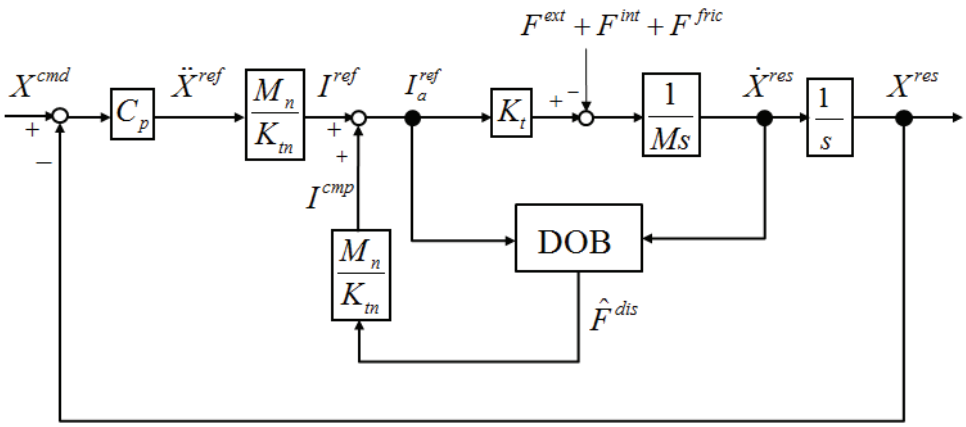

Fig. 2-4: Position control based on acceleration control

to be about 5.0 Hz (31.4 rad/s) for tracking human motion. Considering these factors, position gain K_p is usually set at 900, and velocity gain is set at 60.

2.4 Reaction Force Observer (RFOB)

DOB is utilized for not only estimation of disturbance force but also estimation of reaction force. Reaction Force observer (RFOB) can estimate wider band force information than a force sensor[64]. However, it requires identification of friction force F_{fric} and interactive force F_{int} such as the gravity term in advance. In the case of linear motors, the frictional force is disregarded, because linear motors in this dissertation have little friction effect. The block diagram of RFOB is shown in Fig. 2-6. If the identification of parameters are perfect, estimated external force $\hat{F}^{ext}$ is calculated as follows. In this

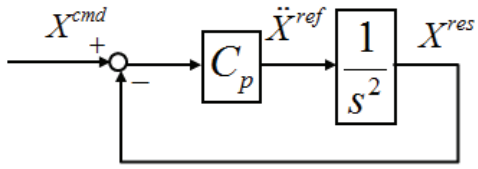

Fig. 2-5: Equivalent system of Fig. 2-4

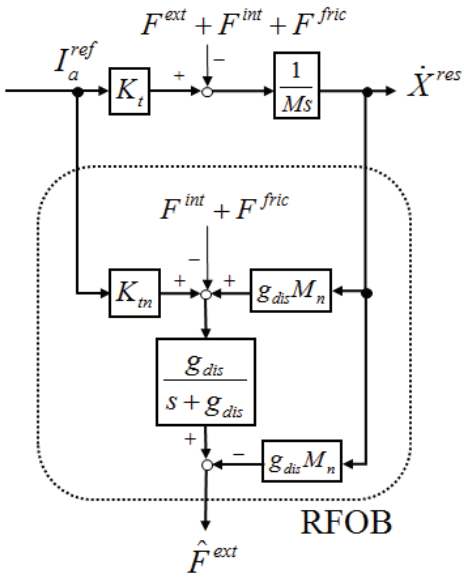

Fig. 2-6: Block diagram of RFOB

dissertation, the cutoff frequency of RFOB is same with that of DOB.

$$\hat{F}^{ext} = \frac{g_{dis}}{s + g_{dis}} F^{ext} \tag{2.5}$$

2.5 Force Control Based on Robust Acceleration Control

The block diagram of a force control system based on robust acceleration control is shown in Fig. 2-7. $C_f(= K_f)$ is force P controller. Fig. 2-8 is the equivalent system of Fig. 2-7. In Fig. 2-8, Z_e is environmental impedance. Estimated force response is described as follows.

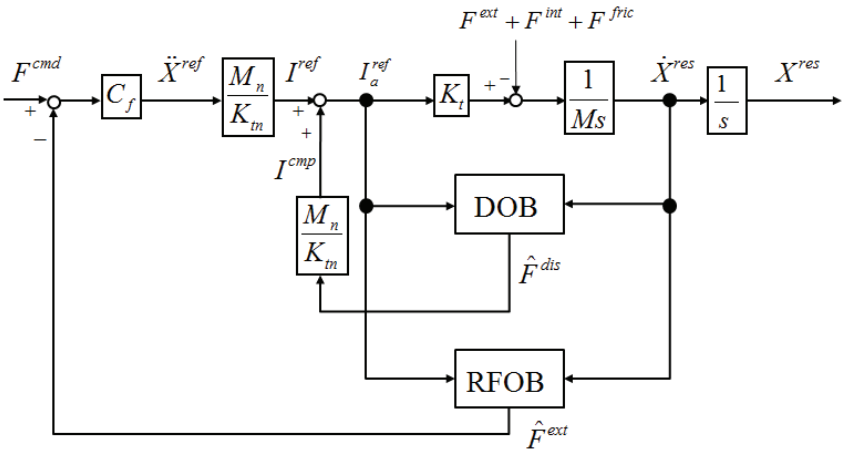

Fig. 2-7: Force control based on acceleration control

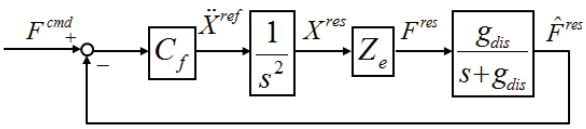

Fig. 2-8: Equivalent system of Fig. 2-7

$$\hat{F}^{res} = \frac{C_f Z_e g_{dis}}{s^2(s+g_{dis})}(F^{cmd} - \hat{F}^{res}) \tag{2.6}$$

(2.6) is transformed as follows.

$$\frac{\hat{F}^{res}}{F^{cmd}} = \frac{1}{\frac{s^2(s+g_{dis})}{C_f Z_e g_{dis}} + 1} \tag{2.7}$$

From (2.7), force gain $C_f(= K_f)$ should be as large as possible to improve the performance. However, force information has some noise. Considering the noise problem, we determine force gain by trial and error. In this dissertation, K_f is usually set at 1.0.

2.6 Summary

This chapter described robust acceleration control based on disturbance observer (DOB). Position control and Force control based on robust acceleration control were also explained.

Chapter 3

Acceleration-Based Bilateral Control (ABC) under Time Delay

3.1 Introduction

Chapter 3 explains the principle of four-channel acceleration-based bilateral control (4ch ABC). Furthermore, destabilization caused by time delay is described. Firstly, modal decomposition of 4ch ABC is explained. Secondly, the feedback loop of each modal space is analyzed. Thirdly, the necessary and sufficient stability condition of ABC is explained. Fourthly, the destabilization caused by time delay is described.

3.2 Modal Decomposition of 4ch ABC

The block diagram of 4ch ABC is shown in Fig. 3-1. 4ch ABC is achieved in virtual orthogonally-crossed two modal spaces: force controller in the common modal space and position controller in differential modal space. Force in the common modal space F_c and position in the differential modal space X_d are defined as follows.

$$F_c = F_m + F_s \tag{3.1}$$

$$X_d = X_m - X_s \tag{3.2}$$

However, force control and position control cannot be achieved simultaneously on the same axis. Therefore, in acceleration dimension, above equations are rewritten as follows by using a second-order Hadamard

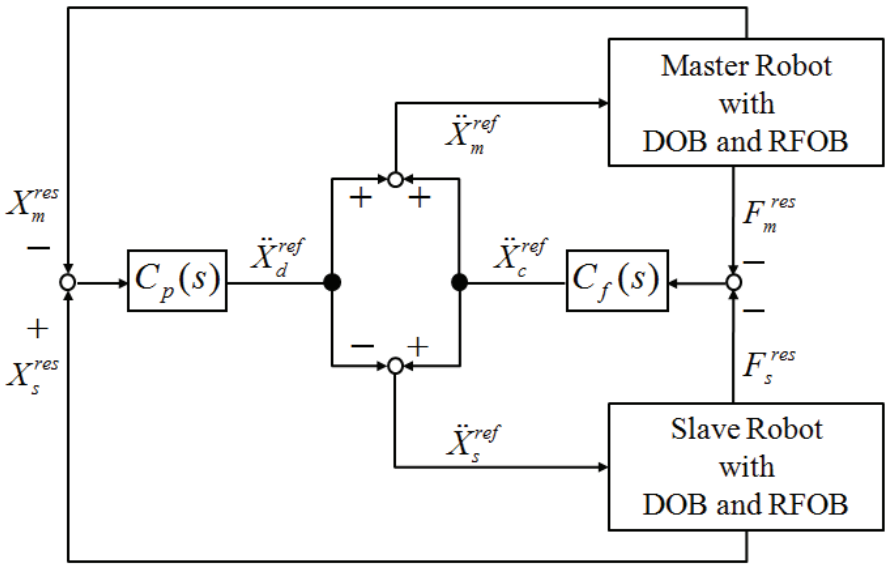

Fig. 3-1: Block diagram of 4ch ABC

matrix $\boldsymbol{H}$.

$$\begin{aligned} \begin{bmatrix} s^2X_c \\ s^2X_d \end{bmatrix} &= \underbrace{\begin{bmatrix} 1 & 1 \\ 1 & -1 \end{bmatrix}}_{H} \begin{bmatrix} s^2X_m \\ s^2X_s \end{bmatrix} \\ \Leftrightarrow \begin{bmatrix} s^2X_m \\ s^2X_s \end{bmatrix} &= \underbrace{\frac{1}{2}\begin{bmatrix} 1 & 1 \\ 1 & -1 \end{bmatrix}}_{H^{-1}} \begin{bmatrix} s^2X_c \\ s^2X_d \end{bmatrix} \end{aligned} \tag{3.3}$$

The objectives of 4ch ABC are such as follows.

$$s^2X_c^{res} = 0 \tag{3.4}$$

$$s^2X_d^{res} = 0 \tag{3.5}$$

To satisfy the previous equations, the common modal space is force-controlled, and the differential modal space is position-controlled as follows. $\hat{F}$ is estimated reaction force value by RFOB.

$$s^2 X_c^{ref} = -2C_f(\hat{F}_m + \hat{F}_s) \tag{3.6}$$

$$s^2 X_d^{ref} = -2C_p(X_m - X_s) \tag{3.7}$$

Using above equations and a second-order inverse Hadamard matrix $\boldsymbol{H^{-1}}$, the reference values of master and slave robots are given as follows. If g_{dis} is large enough, the response value X^{res} is almost the same with the reference value X^{ref}.

$$s^2 X_m^{ref} = s^2 X_m^{res} = C_p(X_s - X_m) - C_f(\hat{F}_m + \hat{F}_s) \tag{3.8}$$

$$s^2 X_s^{ref} = s^2 X_s^{res} = C_p(X_m - X_s) - C_f(\hat{F}_m + \hat{F}_s) \tag{3.9}$$

Therefore, (3.4) and (3.5) are realized by robust acceleration-based bilateral control. However, if g_{dis} is not enough large, robust acceleration control cannot be guaranteed in high frequency area above g_{dis}. As a result, the orthogonality cannot be kept in high frequency area area above g_{dis}.

3.3 Analysis of Each Modal Space in 4ch ABC

4ch ABC is achieved in two virtual modal spaces. Force control is realized in common modal space, and position control is realized in differential modal space. The purpose of the control is realization of next two states.

$$X_m - X_s = 0 \tag{3.10}$$

$$F_m + F_s = 0 \tag{3.11}$$

Then acceleration reference of both master and slave are given as follows. $C_p(= K_p + sK_v)$ means position controller, and $C_f(= K_f)$ means force controller. If g_{dis} is infinity, response value $s^2 X^{res}$ is almost same as reference value $s^2 X^{ref}$.

$$s^2 X_m^{ref} = s^2 X_m^{res} = C_p(X_s - X_m) - C_f(\hat{F}_m + \hat{F}_s) \tag{3.12}$$

$$s^2 X_s^{ref} = s^2 X_s^{res} = C_p(X_m - X_s) - C_f(\hat{F}_m + \hat{F}_s) \tag{3.13}$$

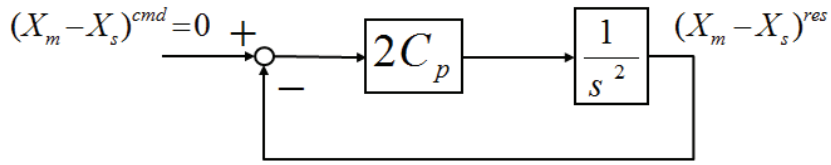

Fig. 3-2: Position control in differential modal space (4ch ABC)

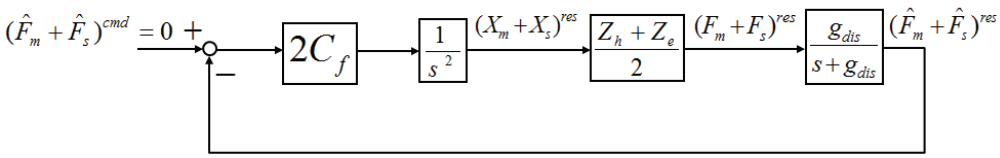

Fig. 3-3: Force control in common modal space (4ch ABC)

3.3.1 Position control of 4ch ABC

Position control in differential modal space is given by subtracting (3.12) from (3.13) as follows.

$$s^2(X_m - X_s)^{res} = -2C_p(X_m - X_s) \tag{3.14}$$

Fig. 3-2 shows the block diagram of position control in differential modal space. The position difference is controlled to be zero for position tracking.

3.3.2 Force control of 4ch ABC

Force control in common modal space is given by adding (3.12) and (3.13) as follows.

$$s^2(X_m + X_s)^{res} = -2(\hat{F}_m + \hat{F}_s) \tag{3.15}$$

Then, the sum of force is expressed as follows by using environmental impedance Z_e and human impedance Z_h.

$$\begin{aligned}(F_m + F_s)^{res} &= Z_h X_m^{res} + Z_e X_s^{res} \\ &= \frac{Z_h + Z_e}{2}(X_m + X_s)^{res} + \frac{Z_h - Z_e}{2}(X_m - X_s)^{res}\end{aligned} \tag{3.16}$$

ABC system controls position difference $(= X_m - X_s)$ to be zero in differential modal space, so (3.16) is approximated as follows.

$$(F_m + F_s)^{res} = \frac{Z_h + Z_e}{2}(X_m + X_s)^{res} \tag{3.17}$$

Fig. 3-3 shows the block diagram of force control in common modal space. The sum of force is controlled to be zero to realize the law of action-reaction in common modal space.

3.4 Necessary and Sufficient Stability Condition of ABC

This section shows the relation between the modal space stability and the total stability. (3.18) shows the relation.

$$\begin{cases} \lim_{t\to\infty}\{\ddot{x}_m + \ddot{x}_s\} \to 0 \\ \lim_{t\to\infty}\{\ddot{x}_m - \ddot{x}_s\} \to 0 \end{cases} \Longleftrightarrow \begin{cases} \lim_{t\to\infty} \ddot{x}_m \to 0 \\ \lim_{t\to\infty} \ddot{x}_s \to 0 \end{cases} \tag{3.18}$$

(3-18) shows that stability conditions of two modal spaces assure the stability of the whole system (master and slave system). Time delay destabilizes feedback loops of two modal spaces. However, even if there exists time delay on communication line, the control target does not change as follows. Therefore, two modal spaces of control target are still orthogonal even under time delay. From the reason, the stability of each modal space should be analyzed independently.

3.5 Destabilization of 4ch ABC Caused by Time Delay

In case that there exists time delay on communication line, acceleration references are changed to next equations. Block diagram of 4ch ABC under time delay is shown as Fig. 3-4. T_1 means time delay from master to slave, and T_2 means time delay from slave to master. In theoretical analysis, this dissertation assumes constant delay and $T_1 = T_2 = T$. However, in the cases with time-varying delay, these conditions are not usually satisfied. In the case ($T_1 \neq T_2$), it is impossible to analyze the stability of

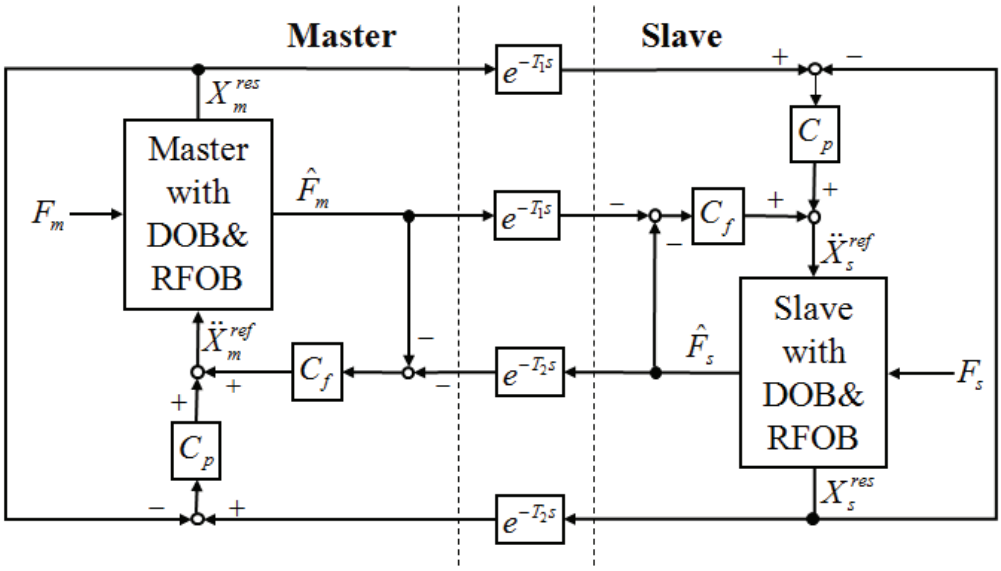

Fig. 3-4: Block diagram of 4ch ABC under Time Delay

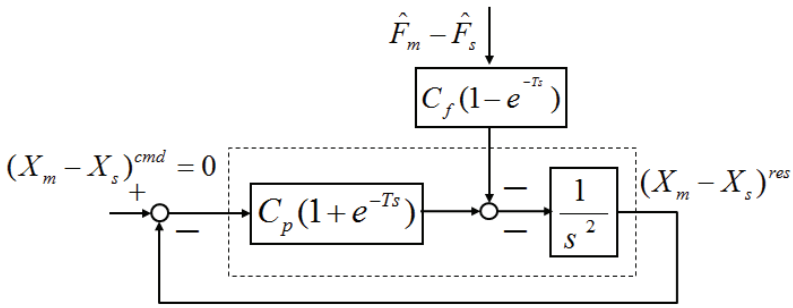

Fig. 3-5: Position control in differential modal space under time delay(4ch ABC)

ABC system because the constructive principle of ABC is based on the symmetric property in master and slave system. Therefore the reliability of the theoretical analysis and effectiveness of proposed method under time-varying delay are experimentally-demonstrated in the latter section.

$$s^2 X_m^{ref} = s^2 X_m^{res} = C_p(X_s e^{-T_2 s} - X_m) - C_f(\hat{F}_m + \hat{F}_s e^{-T_2 s}) \tag{3.19}$$

$$s^2 X_s^{ref} = s^2 X_s^{res} = C_p(X_m e^{-T_1 s} - X_s) - C_f(\hat{F}_m e^{-T_1 s} + \hat{F}_s) \tag{3.20}$$

Table 3-1: Parameters in analysis(proposed system)

Parameter	Meaning	Value	unit
T	Time delay(one way)	0.1	s
K_p	Position gain	900	
K_v	Velocity gain	60	
K_f	Force gain	1.0	
g_{dis}	Cutoff frequency of DOB & RFOB	500	rad/s
Z_h	Impedance of human	1000+10s	N/m
Z_e	Impedance of environment	10000+10s	N/m

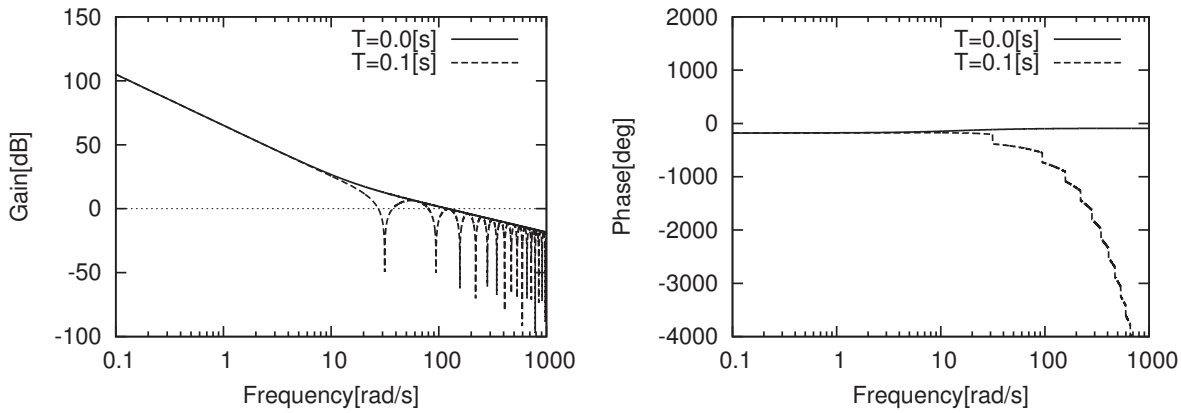

(a) Gain (b) Phase

Fig. 3-6: Bode diagram of L_d (4ch ABC)

3.5.1 Position control of 4ch ABC under time delay

Position control in differential modal space under time delay is given by subtracting (3.20) from (3.19) as follows.

$$s^2(X_m - X_s)^{res} = -C_p(X_m - X_s)(1 + e^{-Ts}) - C_f(1 - e^{-Ts})(\hat{F_m} - \hat{F_s}) \tag{3.21}$$

Fig. 3-5 shows the block diagram of position control in differential modal space under time delay. The part of dotted line is regarded as an open-loop transfer function L_d. Time delay element e^{-Ts} exists in the feedback loop. Time delay element e^{-Ts} in the feedback loop deteriorates the performance and stability. Parameters in analysis are shown as Table 3-1. Fig. 3-6 is Bode diagram of L_d. The gain characteristic shows that the gain-crossover frequency value becomes small due to time delay. This means rapidity

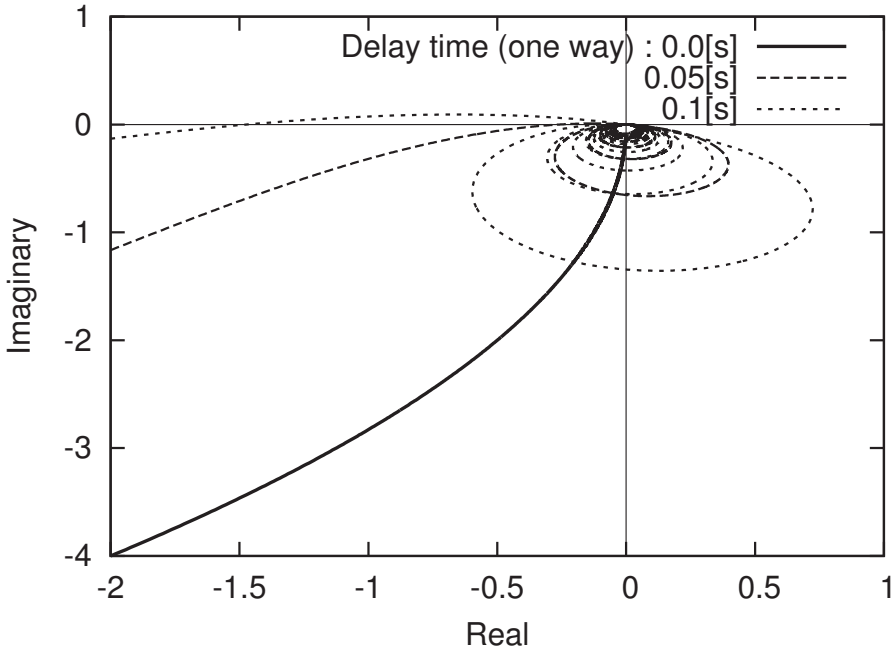

Fig. 3-7: Nyquist plot of differential modal space (4ch ABC)

of the response is deteriorated by time delay. Furthermore, phase characteristic shows that phase delay becomes large in high frequency area. This shows that time delay deteriorates the damping property of position control. Fig. 3-7 is the nyquist plot of position control in differential modal space. Nyquist locus goes through the right of (-1, 0) with the increase of delay time. This shows that time delay deteriorates the stability of position control in differential modal space.

3.5.2 Force control of 4ch ABC under time delay

Force control in common modal space under time delay is given by adding (3.19) and (3.20) as follows.

$$s^2(X_m + X_s)^{res} = -C_p(X_m + X_s)(1 - e^{-Ts}) - C_f(1 + e^{-Ts})(\hat{F_m} + \hat{F_s}) \tag{3.22}$$

Fig. 3-8 shows the block diagram of force control in common modal space. The part of dotted line is regarded as an open-loop transfer function L_c. Time delay element e^{-Ts} also exists in feedback loop. Fig. 3-9 is the bode diagram of L_c, and Fig. 3-10 is Nyquist plot of force control in common modal space. These show that time delay deteriorates the performance and stability of force control in common modal space.

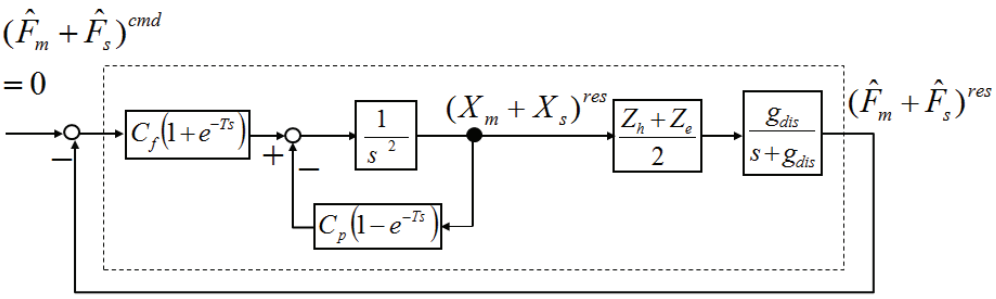

Fig. 3-8: Force control in common modal space under time delay (4ch ABC)

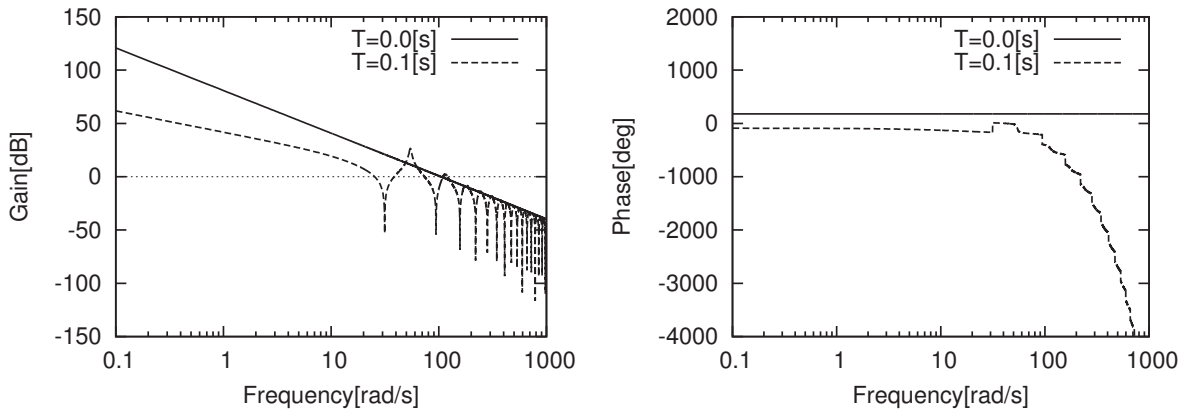

(a) Gain (b) Phase

Fig. 3-9: Bode diagram of L_c (4ch ABC)

3.6 Summary

Chapter 3 explained the structure of ABC under time delay. The destabilization of each modal space due to the time delay was also explained.

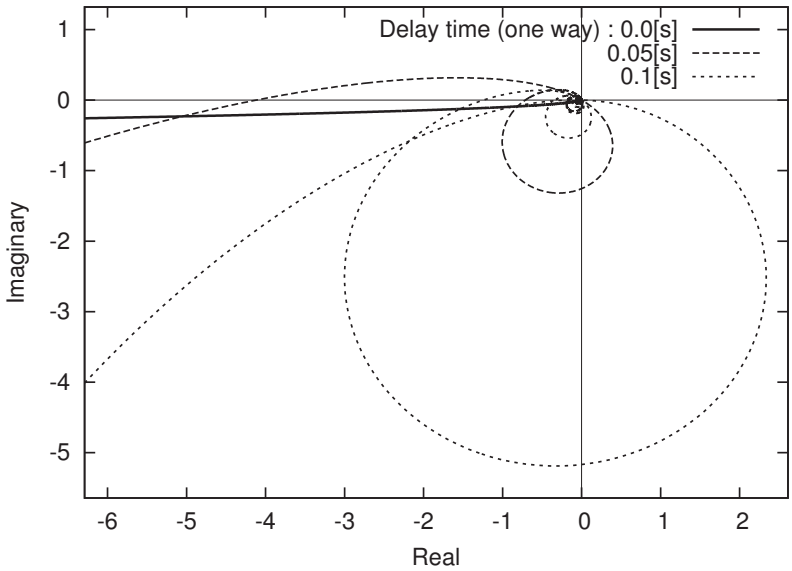

Fig. 3-10: Nyquist plot of common modal space(4ch ABC)

Chapter 4

Reproducibility and Operationality in ABC System

4.1 Introduction

Chapter 4 introduces reproducibility and operationality that are performance indices of ABC system. Firstly, definition of reproducibility and operationality are explained based on hybrid parameters. Secondly, the effect of each modal space on reproducibility and operationality under time delay is analyzed.

4.2 Reproducibility and Operationality Based on Transparency

The relation between master and slave can be formulated by independent variables H, called hybrid parameters[10]. Fig. 4-1 shows network representation of teleoperation systems. Hybrid parameters are defined as follows.

$$\begin{bmatrix} F_m \\ -X_s \end{bmatrix} = \begin{bmatrix} H_{11} & H_{12} \\ H_{21} & H_{22} \end{bmatrix} \begin{bmatrix} X_m \\ -F_s \end{bmatrix} \tag{4.1}$$

If $H_{11} = H_{22} = 0$ and $H_{12} = -H_{21} = 1$ are satisfied, perfect transparency is achieved as follows.

$$F_m = -F_s \tag{4.2}$$

$$X_m = X_s \tag{4.3}$$

Next, slave force is treated as follows.

$$F_s = Z_e X_s \tag{4.4}$$

From (4.1) and (4.4), force in master side is represented as follows.

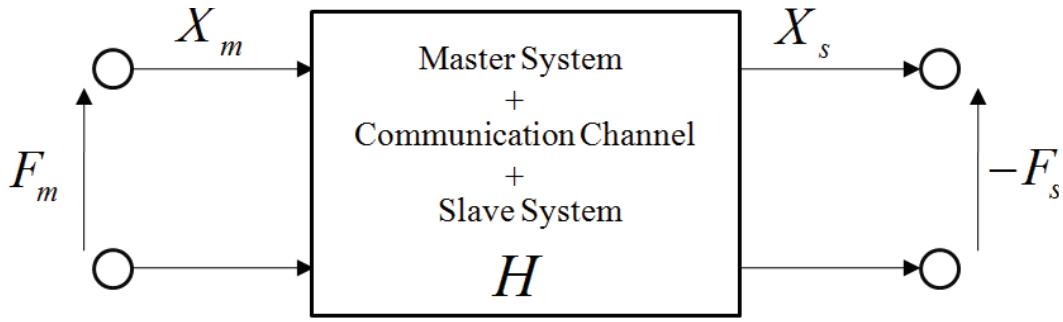

Fig. 4-1: Network representation of master and slave system

$$F_m = (\frac{H_{12}H_{21}}{1 - H_{22}Z_e}Z_e + H_{11})X_m \tag{4.5}$$

P_r and P_o are defined as follows.

$$P_r = \frac{H_{12}H_{21}}{1 - H_{22}Z_e} \tag{4.6}$$

$$P_o = H_{11} \tag{4.7}$$

Hence, (4.5) is represented as follows.

$$F_m = (P_r Z_e + P_o)X_m \tag{4.8}$$

P_r and P_o are defined as "reproducibility" and "operationality"[12]. Reproducibility shows how precisely environmental impedance is reproduced in master side. Operationality shows how smoothly the operator manipulates master robot. Because the reproduction of environmental impedance in master side is important condition in bilateral teleoperation, $|P_r| = 1$ should be satisfied. Additionally, when small operational force, ideally $P_o = 0$, is realized, the operator can feel real environmental impedance naturally. The ideal condition that satisfies perfect reproducibility and operationality is called perfect transparency. In 4ch ABC without time delay, the values of hybrid parameters are obtained as follows.

$$H_{11} = -\frac{s}{C_f} \tag{4.9}$$

$$H_{12} = 1 \tag{4.10}$$

$$H_{21} = -1 \tag{4.11}$$

$$H_{22} = 0 \tag{4.12}$$

Table 4-1: Parameters in analysis and experiment

Parameter	Meaning	Value
T	Time delay(one way)	100[ms]
K_p	Position gain	100
K_f	Force gain	1.0
g_{dis}	Cutoff frequency of DOB	1000[rad/s]
M_n	Nominal mass of motor	0.5[kg]
K_{tn}	Nominal Force coefficient	22.0[N/A]
st	Sampling time	0.1[ms]
Z_e	Impedance of environment	8000+100s
Z_h	Impedance of human	1000+200s
M_n	Nominal inertia of motor	0.5[kg]
K_{tn}	Thrust coefficient	22.0[N/A]
st	Sampling time	0.1[ms]

Then, the reproducibility and the operationality are calculated as follows.

$$P_r = 1 \tag{4.13}$$

$$P_o = -\frac{s}{C_f} \tag{4.14}$$

Therefore, the operator is able to feel the environment impedance exactly when the force control gain C_f is large enough.

4.3 The Effect of Each Control for Reproducibility and Operationality

This section analyzes the effect of each control for reproducibility and operationality under time delay.

4.3.1 The effect of position control for reproducibility and operationality

The effect on reproducibility and operationality is analyzed when position gain changes. Position gain is a gain in position P controller. Each parameter is shown as Table 4-1. Bode diagram of reproducibility and operationality is shown as Fig. 4-2 when position gain changes in 10, 100, 400. As for reproducibility, the band frequency to keep ideal value $P_r = 0[dB]$ is enlarged in low frequency area with the increase of K_p. On the other hand, as for operationality, operational force increases with the increase of K_p. This shows that high position gain improves reproducibility, but deteriorates operationality.

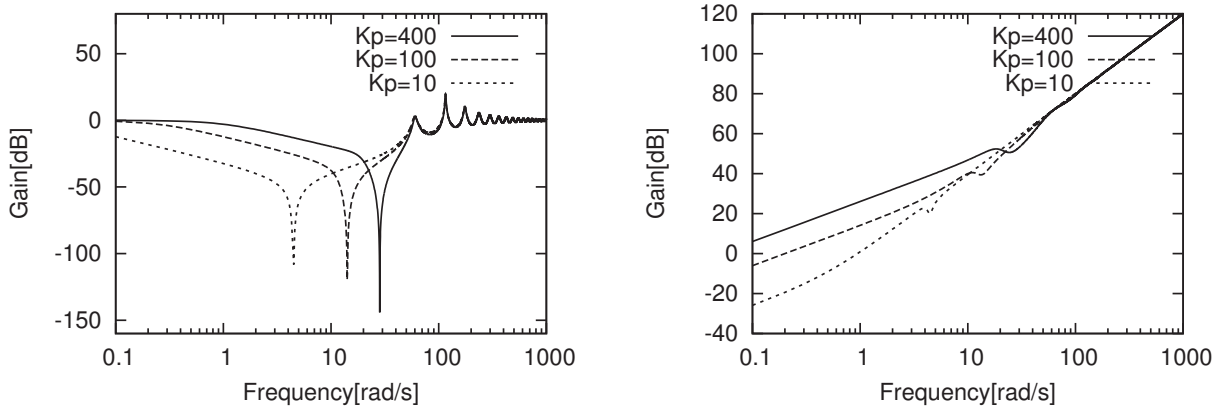

(a) Reproducibility (b) Operationality

Fig. 4-2: Reproducibility and operationality in K_p variation

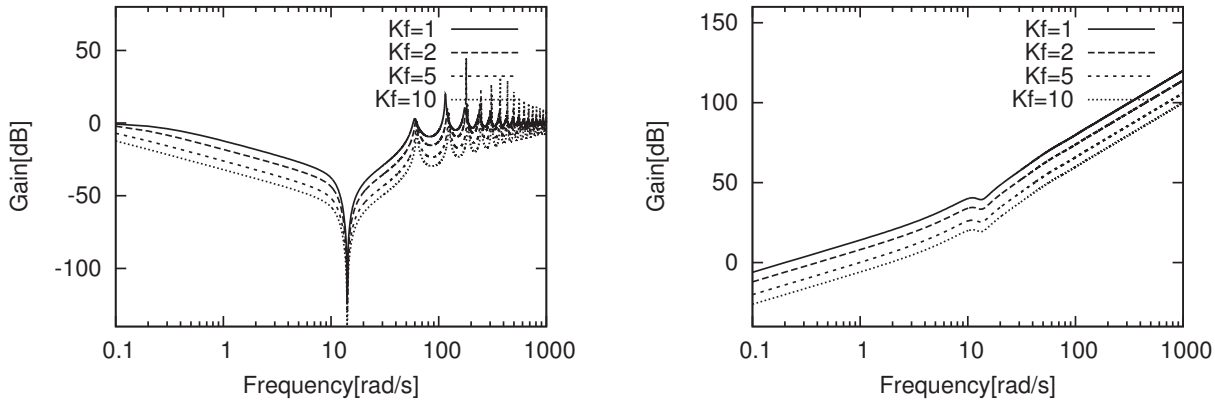

(a) Reproducibility (b) Operationality

Fig. 4-3: Reproducibility and operationality in K_f variation

4.3.2 The effect of force control on reproducibility and operationality

The effect on reproducibility and operationality is analyzed when force gain changes. The bode diagram of reproducibility and operationality is shown as Fig. 4-3 when force gain changes in 1, 2, 5, 10. As for operationality, it is improved with the increase of K_f. On the other hand, as for reproducibility, its gain becomes small under 0[dB] with the increase of K_f. Therefore, high force gain improves operationality, but deteriorates reproducibility.

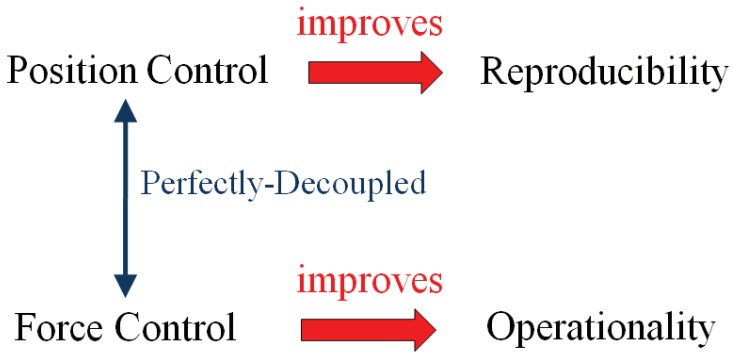

Fig. 4-4: Relation of reproducibility and operationality with each control without time delay

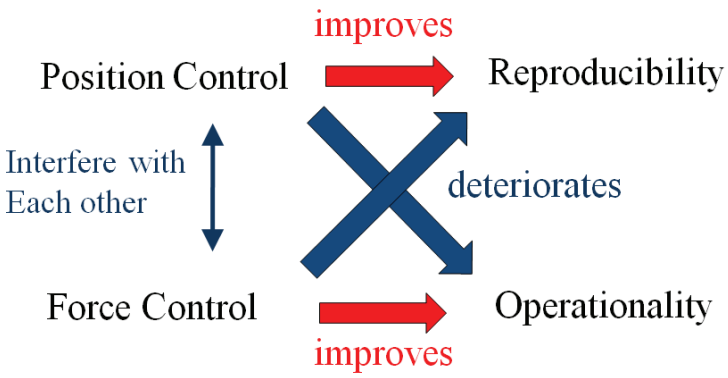

Fig. 4-5: Relation of reproducibility and operationality with each control under time delay

4.4 Summary

Iida described that position control improved reproducibility, and force control improved operationality in 4ch ABC without time delay[12]. This is because position control and force control are perfectly-decoupled in 4ch ABC without time delay showed as Fig. 4-4. However, under time delay, these analyses clarified that position control improved reproducibility but deteriorated operationality, and force control improved operationality but deteriorated reproducibility shown as Fig. 4-5. Even under time delay, control target is that position difference becomes zero: $\int\int(\ddot{x}_m - \ddot{x}_s)dt \rightarrow 0$, and the sum of force becomes zero: $M(\ddot{x}_m + \ddot{x}_s) \rightarrow 0$. Therefore, each control works in two orthogonally-crossed modal space: (1,-1) and (1,+1). However, position control and force control interfere each other on each modal space under time delay. As a result, simple each high gain does not satisfy good reproducibility and operationality.

Chapter 5

Communication Disturbance Observer (CDOB) for ABC System

5.1 Introduction

Chapter 5 introduces time delay compensation by communication disturbance observer (CDOB) which is proposed by Dr. Natori et al., and analyzes the effect on each modal space[60–62]. Firstly, the structure of time delay compensation in 4ch ABC by communication disturbance observer (CDOB) based on the concept of network disturbance (ND) is explained. Secondly, the effect of time delay compensation by CDOB to each modal space is analyzed. Thirdly, the effect of time delay compensation by CDOB to reproducibility and operationality is also analyzed.

5.2 Time Delay Compensation by CDOB

This section explains time delay compensation by communication disturbance observer (CDOB) in 4ch ABC. Fig. 5-1 is block diagram of 4ch ABC with CDOB system, and Fig. 5-2 shows the concept of network disturbance (ND). The effect of time delay is regarded as a disturbance on the slave side. Here the disturbance is defined as network disturbance (ND). In CDOB, an effect of time delay is interpreted as an effect caused by ND on the slave side. This is the concept of ND. ND is estimated by CDOB and the estimated ND is used for time delay compensation as shown in Fig. 5-3, and the internal structure of CDOB is shown in Fig. 5-4. A slave model without time delay is assumed in the master side. CDOB has the same structure as DOB, and calculates the effect of time delay on the system as ND. Estimated ND is described as follows.

$$\begin{aligned} \hat{D}_{net} &= \frac{g_{net}}{s+g_{net}} D_{net} \\ &= \frac{g_{net}}{s+g_{net}} (M_n s^2 X_{sm} - M_n s^2 X_s e^{-T_2 s}) \end{aligned} \tag{5.1}$$

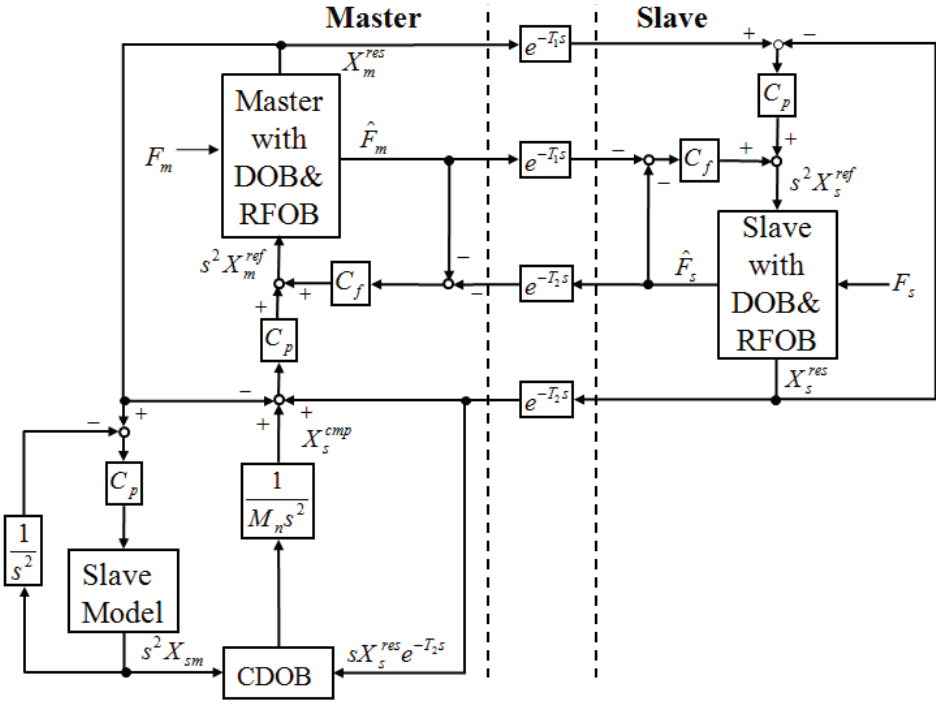

Fig. 5-1: Block diagram of 4ch ABC with CDOB

If the cutoff frequency of LPF in CDOB g_{net} is large enough, (5.1) is changed as follows.

$$\hat{D}_{net} = M_n(s^2 X_{sm} - s^2 X_s e^{-T_2 s}) \tag{5.2}$$

Then compensation value is shown as follows.

$$\begin{aligned} X_s^{cmp} &= \frac{1}{M_n s^2}\hat{D}_{net} \\ &= X_{sm} - X_s e^{-T_2 s} \end{aligned} \tag{5.3}$$

The acceleration response value of master robot with compensation is shown as follows.

$$\begin{aligned} & s^2 X_m^{res} \\ = \; & C_p(X_s e^{-T_2 s} + X_s^{cmp} - X_m) - C_f(\hat{F}_m + \hat{F}_s e^{-T_2 s}) \\ = \; & C_p(X_{sm} - X_m) - C_f(\hat{F}_m + \hat{F}_s e^{-T_2 s}) \end{aligned} \tag{5.4}$$

The acceleration response value of slave model is shown as follows.

$$s^2 X_{sm}^{res} = C_p(X_m - X_{sm}) \tag{5.5}$$

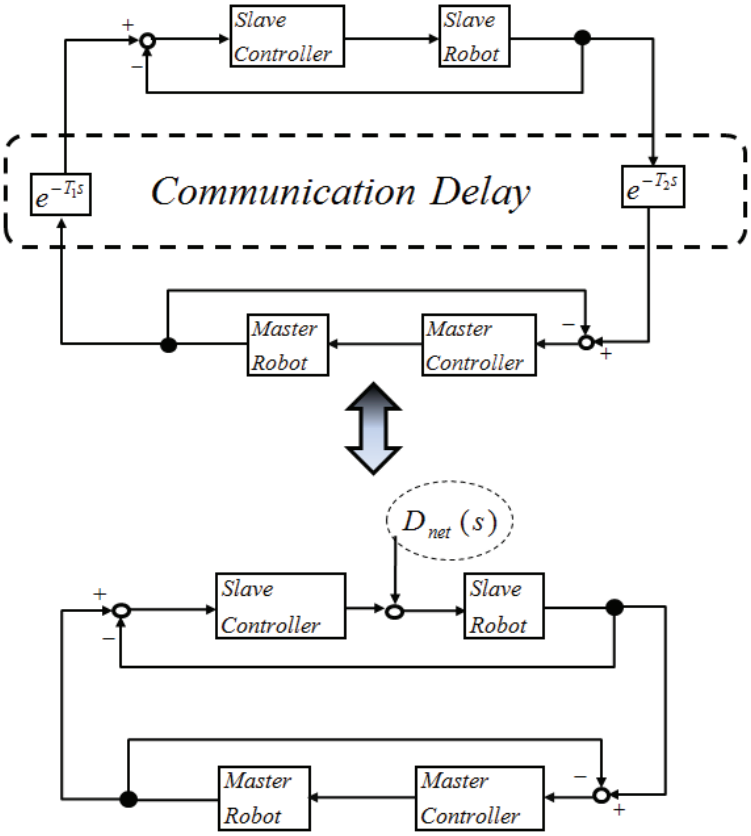

Fig. 5-2: Concept of network disturbance (4ch ABC + CDOB)

(5.5) is changed as follows.

$$X_{sm} = \frac{C_p}{C_p + s^2} X_m \tag{5.6}$$

If (5.6) is substituted to (5.4), (5.7) follows.

$$\begin{aligned} s^2 X_m^{res} &= C_p(X_{sm} - X_m) - C_f(\hat{F}_m + \hat{F}_s e^{-T_2 s}) \\ &= C_p(\frac{C_p}{C_p + s^2} X_m - X_m) - C_f(\hat{F}_m + \hat{F}_s e^{-T_2 s}) \\ &\cong C_p(X_m - X_m) - C_f(\hat{F}_m + \hat{F}_s e^{-T_2 s}) \\ &= -C_f(\hat{F}_m + \hat{F}_s e^{-T_2 s}) \end{aligned} \tag{5.7}$$

(5.7) shows that slave model position X_{sm} and master position X_m cancel each other, so that position control in master robot is removed. Of course, the position control in master robot is necessary to

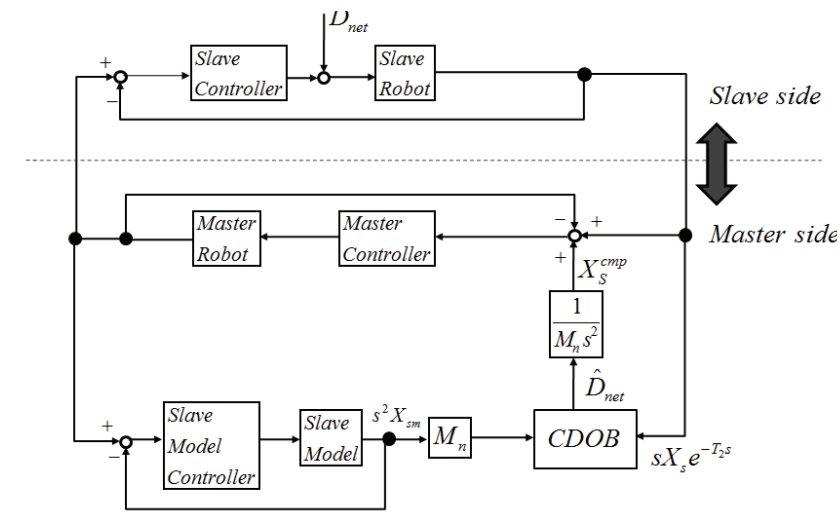

Fig. 5-3: Concept of time delay compensation by CDOB (4ch ABC + CDOB)

improve the performance. However, the model-based control without any model error is very difficult. As a result, position control in master robot is removed by time delay compensation of CDOB. The ultimate acceleration response values of 4ch ABC + CDOB system are given as follows.

$$s^2 X_m^{res} = -C_f(\hat{F}_m + \hat{F}_s e^{-T_2 s}) \tag{5.8}$$

$$s^2 X_s^{res} = C_p(X_m e^{-T_1 s} - X_s) - C_f(\hat{F}_m e^{-T_1 s} + \hat{F}_s) \tag{5.9}$$

5.3 Effect of Time Delay Compensation by CDOB to Each Modal Space

This section analyzes the effect of time delay compensation by CDOB to each modal space. The differential and common modal space of 4ch ABC + CDOB system are analyzed.

5.3.1 Analysis of position control in differential modal space (4ch ABC + CDOB)

The position control in differential modal space of 4ch ABC + CDOB system is given by subtracting (5.9) from (5.8) as follows.

$$s^2(X_m - X_s)^{res} = -C_p(X_m e^{-Ts} - X_s) - C_f(1 - e^{-Ts})(\hat{F_m} - \hat{F_s}) \tag{5.10}$$

(5.10) is rewritten to as follows.

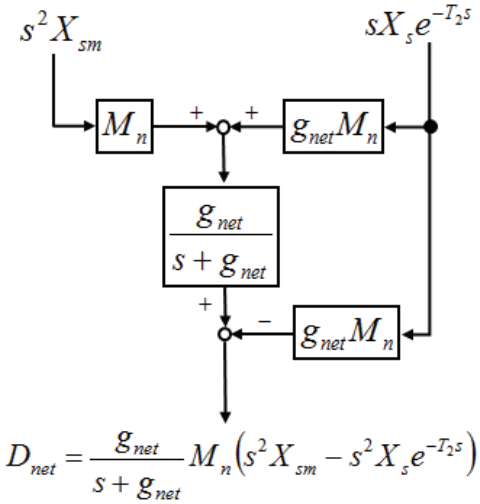

Fig. 5-4: Internal structure of CDOB

$$s^2(X_m - X_s)^{res} = C_p\{(X_m - X_m e^{-Ts}) - (X_m - X_s)\} - C_f(1 - e^{-Ts})(\hat{F_m} - \hat{F_s}) \tag{5.11}$$

Fig. 5-5 shows the block diagram of (5.11). The part of dotted line is regarded as an open-loop transfer function L_d, and the stability of L_d is analyzed. Time delay compensation by CDOB removes time delay e^{-Ts} from the feedback loop in differential modal space. However, the command value of differential modal space changes from 0 to $X_m - X_m e^{-Ts}$. This is because that position control works only in slave robot. Time delay compensation by CDOB removes the position control in master robot, so that the slave position X_s traces the time-delayed master position $X_m e^{-Ts}$ unilaterally. As a result, time delay is removed from the feedback loop in differential modal space, and the command value changes from 0 to $X_m - X_m e^{-Ts}$.

5.3.2 Analysis of force control in common modal space (4ch ABC+ CDOB)

Force control in common modal space of 4ch ABC+ CDOB system is given by adding (5.8) and (5.9) as follows.

$$s^2(X_m + X_s)^{res} = -C_p(X_m + X_s)(1 - e^{-Ts}) - C_f(1 + e^{-Ts})(\hat{F_m} + \hat{F_s}) \tag{5.12}$$

Fig. 5-6 shows the block diagram of force control of 4ch ABC + CDOB system in common modal space. The part of dotted line is regarded as an open-loop transfer function (L_c), and the stability of L_c is

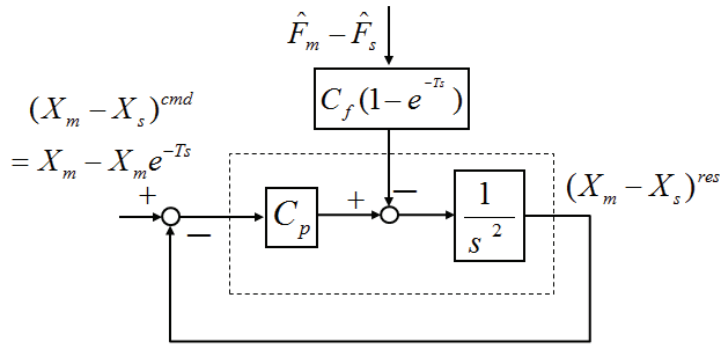

Fig. 5-5: Position control in differential modal space(4ch ABC + CDOB)

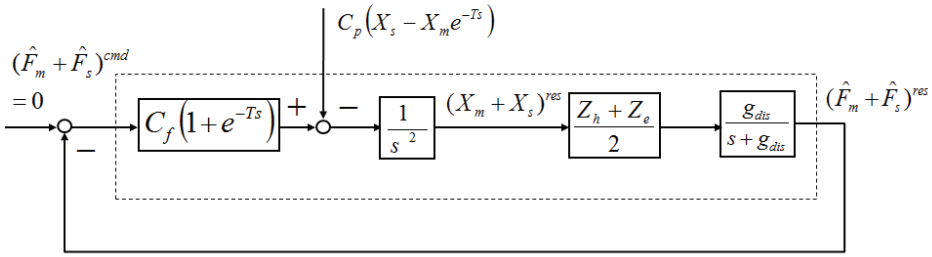

Fig. 5-6: Force control in common modal space(4ch ABC + CDOB)

analyzed. Time delay still exists in feedback loop of force control in common modal space. Time delay compensation by CDOB makes position control in differential modal space stable, but another solution method is required to improve the stability of force control in common modal space. CDOB approach is a kind of model predictive control. However, it is not suitable for force control because the prediction of the reaction force from an environment is impossible.

5.4 Effect of Time Delay Compensation by CDOB for Reproducibility and Operationality

This section analyzes the effect of time delay compensation by CDOB for reproducibility and operationality. Bode diagram of reoroducibility and operationality in 4ch ABC + CDOB and conventional 4ch ABC is shown as Fig. 5-7. Parameters are shown as Table 5-1. Time delay compensation by CDOB improves operationality very much. However, on the other hand, it deteriorates reproducibility. This is because time delay compensation removes the position control of master robot. As explained in chapter 4, position control improves reproducibility, but deteriorates operationality under time delay. Furthermore,

Table 5-1: Parameters in stability and performane analysis

Parameter	Meaning	Value
T	Time delay(one way)	100[ms]
K_p	Position gain	900
K_v	Velocity gain	60
K_f	Force gain	1.0
g_{dis}	Cutoff frequency of DOB	800[rad/s]
g_{net}	Cutoff frequency of CDOB	800[rad/s]
Z_h	Impedance of human	1000+200s
Z_e	Impedance of environment	10000+50s
st	Sampling time	0.1[ms]
M_n	Nominal inertia of motor	0.5 [kg]
K_{tn}	Torque coefficient	22.0 [N/A]

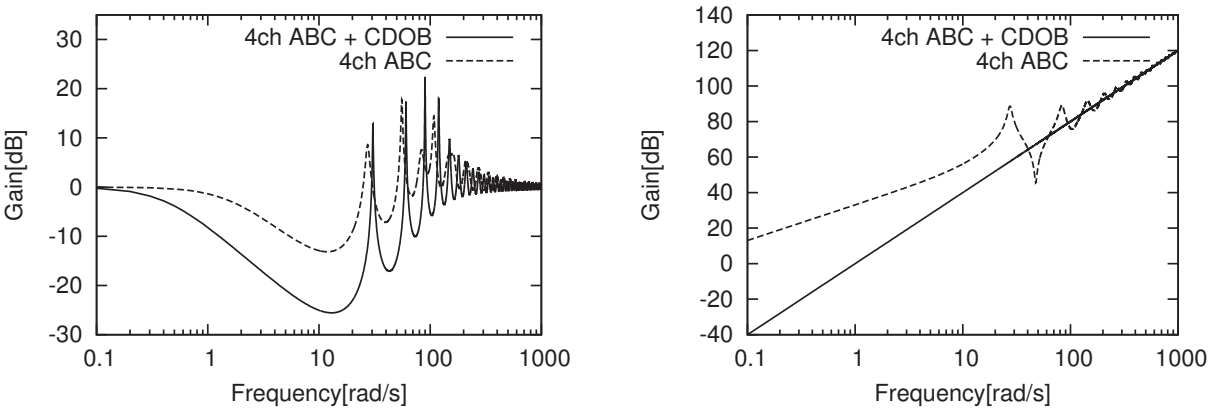

(a) Reproducibility

(b) Operationality

Fig. 5-7: Reproducibility and operationality in 4ch ABC + CDOB

it also breaks the symmetric property between the master and the slave. As a result, the manipulation from slave side becomes impossible.

5.5 Summary

Chapter 5 introduced time delay compensation by communication disturbance observer (CDOB), and analyzed the effect on each modal space. Firstly, the structure of time delay compensation in 4ch ABC by communication disturbance observer (CDOB) based on the concept of network disturbance (ND) was

explained. Secondly, the effect of time delay compensation by CDOB to each modal space was analyzed. Thirdly, the effect of time delay compensation by CDOB to reproducibility and operationality was also analyzed.

Chapter 6

Damping Injection to ABC system

6.1 Introduction

Chapter 6 analyzes the effect of damping injection on ABC system. Previous chapter 5 proves that time delay compensation by CDOB stabilizes position control in differential modal space. However, another solution method is required to improve the stability of force control. A major method for stabilization of force control is damping injection by the local velocity feedback[65]. There are some researchers who proposed damping injection to ABC, and analyzed the effect on transparency[66, 67]. This chapter 6 describes damping injection to the master and the slave robots, and analyzes the effect of damping injection to each modal space. The acceleration reference values of 4ch ABC + CDOB + Damping system are given by the following equations. K_{dm} means damping gain. Here, the differential process such $\frac{sg_{dis}}{s+g_{dis}}$ is regarded as a simple differentiator s on the assumption that g_{dis} is large enough.

$$s^2 X_m^{ref} = s^2 X_m^{res} = -C_f(\hat{F}_m + \hat{F}_s e^{-T_2 s}) - K_{dm} s X_m \tag{6.1}$$

$$s^2 X_s^{ref} = s^2 X_s^{res} = C_p(X_m e^{-T_1 s} - X_s) - C_f(\hat{F}_m e^{-T_1 s} + \hat{F}_s) - K_{dm} s X_s \tag{6.2}$$

6.2 Analysis of Position Contol in Differential Modal Space (4ch ABC + CDOB + Damping)

The position control in differential modal space of 4ch ABC+ CDOB + Damping system is given by subtracting (6.2) from (6.1) as follows.

$$\begin{aligned} s^2(X_m - X_s)^{res} = C_p\{(X_m - X_m e^{-Ts}) - (X_m - X_s)\} \\ -C_f(1 - e^{-Ts})(\hat{F_m} - \hat{F_s}) - K_{dm}(sX_m - sX_s) \end{aligned} \tag{6.3}$$

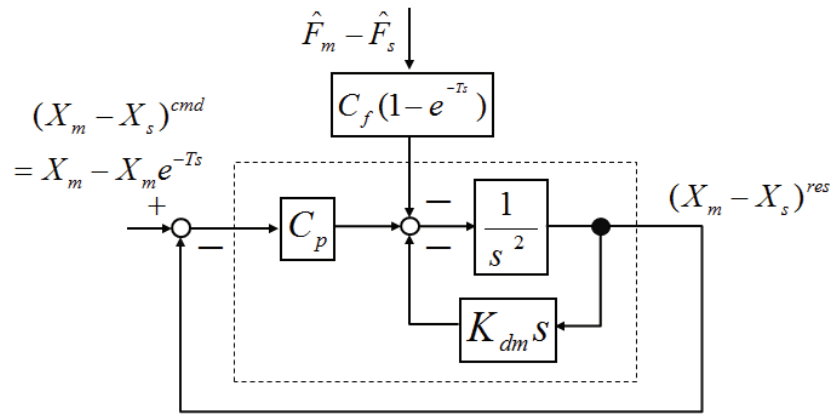

Fig. 6-1: Position control in differential modal space (4ch ABC + CDOB + Damping)

Table 6-1: Parameters in stability and performane analysis

Parameter	Meaning	Value
T	Time delay(one way)	100[ms]
K_p	Position gain	900
K_v	Velocity gain	60
K_f	Force gain	1.0
g_{dis}	Cutoff frequency of DOB	800[rad/s]
g_{net}	Cutoff frequency of CDOB	800[rad/s]
Z_h	Impedance of human	1000+200s
Z_e	Impedance of environment	10000+50s
K_{dm}	Damping gain	40.0
st	Sampling time	0.1[ms]

Fig. 6-1 shows the block diagram of position control in differential modal space of 4ch ABC + CDOB + Damping system. The part of dotted line is regarded as an open-loop transfer function (L_d), and the stability of L_d is analyzed. The stability of L_d is analyzed by Nyquist plot in Fig. 6-2. Parameters in analysis are shown as Table 6-1. Fig. 6-2 shows that damping injection leads the phase of position control in differential modal space, so that the stability of position control is improved.

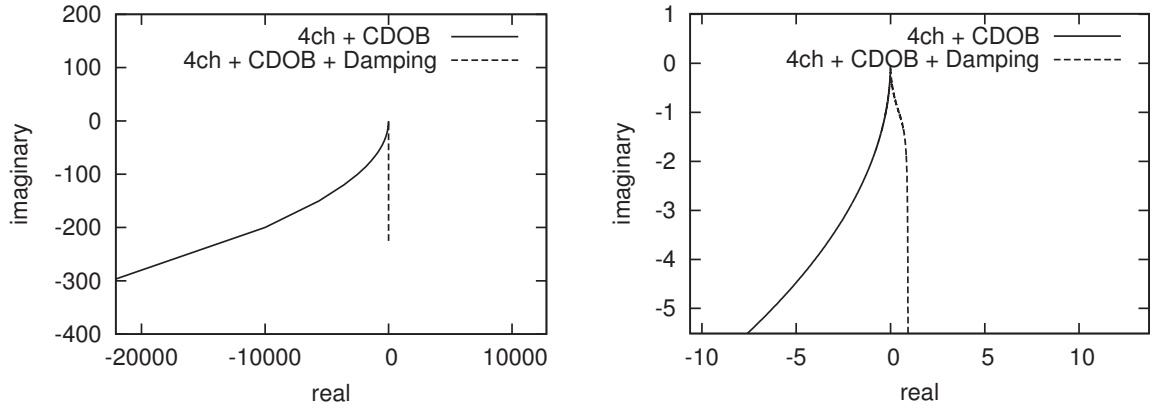

(a) Overall view (b) Closeup to (0,0)

Fig. 6-2: Nyquist plot of differential modal space (4ch ABC + CDOB + Damping)

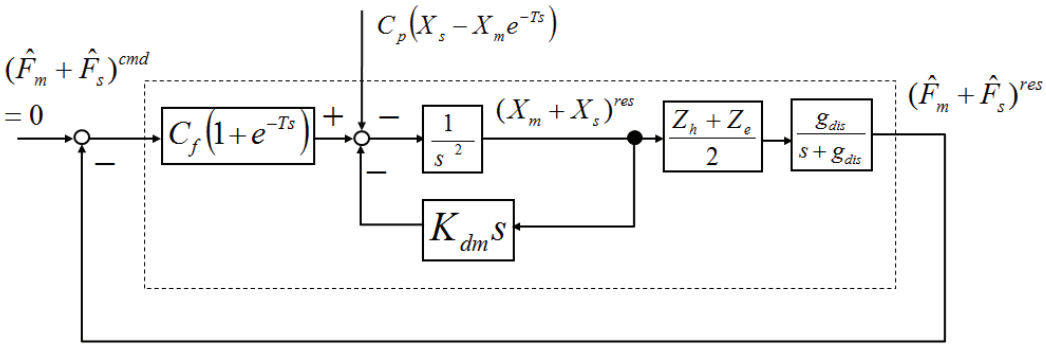

Fig. 6-3: Force control in common modal space (4ch ABC + CDOB + Damping)

6.3 Analysis of Force Contol in Common Modal Space (4ch ABC + CDOB + Damping)

The force control of 4ch ABC + CDOB + damping system in common modal space is shown as follows by adding (6.1) and (6.2).

$$s^2(X_m + X_s)^{res} = -C_f(1 + e^{-Ts})(\hat{F}_m + \hat{F}_s) + C_p(X_m e^{-Ts} - X_s) - K_{dm}s(X_m + X_s) \quad (6.4)$$

Block diagram of (6.4) is shown in Fig. 6-3. The part of dotted line is regarded as an open loop transfer function (L_c). The stability of L_c is analyzed by Nyquist plot in Fig. 6-4. Fig. 6-4 shows that damping injection leads the phase of force control in common modal space, so that the stability of force control is

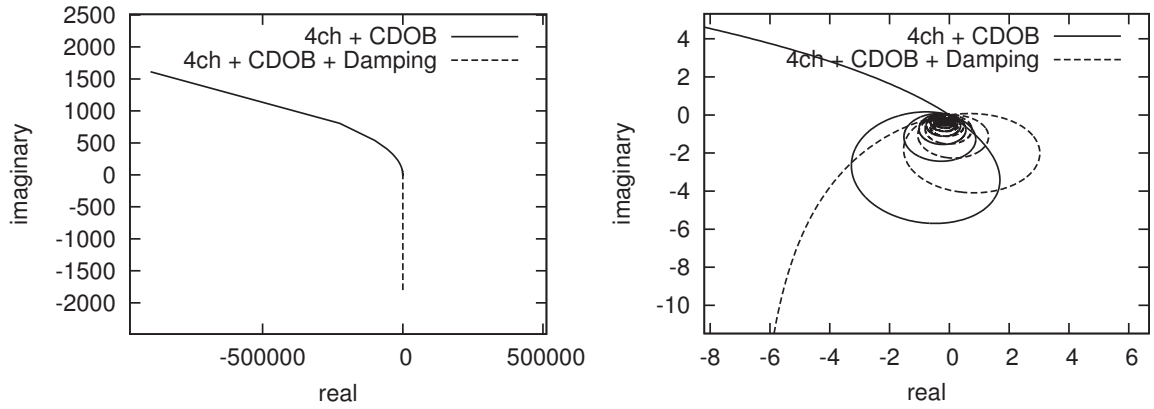

(a) Overall view (b) Closeup to (0,0)

Fig. 6-4: Nyquist plot of common modal space (4ch ABC + CDOB + damping)

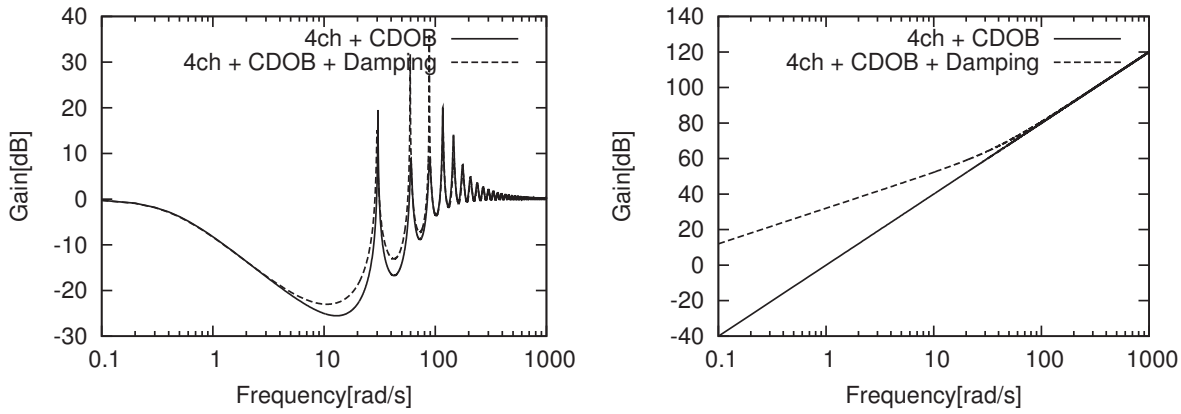

(a) reproducibility (b) operationality

Fig. 6-5: Gain characteristic of reproducibility and operationality (4ch ABC + CDOB + damping)

also improved. Gain margin is 12.2[dB], and phase margin is 13.3[deg].

6.4 Reproducibility and Operationality (4ch ABC + CDOB + Damping)

Fig. 6-5 shows gain characteristics of reproducibility and operationality[12]. The ideal value of reroducibility is 1(=0[dB]), and operationality is 0(= - ∞[dB]). Damping injection has almost no influence to reproducibility. However, damping injection deteriorates operationality in low frequency area. From these analyses, damping injection improves the stability of each modal space under time delay, but it simultaneously deteriorates operationality in low frequency area. There is a trade-off relation between stability and operationality in damping injection.

6.5 Summary

Chapter 6 introduced damping injection by velocity feedback in ABC system, and analyzed the effect on each modal space. Furthermore, the effect to reproducibility and operationality was also analyzed. Analysis result showed that there was a trade-off relation between stability and operationality in damping injection.

Chapter 7

Frequency-Domain Damping Design (FDD) for ABC System

7.1 Introduction

To solve the previous trade-off problem between robust stability and operationality in damping injection, this chapter 7 proposes "frequency-domain damping design (FDD)". Appropriate frequency-domain damping injection is achieved by using loop-shaping high-pass filter (HPF). The design of HPF is determined based on robust H_∞ stability condition.

7.2 Concept of FDD

Damping controller C_{dm} is shown as follows. K_{fdd} is the gain of FDD. G_{hpf} is the transfer function of HPF.

$$C_{dm} = K_{fdd} G_{hpf} \tag{7.1}$$

The acceleration response values of proposed system (4ch ABC + CDOB + FDD) are given by the following equations.

$$s^2 X_m^{res} = -C_f(\hat{F}_m + \hat{F}_s e^{-T_2 s}) - C_{dm} s X_m \tag{7.2}$$

$$s^2 X_s^{res} = C_p(X_m e^{-T_1 s} - X_s) - C_f(\hat{F}_m e^{-T_1 s} + \hat{F}_s) - C_{dm} s X_s \tag{7.3}$$

The characteristic of time delay element e^{-Ts} in the frequency domain is described as follows.

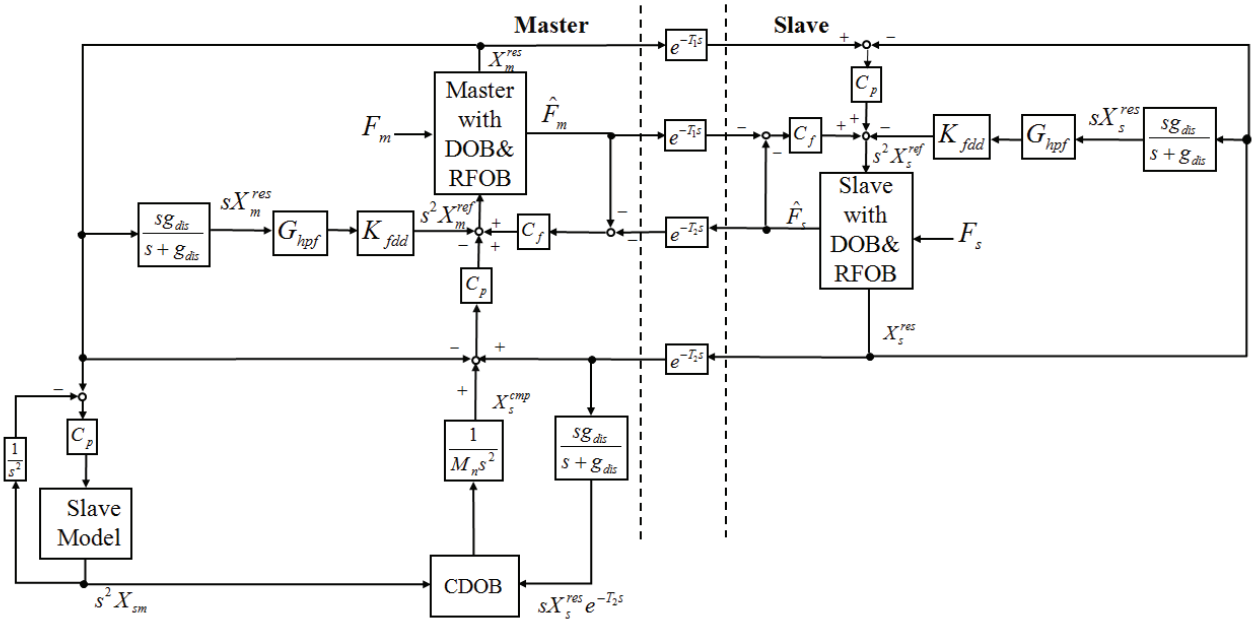

Fig. 7-1: Block diagram of 4ch ABC + CDOB + FDD

$$|e^{-j\omega T}| = 1 \tag{7.4}$$

$$\angle e^{-j\omega T} = -\omega T \tag{7.5}$$

Time delay element e^{-Ts} delays the phase of any control system in proportion to frequency value ω. This means that the control system which has time delay element e^{-Ts} tends to become unstable in high frequency area. From this reason, this section proposes high damping injection only in high frequency area using loop-shaping HPF to suppress only the high frequency oscillations at contact. FDD realizes a high-performance and stable bilateral teleoperation system under time delay. The block diagram of proposed system is shown as Fig. 7-1.

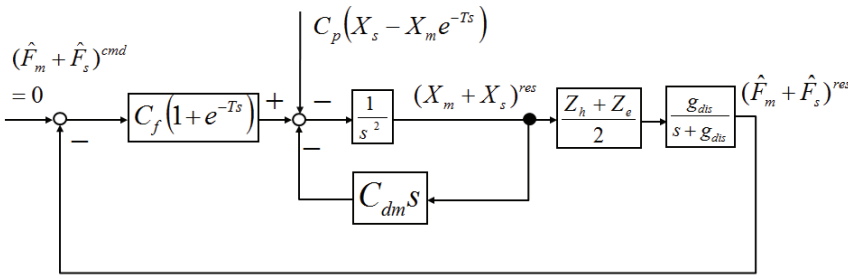

Fig. 7-2: Force control in common modal space(4ch ABC + CDOB + FDD)

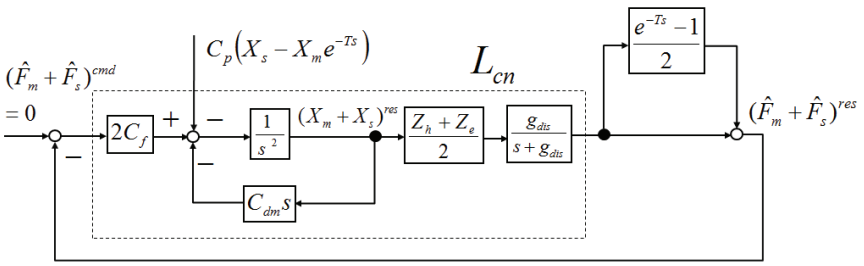

Fig. 7-3: Multiplicative representation of time delay effect on common modal space

Table 7-1: Parameters in stability and performane analysis

Parameter	Meaning	Value
T	Time delay(one way)	150[ms]
K_p	Position gain	900
K_v	Velocity gain	60
K_f	Force gain	1.0
g_{dis}	Cutoff frequency of DOB	800[rad/s]
g_{net}	Cutoff frequency of CDOB	800[rad/s]
Z_h	Impedance of human	1000+200s
Z_e	Impedance of environment	10000+50s
K_{dm}	Damping gain	100.0
K_{fdd}	FDD gain	90.0
st	Sampling time	0.1[ms]
M_n	Nominal inertia of motor	0.5[kg]
K_{tn}	Torque coefficient	22.0[N/A]

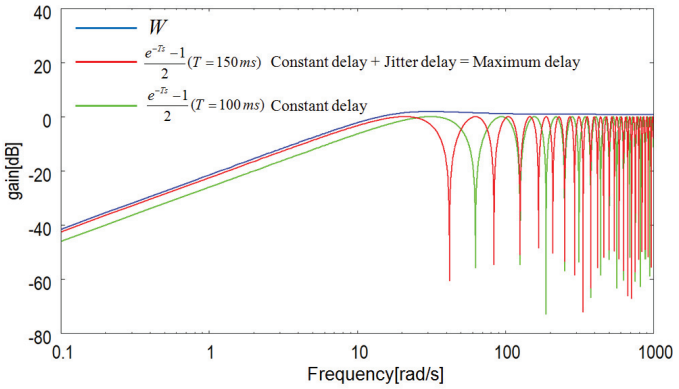

Fig. 7-4: Bode diagram of weighting function

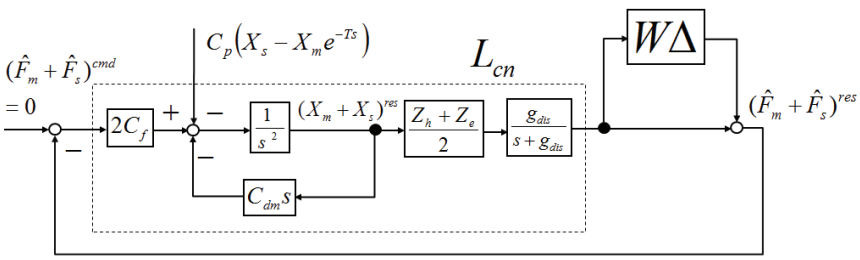

Fig. 7-5: Multiplicative representaion of time delay effect using weighting function

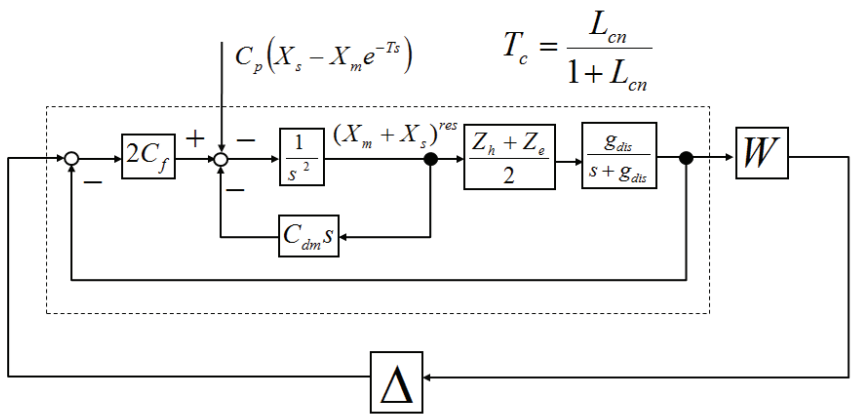

Fig. 7-6: Equivalent transformation of Fig. 7-5

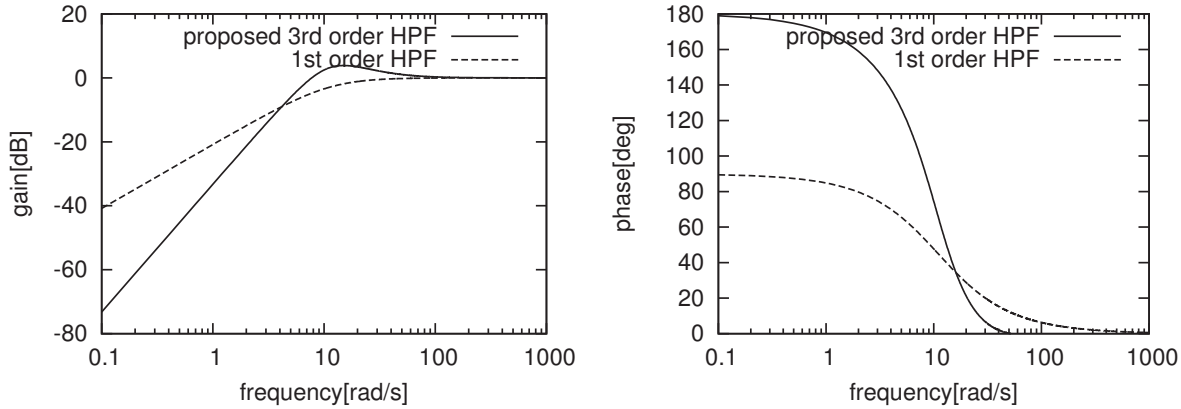

(a) Gain (b) Phase

Fig. 7-7: Bode diagram of proposed 3rd order HPF

7.3 Design of HPF Based on Robust H_∞ Stability Condition

This section explains the procedure of design of loop-shaping HPF based on robust H_∞ stability condition.

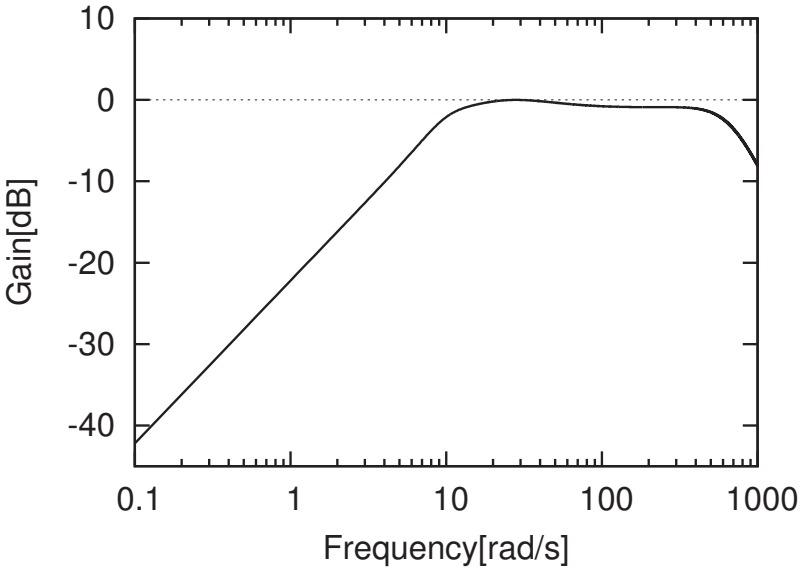

Fig. 7-8: Gain characteristic of $W(j\omega)T_c(j\omega)$

Table 7-2: Corresponding parameters to other time delay cases

T_{max}[ms]	g_h[rad/s]	K_{fdd}
150	11	90
200	8.0	93
250	6.0	96
300	3.0	100

7.3.1 Robust stability condition of force control in common modal space

The block diagram of common modal space is shown as Fig. 7-2. Fig. 7-2 is transformed into Fig. 7-3 equivalently. Fig. 7-3 is multiplicative representation of time delay effect on common modal space. The dotted part is regarded as the nominal open-loop transfer function of common modal space L_{cn}. The multiplicative uncertainty is represented by weighting function $W(s)$ as follows. $\Delta(s)$ shows uncertainty.

$$\frac{e^{-Ts}-1}{2} = W(s)\Delta(s), \quad |\Delta(jw)| < 1, \ \forall w \tag{7.6}$$

The transfer function of $W(s)$ is described as follows. $W(s)$ is designed to cover any time delay uncertainty as tightly as possible for improvement of operationality. In this chapter, maximum delay time T_{max} is set at 150 ms. Constant time delay is 100 ms, and jitter delay is +-50 ms. Other parameters are shown as Table 7-1.

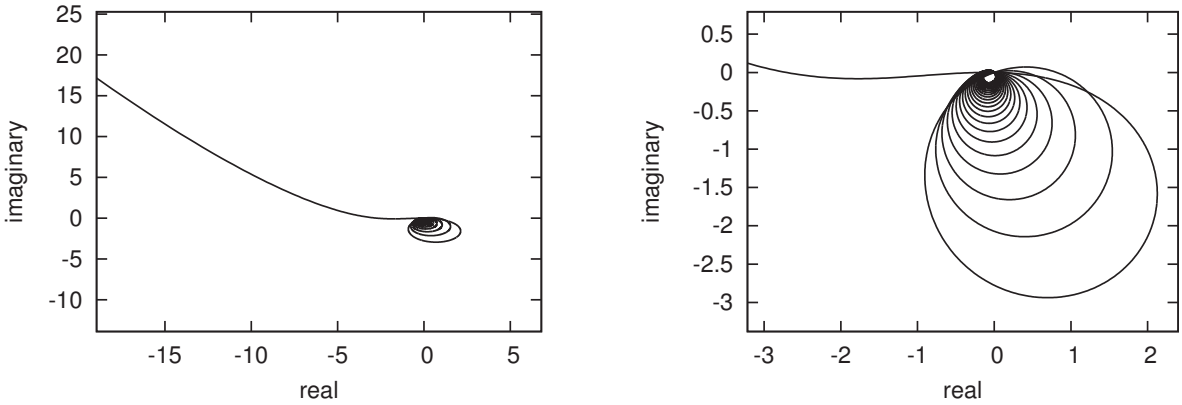

(a) Reproducibility (b) Operationality

Fig. 7-9: Nyquist plot of common modal space (4ch ABC + CDOB + FDD)

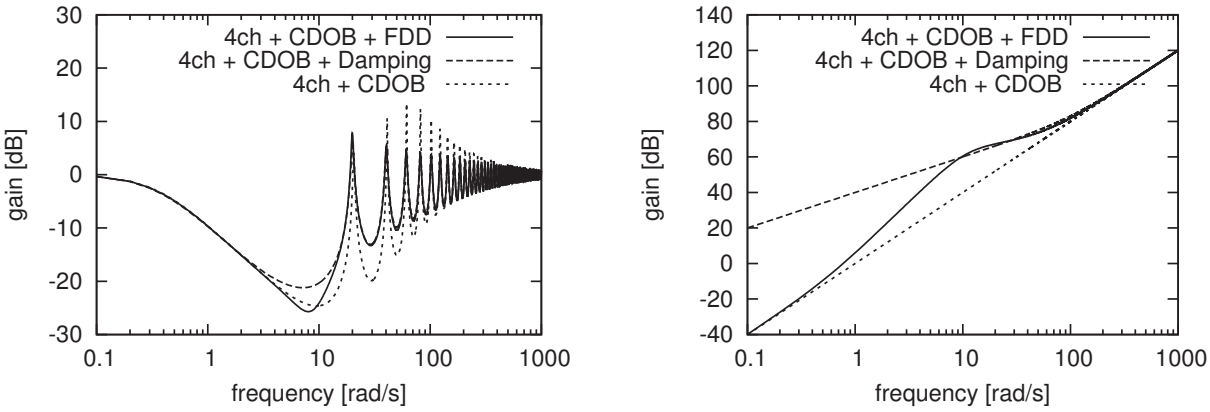

(a) Reproducibility (b) Operationality

Fig. 7-10: Reproducibility and operationality in 4ch ABC + CDOB + FDD

$$W(s) = \frac{11s(s+36)(s+17)}{10(s^2+36s+400)(s+20)} \tag{7.7}$$

Gain characteristic of $W(s)$ is shown as Fig. 7-4. The time delay uncertainty under 150 ms is tightly-covered with the weighting function in all frequency area. Green line is the constant time delay uncertainty, and red line is the assumed maximum time delay (constant delay + jitter delay). Fig. 7-4 shows that blue line of weighting function covers with any time delay uncertainty. Therefore, if there exists any jitter time delay within 50 ms, the robust stability is retained by the following condition.

By using $W(s)$, Fig. 7-3 is transformed into Fig. 7-5. Fig. 7-5 is equivalently transformed into Fig. 7-6. The design objective is to minimize the weighted complementary sensitivity function (nominal closed-

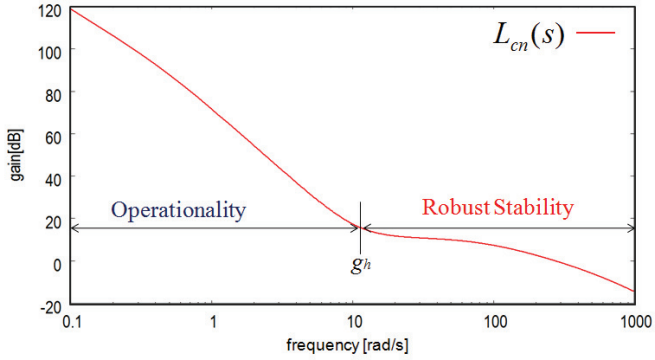

Fig. 7-11: Frequency-domain shaping of L_{cn}

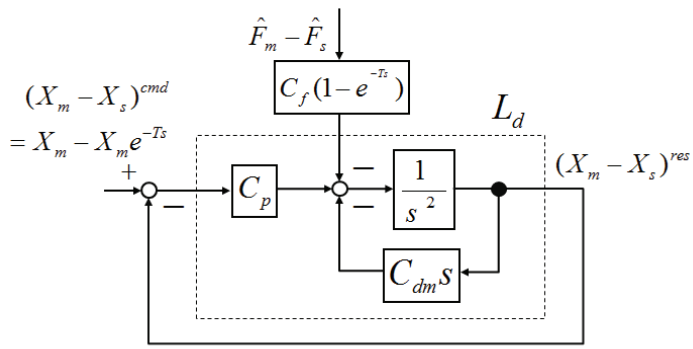

Fig. 7-12: Position control in differential modal space (4ch ABC + CDOB + FDD)

loop transfer function) $T_c = L_{cn}/(1 + L_{cn})$. The robust stability condition is as follows.

$$\begin{aligned} ||W(s)T_c(s)||_\infty &< 1 \\ \Leftrightarrow |W(j\omega)T_c(j\omega)| &< 1, \ \forall\omega \end{aligned} \tag{7.8}$$

7.3.2 Design of loop-shaping HPF

To satisfy (7.8), Damping gain K_{fdd} is set at 90, and a 3rd order HPF is designed as follows.

$$G_{HPF} = \frac{s^2(s+29)}{(s^2+15s+11^2)(s+11)} \tag{7.9}$$

Cutoff frequency of HPF g_h is set to 11.0 rad/s. In general, high order HPF has better gain characteristic than low order HPF. However, high order HPF has its large phase lead element. This large phase lead

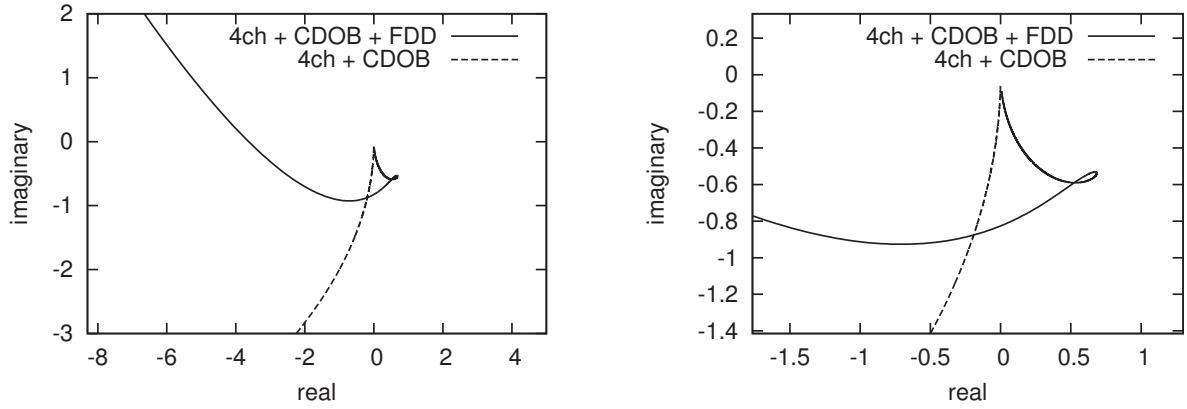

(a) Reproducibility (b) Operationality

Fig. 7-13: Nyquist plot of differential modal space (4ch ABC + CDOB + FDD)

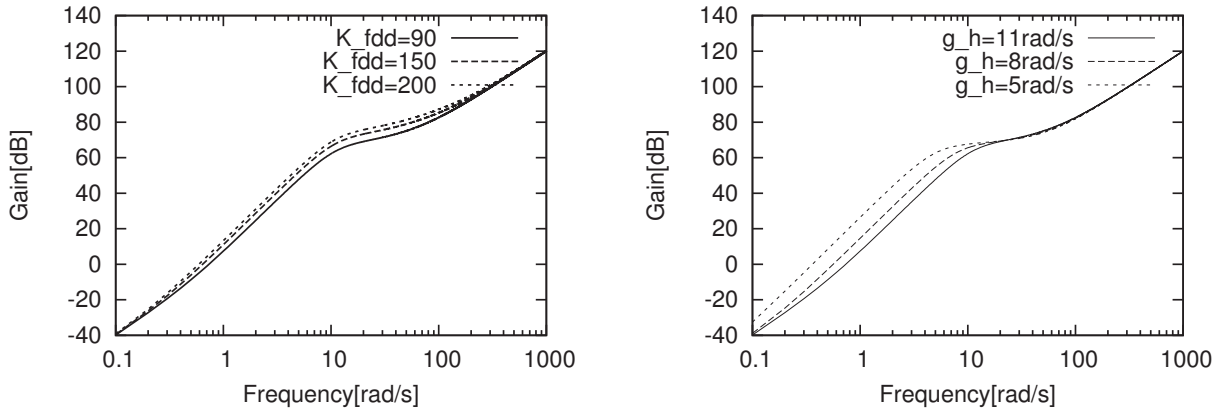

(a) K_{fdd} variation (b) g_h variation

Fig. 7-14: Operationality in K_{fdd} and g_h variation

changes the velocity feedback into the acceleration feedback, and might cause destabilization. Considering these factors, this chapter designs 3rd order HPF. Bode diagram of proposed 3rd order HPF is shown as Fig. 7-7 compared with conventional 1st order HPF $s/(s+11)$. As for gain characteristic, proposed 3rd-order HPF retains much smaller gain characteristic in low frequency area than conventional 1st-order HPF. On the other hand, as for phase characteristic, phase lead of proposed 3rd order HPF above g_h is relieved as much as that of conventional 1st order HPF. Then the gain characteristic of the weighted complementary sensitivity function $W(s)T_c(s)$ is shown as Fig. 7-8. In all frequency area, gain value is smaller than 1(=0[dB]). It shows that robust stability is satisfied by proposed FDD. In addition, Nyquist plot is shown as Fig. 7-9. However, if the maximum delay time is set at more than 150 ms, the cutoff frequency g_h should be redesigned to be smaller than 11 rad/s, and the other parameters might need some

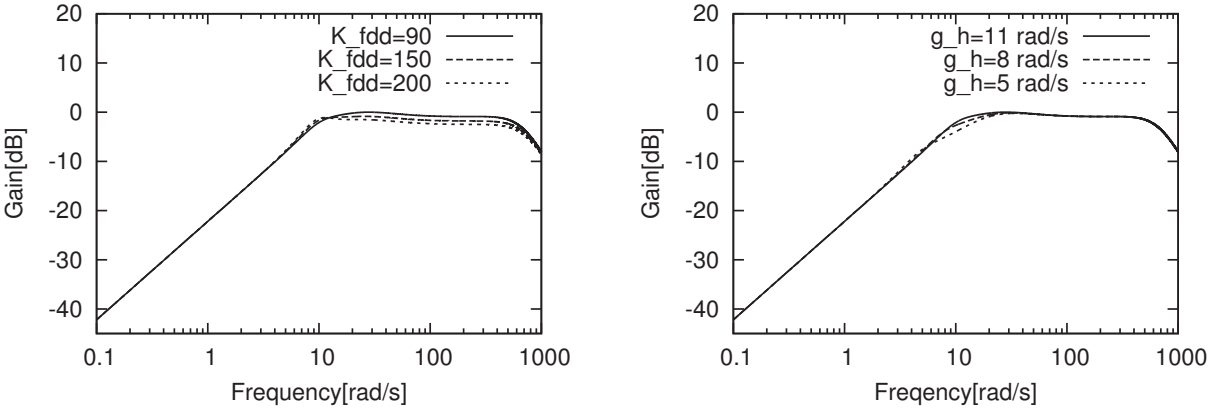

(a) K_{fdd} variation (b) g_h variation

Fig. 7-15: H_∞ norm in K_{fdd} and g_h variation

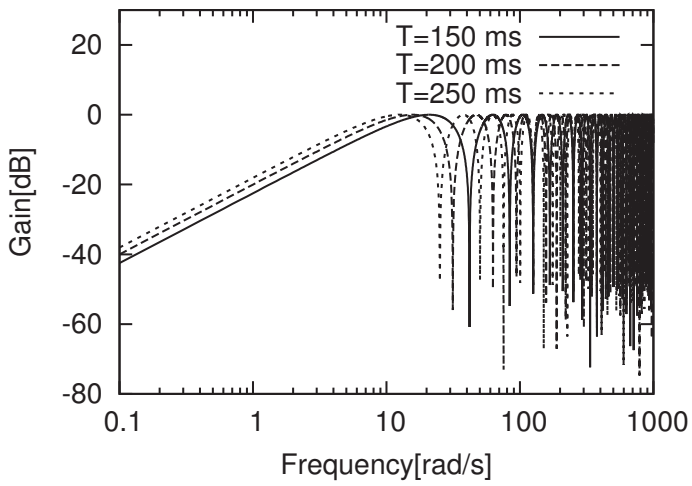

Fig. 7-16: Time delay uncertainty in delay time variation

adjustment to satisfy the robust stability condition. Table 7-2 shows corresponding parameter values of g_h and K_{fdd} to other time delay cases. T_{max} means the maximum delay time.

7.3.3 Mixed sensitivity problem between operationality and robust stability

Hybrid parameters of proposed system are described as follows.

$$H_{11}(P_o) = -\frac{s(s+C_{dm})}{C_f} \tag{7.10}$$

$$H_{12} = e^{-Ts} \tag{7.11}$$

$$H_{21} = -e^{-Ts} \tag{7.12}$$

$$H_{22} = \frac{C_f(-1+e^{-2Ts})}{C_p+s(s+C_{dm})} \tag{7.13}$$

From (7.10), operationality P_o is proportional to force gain, and damping injection deteriorates operationality. Fig. 7-10 shows gain characteristic of reproducibility and operationality. As for reproducibility, FDD has almost no influence on it. On the other hand, as for operationality, operationality in low frequency area under g_h is improved compared with conventional damping injection. Furthermore, Fig. 7-11 shows Bode diagram of the nominal open loop transfer function in common modal space L_{cn}. It shows frequency-domain loop-shaping of L_{cn}. In low frequency area under g_h, $|L_{cn}|$ becomes large to improve operationality. On the other hand, in high frequency area above g_h, $|L_{cn}|$ becomes small by damping injection to assure robust stability. This is the mixed sensitivity problem between operationality and robust stability. However, the value of g_h depends on the maximum delay time. Robust stability is more important than operationality. As a result, improvement of operationality by FDD is limited by the maximum delay time.

7.3.4 Analysis of position control in differential modal space (4ch ABC + CDOB + FDD)

The position control in differential modal space of proposed system (4ch ABC+ CDOB + FDD) is given by subtracting (7.3) from (7.2) as follows

$$\begin{aligned} s^2(X_m - X_s)^{res} = C_p\{(X_m - X_m e^{-Ts}) - (X_m - X_s)\} \\ -C_f(1-e^{-Ts})(\hat{F_m} - \hat{F_s}) - C_{dm}(sX_m - sX_s) \end{aligned} \tag{7.14}$$

Fig. 7-12 shows the block diagram of position control in differential modal space of 4ch ABC + CDOB + FDD system. The part of dotted line is regarded as an open-loop transfer function (L_d), and the stability of L_d is analyzed. The stability of L_d is analyzed by Nyquist plot in Fig. 7-13. Parameters in analysis are shown as Table 7-1. Fig. 7-13 shows that the stability of position control in proposed system is also stable.

7.3.5 Procedure of parameter tuning of FDD

Fig. 7-14 shows the change of operationality in K_{fdd} and g_h variation. With the increase of K_{fdd}, operationality is deteriorated in all frequency area a little. On the other hand, with the decrease of g_h, operationality is deteriorated in some degree in low frequency area. From this analysis, the value of g_h has much more influence to operationality than that of K_{fdd}, so g_h should be as large as possible for

operationality in the satisfaction of robust stability. Furthermore, Fig. 7-15 shows the change of H_∞ norm in K_{fdd} and g_h variation. With the increase of K_{fdd}, H_∞ norm in high frequency becomes small. On the other hand, with the decrease of g_h, H_∞ norm around g_h becomes small. Fig. 7-16 shows the change of time delay uncertainty in delay time variation. The gain value of time delay uncertainty in low frequency area becomes large as delay time becomes large. Therefore, if delay time increases, there is no choice to make the value of g_h small to satsify robust stability. Table 7-2 shows corresponding parameter values of g_h and K_{dm} to other time delay cases. T_{max} means the maximum delay time. As shown as Table 7-2, g_h becomes small as T_{max} becomes large.

7.4 Experiments

Fig. 7-17 shows the experimental system. Linear motor is controlled by real time OS:RTAI. Communication protocol is RTNet. Time delay is produced by network emulator. The master and slave system consists of 1-DOF robots. The robots consist of linear motors and position encoders.

Three controllers are compared: 4ch ABC + CDOB, 4ch ABC + CDOB + damping and 4ch ABC + CDOB + FDD. Experimental parameters are set as Table 7-1. The experiment is conducted under constant delay and time-varying delay. As for constant delay, delay time is set at 150 ms. In time-varying delay case, it changes from 50 ms to 150 ms. Time delay is varying by linear jitter produced by network emulator. Fig.7-18 shows the dynamic change of time delay with linear jitter. Time delay changes by 1ms in one sampling time of packet transmission. Fig. 7-19 shows the experimental instruments.

7.4.1 Free motion

Experiments for free motion are done. The operator handles master robot with back-and-forth motion. The experimental results under constant delay are in Figs. 7-20 $\sim$ 7-22, and those under time-varying delay are shown in Figs. 7-23 $\sim$ 7-25. Each slave robot follows the position of its master robot precisely. The stability of each controller is well even under time-varying delay. This is because time delay compensation by CDOB makes the position control stable. However in damping injection case, some extra force is necessary in free motion. As a result, the operator feels stress in manipulation. On the other hand, proposed FDD reduces the operational force drastically compared with conventional damping injection. Yet the operational force of proposed system (4ch ABC + CDOB + FDD) is still larger than that of 4ch ABC + CDOB. This means that HPF cannot filter out the damping injection perfectly in free motion.

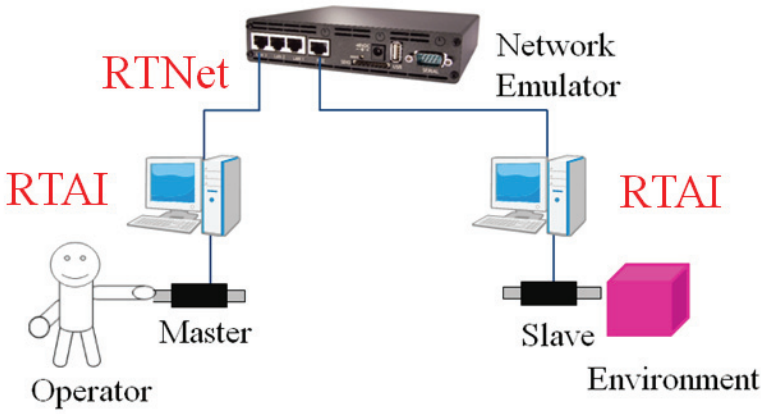

Fig. 7-17: Experimental system

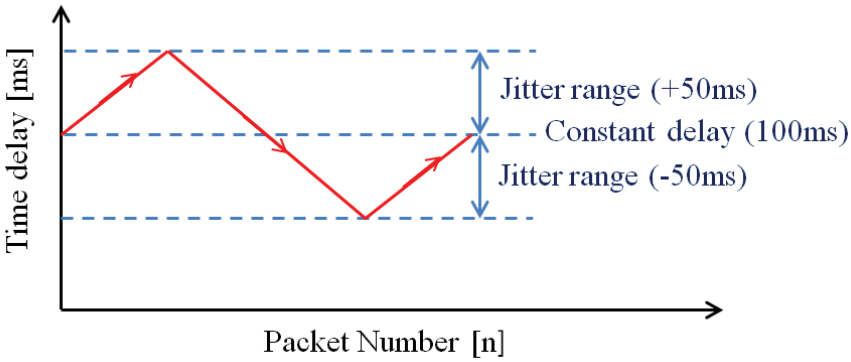

Fig. 7-18: Dynamic change of time delay with linear jitter

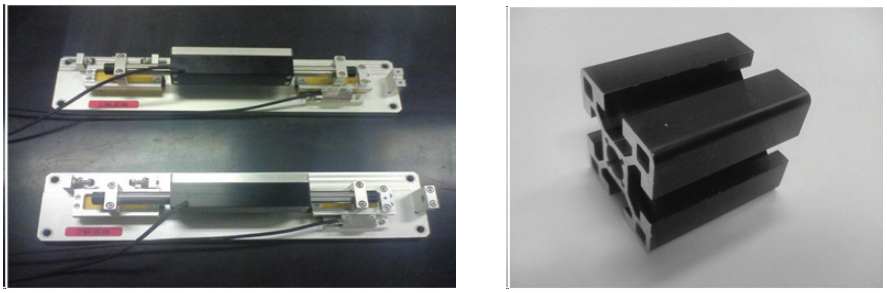

(a) Two linear motors (b) Hard environment (aluminium)

Fig. 7-19: Experimental instruments

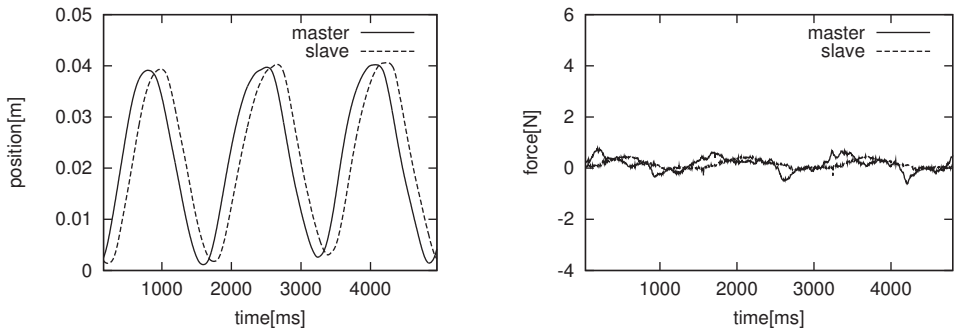

(a) Position response (b) Force response

Fig. 7-20: Free motion under constant delay (4ch ABC + CDOB)

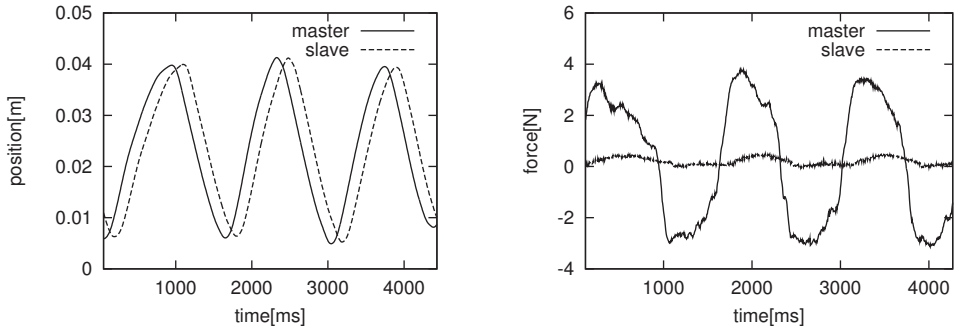

(a) Position response (b) Force response

Fig. 7-21: Free motion under constant delay (4ch ABC + CDOB + Damping)

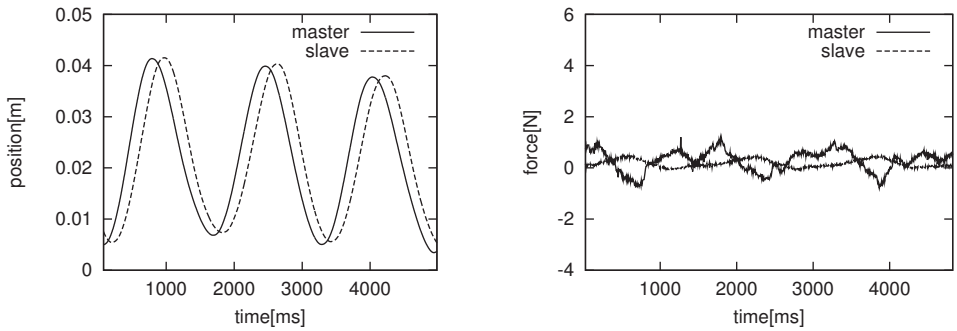

(a) Position response (b) Force response

Fig. 7-22: Free motion under constant delay (4ch ABC + CDOB + FDD)

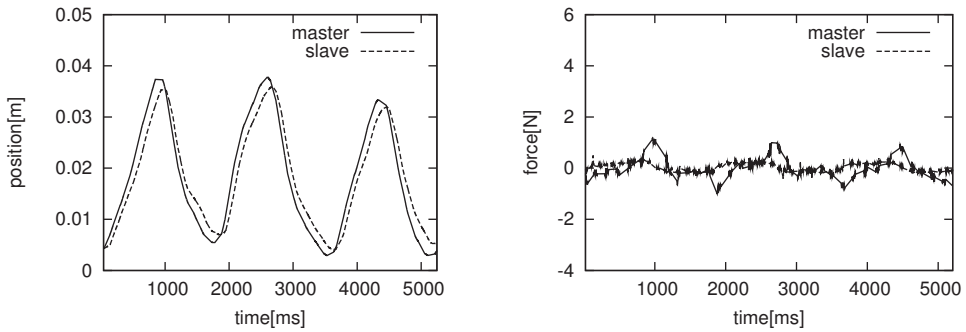

(a) Position response (b) Force response

Fig. 7-23: Free motion under time-varying delay (4ch ABC + CDOB)

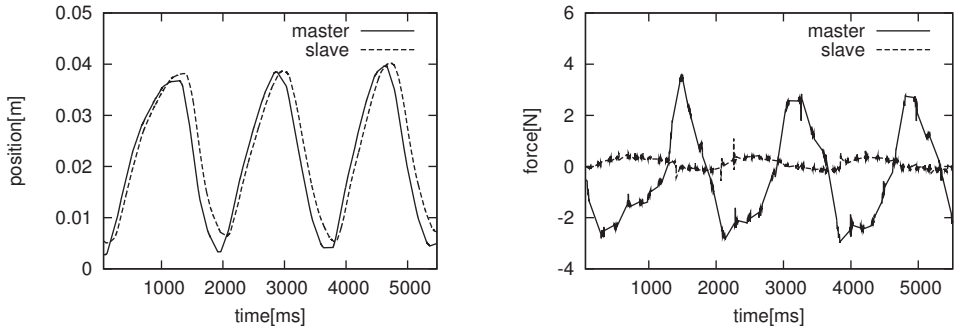

(a) Position response (b) Force response

Fig. 7-24: Free motion under time-varying delay (4ch ABC + CDOB + Damping)

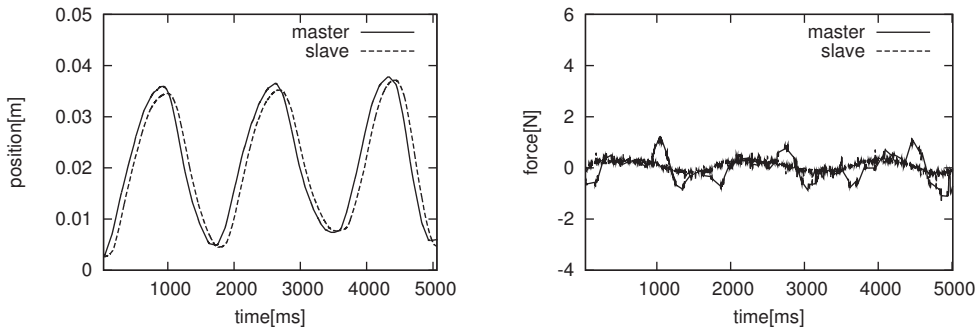

(a) Position response (b) Force response

Fig. 7-25: Free motion under time-varying delay (4ch ABC + CDOB + FDD)

7.4.2 Contact motion

The experimental results of contact motion are shown in Figs. 7-26∼7-34. Figs. 7-26∼7-28 are the results of contact motion with a hard environment under constant delay. With 4ch ABC + CDOB, there are oscillations in contact motion. This is because the force control in the common modal space is unstable. On the other hand, with damping injection, oscillations are suppressed well. It proves that damping injection improves the stability of force control in the common modal space. Proposed system (4ch ABC + CDOB + FDD) also realizes stable contact motion. FDD suppresses high frequency oscillations in contact motion, and stabilizes the force control in the common modal space.

Figs. 7-29∼7-31 are the results of contact motion with a soft environment under constant delay. It is clear that the soft environment absorbs oscillations. As a result, the stability of each controller is improved compared as the case with the hard environment.

Figs. 7-32∼7-34 are the results of contact motion with the hard environment under time-varying delay. Network jitter intensifies oscillations in contact motion with 4ch ABC + CDOB. However, the controller with damping injection still realizes the stable contact motion with the hard environment even under time-varying delay. Proposed controller with FDD also achieved the stable contact motion with the hard environment under time-varying delay. The effectiveness of FDD is demonstrated even under time-varying delay.

From experimental results of contact motion, it is proved that satisfaction of stability conditions of two modal spaces assure the whole stability of ABC. Time delay compensation by CDOB stabilizes the position control in differential modal space. Surely, position control in free motion is stable. However 4ch ABC + CDOB system gets unstable in contact motion. This is because the stability of force control in common modal space is still inferior. Stabilization of common modal space is necessary to realize stable contact motion. Damping injection stabilizes force control in common modal space, and stable contact motion is achieved in experimental results. However damping injection drastically deteriorates the operationality in manipulation. On the other hand, FDD realizes the stabilization of two modal space with a bit deterioration of operationality compared with conventional damping injection.

7.5 Summary

This chapter proposed frequency-domain damping design (FDD) to 4ch ABC + CDOB system. HPF of FDD is designed based on robust H_∞ stability. With the experimental and analytical results, proposed damping method improved the stability of contact motion with environments, maintaining good operationality. The proposed FDD method is easily implementable and adjustable by the design of H_∞ norm if the maximum delay time value including jitter delay is known in advance. The validity of the proposed control system was confirmed with some experimental results.

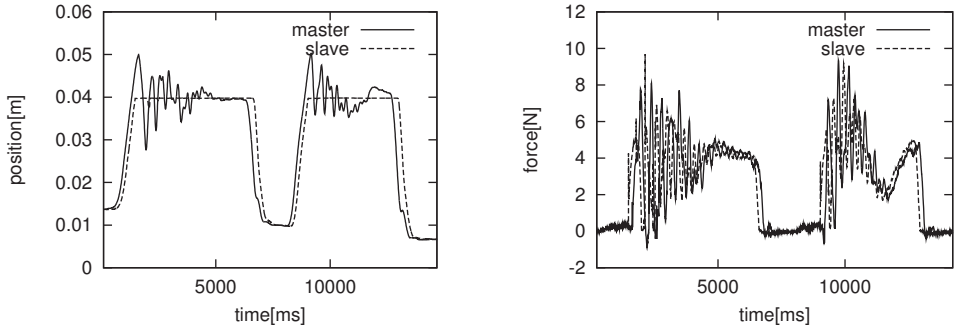

(a) Position response (b) Force response

Fig. 7-26: Contact motion with hard environment under constant delay (4ch ABC + CDOB)

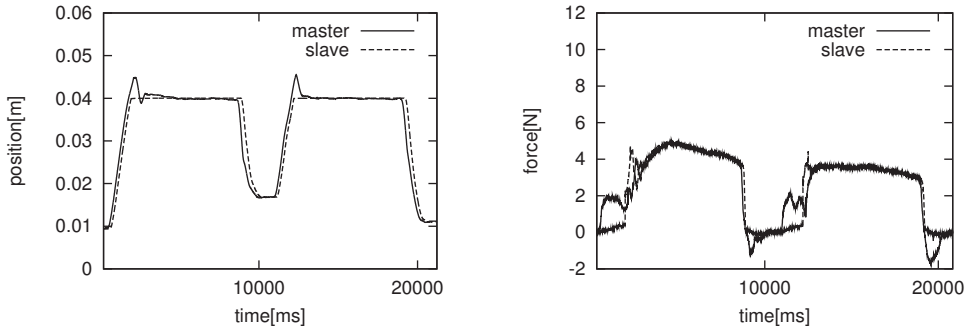

(a) Position response (b) Force response

Fig. 7-27: Contact motion with hard environment under constant delay (4ch ABC + CDOB + Damping)

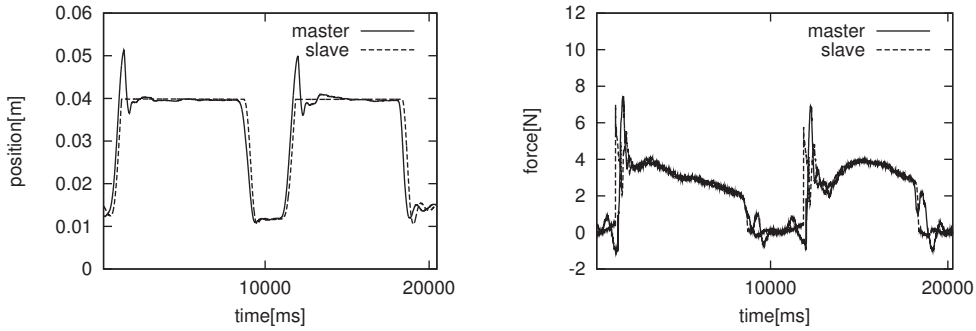

(a) Position response (b) Force response

Fig. 7-28: Contact motion with hard environment under constant delay (4ch ABC + CDOB + FDD)

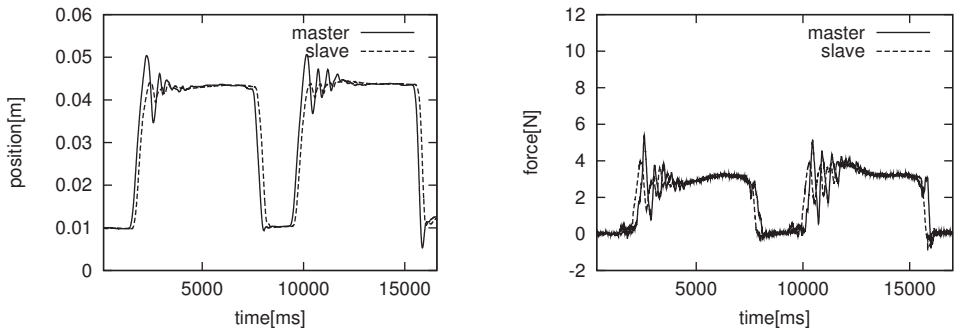

(a) Position response (b) Force response

Fig. 7-29: Contact motion with soft environment under constant delay (4ch ABC + CDOB)

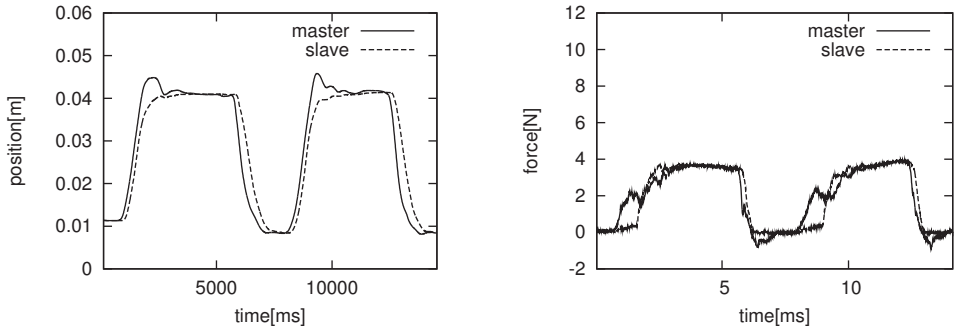

(a) Position response (b) Force response

Fig. 7-30: Contact motion with soft environment under constant delay (4ch ABC + CDOB + Damping)

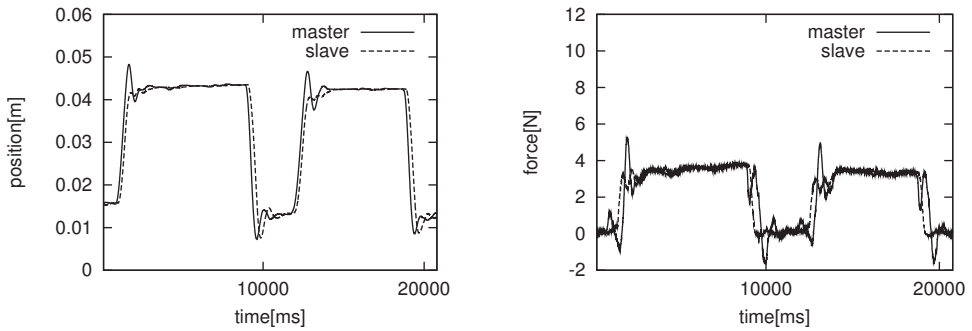

(a) Position response (b) Force response

Fig. 7-31: Contact motion with soft environment under constant delay (4ch ABC + CDOB + FDD)

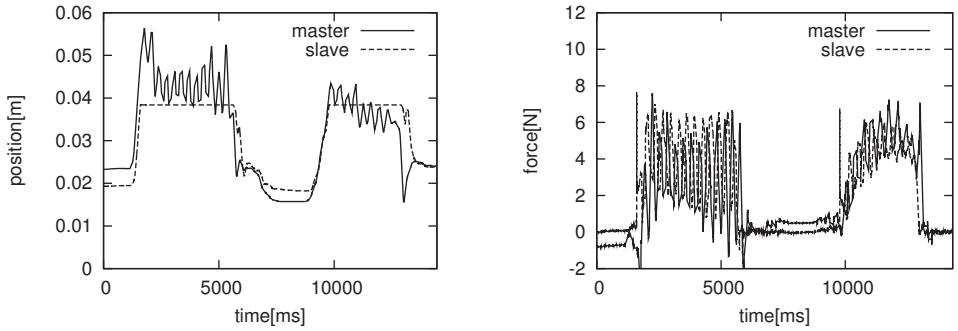

(a) Position response (b) Force response

Fig. 7-32: Contact motion with hard environment under time-varying delay (4ch ABC + CDOB)

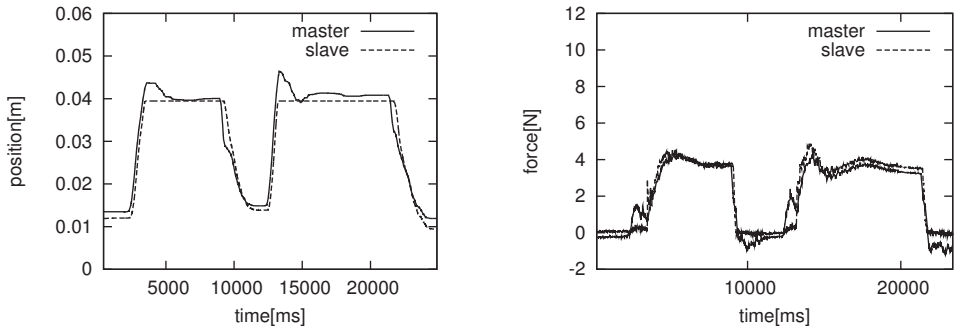

(a) Position response (b) Force response

Fig. 7-33: Contact motion with hard environment under time-varying delay (4ch ABC + CDOB + Damping)

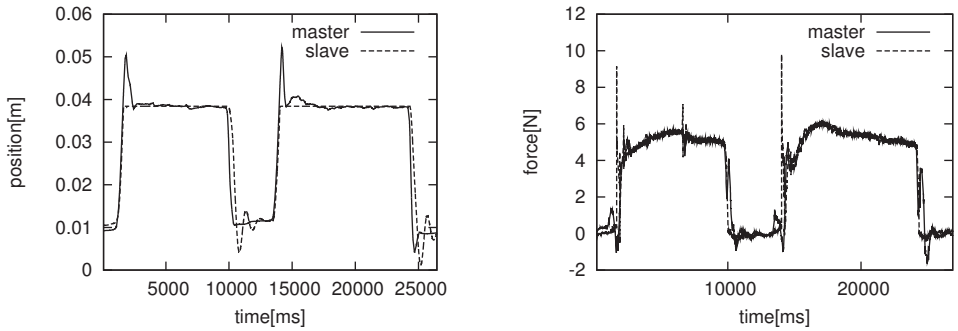

(a) Position response (b) Force response

Fig. 7-34: Contact motion with hard environment under time-varying delay (4ch ABC + CDOB + FDD)

Chapter 8

Novel 4ch ABC Design for Haptic Communication under Time Delay

8.1 Introduction

Chapter 8 introduces a novel 4ch ABC design for haptic communication under time delay. Time delay compensation by CDOB improves operationality from master side. However, time delay compensation by CDOB weakens position control of master robot. As a result, the symmetric property between master and slave is broken, and manipulation from slave side becomes impossible. To realize haptic communication between two operator, the perfect symmetric property between master and slave system is essential. Chapter 8 introduces a novel four-channel ABC architecture using two degrees of freedom proportional derivative (PD) control for haptic communication under time delay. In proposed 4ch ABC, the difference of position is controlled to be zero by P-D control (differential proactive PD control), and the sum of force is controlled to be zero by damping-injected force P control. Furthermore, frequency-domain damping design (FDD) is utilized to realize both high performance and stability based on delay-dependent robust H_∞ stability. Proposed 4ch ABC improves the stability of each modal space under time delay, keeping the symmetric property. The validity of the proposed control system is confirmed by some experimental results.

8.2 Architecture of Proposed Novel 4ch ABC

This section introduces a novel 4ch ABC architecture for stable haptic communication under time delay. Acceleration reference values of proposed 4ch ABC are described as follows. $C_p'(= K_p)$ is position P controller. Here C_{dm} means damping controller. Velocity control is changed to local velociy feedback. The block diagram of proposed 4ch ABC is shown as Fig. 8-1.

$$s^2 X_m^{ref} = s^2 X_m^{res} = C_p'(X_s e^{-T_2 s} - X_m) - C_f(\hat{F}_m + \hat{F}_s e^{-T_2 s}) - C_{dm} s X_m \tag{8.1}$$

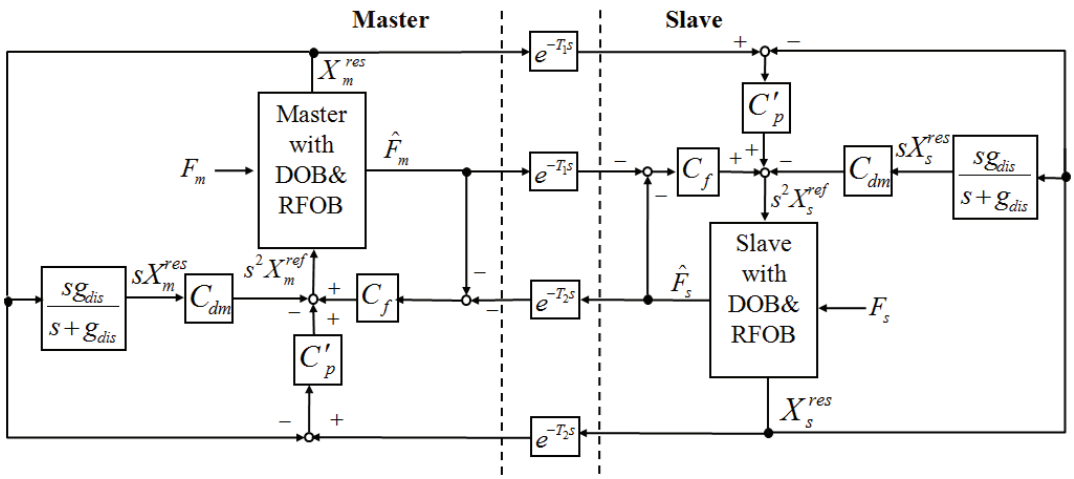

Fig. 8-1: Block diagram of the proposed novel 4ch ABC

$$s^2 X_s^{ref} = s^2 X_s^{res} = C_p'(X_m e^{-T_1 s} - X_s) - C_f(\hat{F}_m e^{-T_1 s} + \hat{F}_s) - C_{dm} s X_s \tag{8.2}$$

8.2.1 Position control (Proposed Novel 4ch ABC)

Position control of proposed 4ch ABC in differential modal space is given by subtracting (8.2) from (8.1) as follows.

$$s^2(X_m - X_s)^{res} = -C_p'(X_m - X_s)(1 + e^{-Ts}) - C_f(1 - e^{-Ts})(\hat{F}_m - \hat{F}_s) - C_{dm}(sX_m - sX_s) \tag{8.3}$$

Fig. 8-2 shows the block diagram of position control of proposed 4ch ABC in differential modal space. The position difference is controlled to be zero by P-D control (differential proactive PD control). In proposed 4ch ABC, velocity feedback is not affected by time delay e^{-Ts}. As a result, the stability is much more improved compared with conventional 4ch ABC.

8.2.2 Force control (Proposed Novel 4ch ABC)

Force control in common modal space is given by adding (8.1) and (8.2) as follows.

$$s^2(X_m + X_s)^{res} = -C_p'(X_m + X_s)(1 - e^{-Ts}) - C_f(1 + e^{-Ts})(\hat{F}_m + \hat{F}_s) - C_{dm}(sX_m + sX_s) \tag{8.4}$$

Fig. 8-3 shows the block diagram of force control in common modal space. Velocity damping loop is injected to the force control in common modal space. Damping injection improves the stability of force control. The stability of force control is also improved.

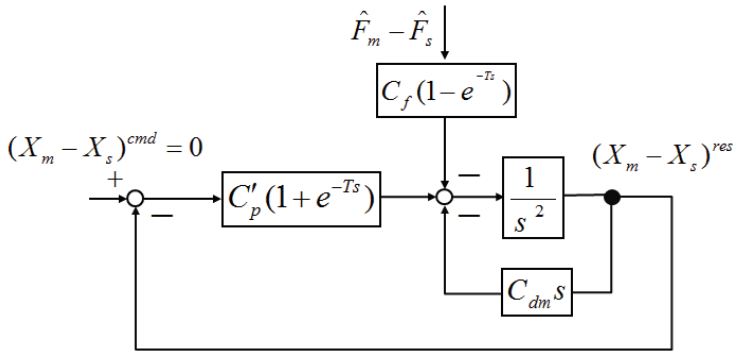

Fig. 8-2: Block diagram of position control in the differential modal space (proposed novel 4ch ABC)

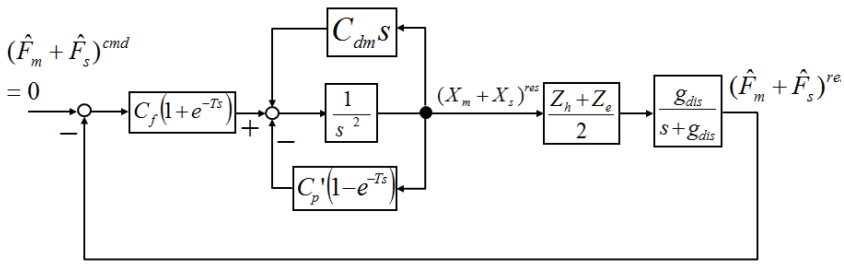

Fig. 8-3: Block diagram of force control in the common modal space (proposed novel 4ch ABC)

8.3 Frequency-Domain Damping Design (FDD)

Velocity damping by local velocity feedback improves the stability of each modal space. However, it deteriorates the performance of robust acceleration control. Damping injection changes plant model from $1/s^2$ to $1/s(s + C_{dm})$, so appropriate minimal amount of damping should be injected to keep high performance. To realize both high performance and stability, this section utilizes "frequency-domain damping design (FDD)". Appropriate frequency-domain damping injection is achieved by using loop-shaping high pass filter (HPF). The design of loop-shaping HPF and the damping gain are determined based on delay dependent robust H_∞ stability condition.

8.3.1 Concept of FDD

Damping controller C_{dm} is shown as follows. K_{fdd} is damping gain. g_h is cutoff frequency of HPF. ζ is damping ratio, and g_h is cutoff frequency of HPF.

$$C_{dm} = K_{fdd}\frac{s^2 + 2\zeta g_h s}{s^2 + 2\zeta g_h s + {g_h}^2} \tag{8.5}$$

The characteristic of time delay element e^{-Ts} in the frequency domain is described as follows.

$$|e^{-j\omega T}| = 1 \tag{8.6}$$

$$\angle e^{-j\omega T} = -\omega T \tag{8.7}$$

The time delay element e^{-Ts} delays the phase of any control system in proportion to frequency value ω. This means that the control system which has time delay element e^{-Ts} tends to become unstable in high frequency area. From this reason, this section proposes high damping injection only in high frequency area using HPF. This frequency-domain damping design (FDD) realizes high-performance and stable bilateral teleoperation system even under time delay.

8.3.2 Design of HPF for FDD

Here, the design of HPF for FDD is introduced. At first, the bode diagram of 1st order HPF and 2nd order HPF is compared. The transfer function of each HPF is shown as follows.

$$G_{1st\,HPF} = \frac{s}{s+g_h} \tag{8.8}$$

$$G_{2nd\,HPF} = \frac{s^2}{s^2+2\zeta g_h s+{g_h}^2} \tag{8.9}$$

Bode diagram of each HPF is shown as Fig. 8-4. Fig. 8-4(a) shows that the gain characteristic of 2nd order HPF is better than that of 1st order HPF. However, Fig. 8-4(b) shows that 2nd order HPF leads phase too much. To prepare an appropriate HPF for FDD, this section injects 2nd order BPF(band pass filter) to 2nd order HPF. The injection of BPF mitigates the rapid phase change around g_h. The transfer function of proposed HPF(2nd order HPF + 2nd order BPF) is described as follows.

$$\begin{aligned} G_{HPF} &= \underbrace{\frac{s^2}{s^2+2\zeta g_h s+{g_h}^2}}_{2nd\,HPF} + \underbrace{\frac{2\zeta g_h s}{s^2+2\zeta g_h s+{g_h}^2}}_{2nd\,BPF} \\ &= \frac{s^2+2\zeta g_h s}{s^2+2\zeta g_h s+{g_h}^2} \end{aligned} \tag{8.10}$$

Bode diagram of proposed HPF is shown as Fig. 8-5. As for gain characteristic, the gain characteristic of proposed HPF(2nd order HPF + 2nd order BPF) is better than that of 1st order HPF. As for phase characteristic, phase change around g_h is mitigated compared with 2nd order HPF. From this analysis, it is clear that proposed HPF is appropriate for FDD.

8.3.3 Determination of parameters based on delay dependent robust H_∞ stability condition

The block diagram of differential modal space is transformed into Fig. 8-6. Fig. 8-6 is multiplicative representation of time delay effect on differential modal space. The dotted part is regarded as the nominal

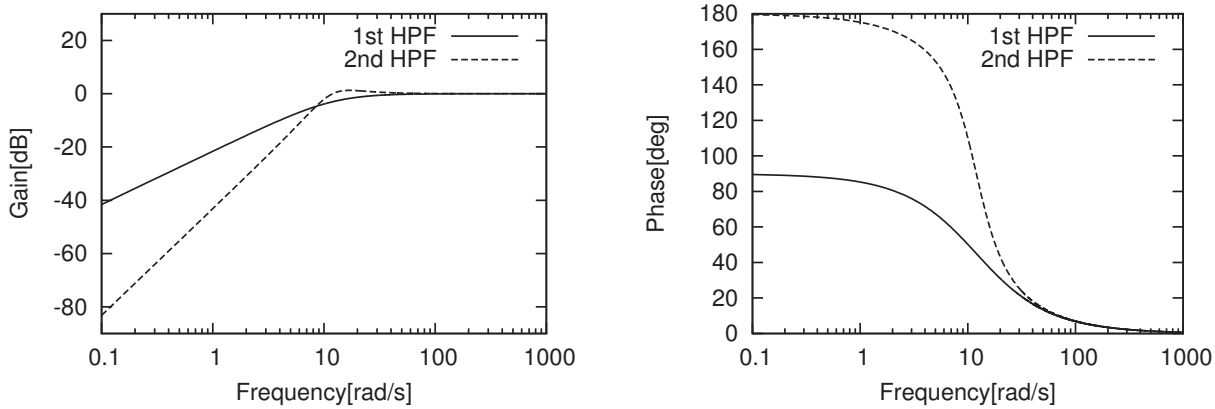

(a) Gain (b) Phase

Fig. 8-4: Bode diagram of 1st order and 2nd order HPF

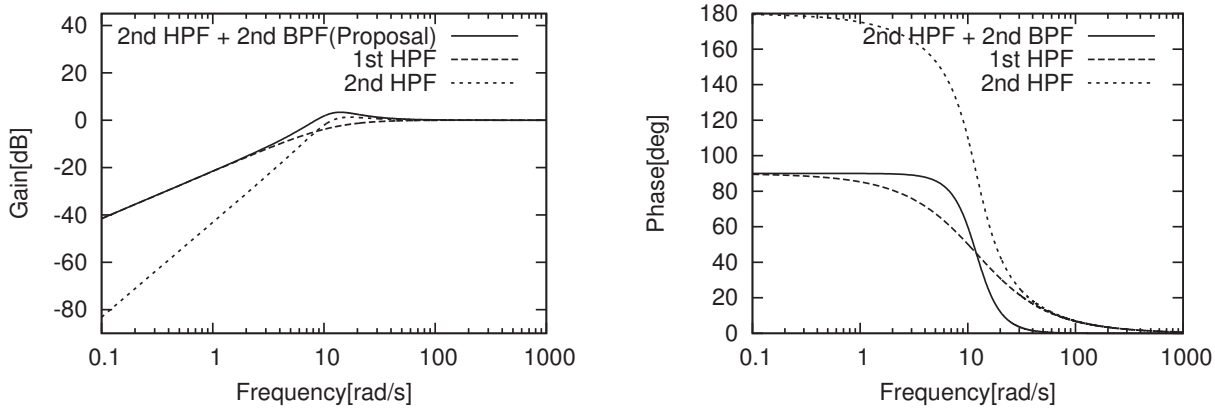

(a) Gain (b) Phase

Fig. 8-5: Bode diagram of the proposed HPF (2nd order HPF + 2nd order BPF)

open-loop transfer function of differential modal space L_{dn}. The multiplicative uncertainty is represented by weighting function $W(s)$ as follows. $\Delta(s)$ shows uncertainty.

$$\frac{e^{-Ts}-1}{2} = W(s)\Delta(s), \quad |\Delta(j\omega)| < 1, \ \forall w \tag{8.11}$$

The transfer function of $W(s)$ is described as follows. $W(s)$ is designed to cover time delay uncertainty as tightly as possible for improvement of performance. In this section, maximum delay time is set at 120 ms. $W(s)$ is designed to cover time delay uncertainty as tightly as possible for improvement of performance.

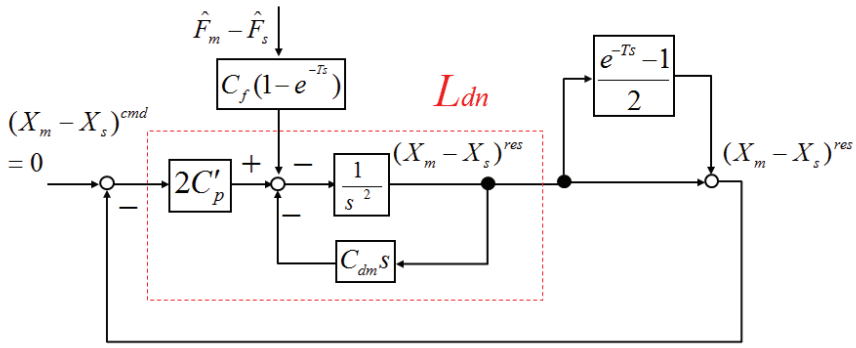

Fig. 8-6: Multiplicative representation of time delay effect on the differential modal space

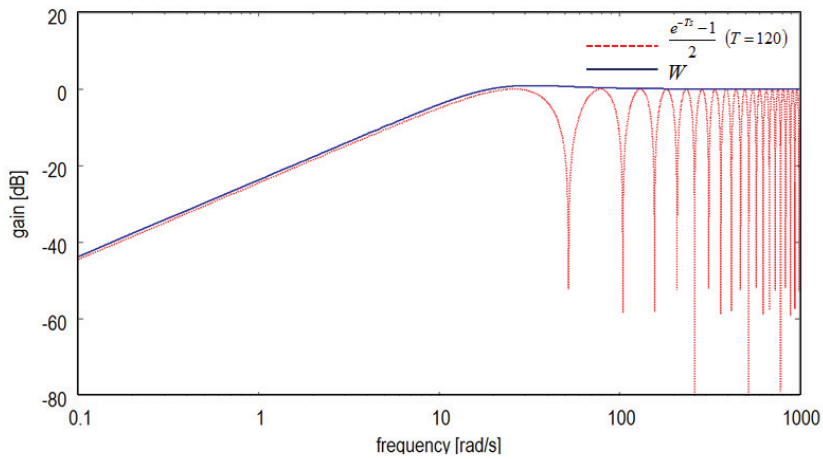

Fig. 8-7: Bode diagram of the weighting function

$$W(s) = \frac{(s^2 + 35s)(s + 22)}{(s^2 + 35s + 435)(s + 27)} \tag{8.12}$$

The gain characteristic of $W(s)$ is shown as Fig. 8-7. The time delay uncertainty under 120 ms is tightly-covered with the weighting function in all frequency area. By using $W(s)$, Fig. 8-6 is transformed into Fig. 8-8. The design objective is to minimize the weighted complementary sensitivity function (nominal closed-loop transfer function) of differential modal space $T_d = L_{dn}/(1 + L_{dn})$. The robust stability condition of differential modal space is as follows.

$$\begin{aligned} ||W(s)T_d(s)||_\infty &< 1 \\ \Leftrightarrow |W(j\omega)T_d(j\omega)| &< 1, \ \forall w \end{aligned} \tag{8.13}$$

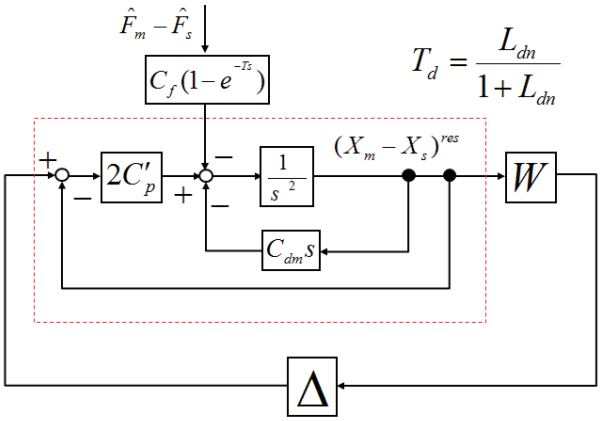

Fig. 8-8: Block diagram of robust stability condition in the differential modal space

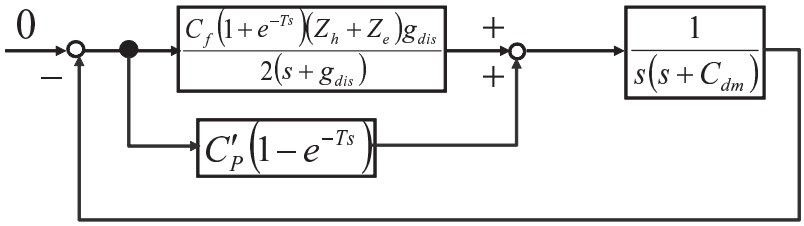

Fig. 8-9: Block diagram of the common modal space (version II)

On the other hand, it is difficult to introduce the robust stability condition of force control in common modal space, because there are two time delay elements in the feedback loop. The block diagram of force control is transformed as in Figs. 8-3, and 8-9 ∼ 8-11. Fig. 8-10 is multiplicative representation of time delay effect on common modal space. In Fig. 8-10, two transfer functions are defined as follows.

$$G_{c1} = \frac{C_f(Z_h+Z_e)g_{dis}}{s(s+g_{dis})(s+C_{dm})} \tag{8.14}$$

$$G_{c2} = \frac{C_f(Z_h+Z_e)g_{dis} - 2C'_p(s+g_{dis})}{C_f(Z_h+Z_e)g_{dis}} \tag{8.15}$$

Finally, Fig. 8-10 is equivalently transformed into Fig. 8-11. The robust stability condition of common modal space is as follows.

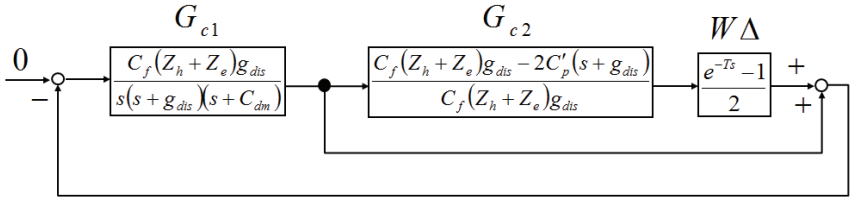

Fig. 8-10: Block diagram of the common modal space (version III)

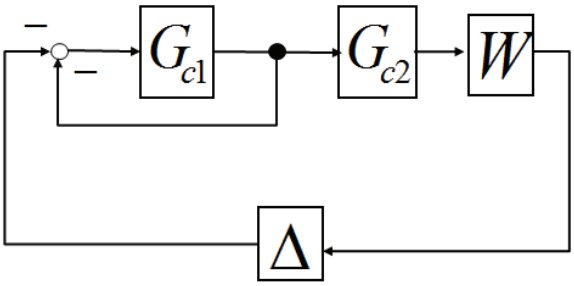

Fig. 8-11: Block diagram of the robust stability condition in the common modal space

$$
\begin{aligned}
&||\frac{G_{c1}(s)G_{c2}(s)W(s)}{1+G_{c1}(s)}||_\infty &< \quad 1 \\
\Leftrightarrow &|\frac{G_{c1}(j\omega)G_{c2}(j\omega)W(j\omega)}{1+G_{c1}(j\omega)}| &< \quad 1, \ \forall\omega
\end{aligned}
\tag{8.16}
$$

ABC consists of position control and force control in two orthogonally-crossed modal spaces independently. Hence, satisfying the stability conditions of two modal spaces ensures the stability of the whole ABC system. The robust stability condition of the whole ABC system is as follows.

$$
\begin{cases}
||W(s)T_d(s)||_\infty < 1 \\
||\frac{G_{c1}(s)G_{c2}(s)W(s)}{1+G_{c1}(s)}||_\infty < 1
\end{cases}
$$

$$
\Leftrightarrow \begin{cases}
|W(j\omega)T_d(j\omega)| < 1, \ \forall\omega \\
|\frac{G_{c1}(j\omega)G_{c2}(j\omega)W(j\omega)}{1+G_{c1}(j\omega)}| < 1, \ \forall\omega
\end{cases}
\tag{8.17}
$$

To satisfy (8-17), K_{fdd} is set at 65, and cutoff frequency of HPF g_h is set at 12.56 rad/s, and other parameters are shown in Table 8-1. Then the robust stability condition is satisfied as like Fig. 8-12. Each gain characteristic is smaller than 1(=0 dB). However, if the maximum delay time is set at more than

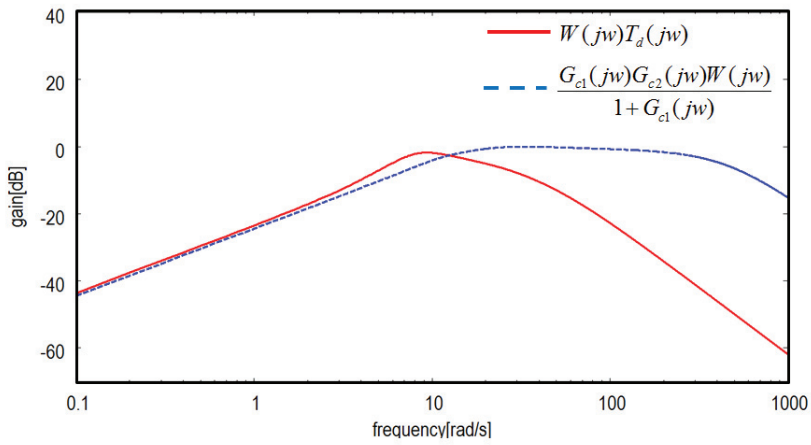

Fig. 8-12: Satisfaction of robust stability

Table 8-1: Parameters of analysis

Parameter	Meaning	Value
T	Time delay(one way)	120[ms]
K_p	Position gain	400
K_v	Velocity gain	65
K_f	Force gain	1.0
K_{fdd}	Damping gain of FDD	65
g_h	Cutoff frequency of HPF	12.56[rad/s]
ζ	Damping ratio of HPF	0.5
g_{dis}	Cutoff frequency of DOB	800[rad/s]
Z_h	Impedance of human	1000+200s[N/m]
Z_e	Impedance of environment	9000+100s[N/m]
M_n	Nominal inertia of motor	0.5[kg]
K_{tn}	Thrust coefficient	22.0[N/A]
st	Sampling time	0.1[ms]

120 ms, the cutoff frequency g_h should be modified smaller than 12.56 rad/s, and the other parameters might need some adjustment to satisfy the robust stability condition. Table 8-2 shows the corresponding parameter values of g_h and K_{fdd} to other time delay cases. T_{max} means the maximum delay time.

Table 8-2: Corresponding parameters to other time delay cases

T_{max}[ms]	g_h[rad/s]	K_{fdd}
120	12.56	65
150	9.0	145
200	6.0	280

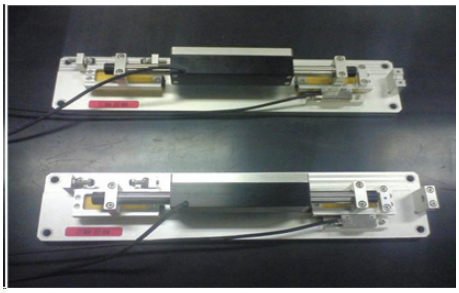

(a) Two linear motors

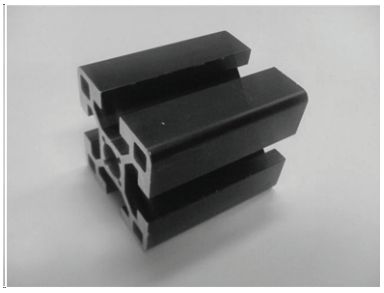

(b) Hard environment (aluminium)

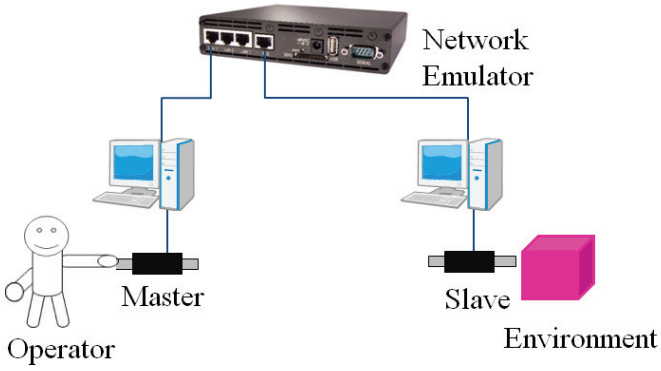

(c) Overview of experimental system

Fig. 8-13: Experimental system

8.4 Experiments

Fig. 8-13 shows the experimental system. The master and slave system consists of 1-DOF robots. The robots consist of linear motors and position encoders. Proposed novel 4ch ABC and conventional 4ch ABC are compared. Time delay is varying by linear jitter produced by network emulator. Central value is 100 ms, and jitter value is + - 20 ms. Other experimental parameters are set as Table 8-1.

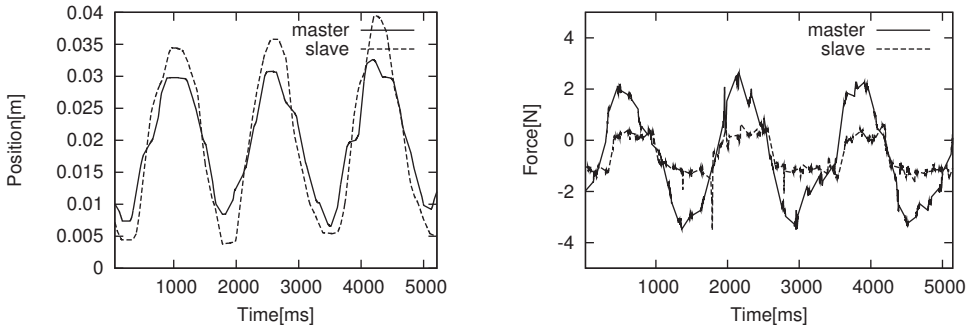

(a) Position response (b) Force response

Fig. 8-14: Free motion (conventional 4ch ABC)

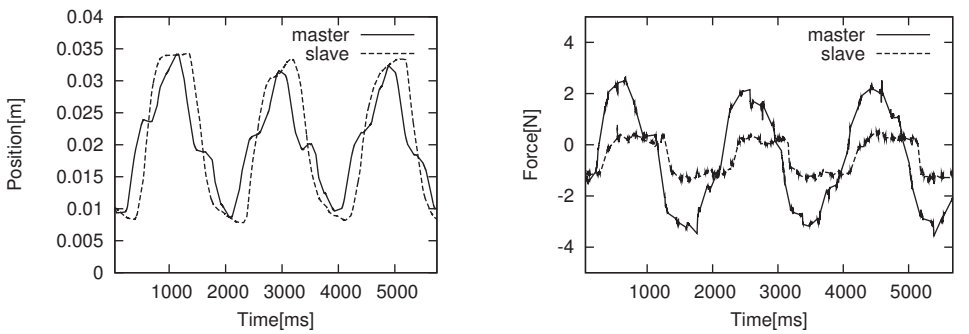

(a) Position response (b) Force response

Fig. 8-15: Free motion (proposed novel 4ch ABC)

8.4.1 Free motion

Experiment in free motion is implemented. The operator handles master robot with back-and-forth motion. The experimental results of free motion are shown in Fig. 8-14 and Fig. 8-15. Overshoot and position error in go-back motion is outstanding with conventional 4ch ABC. On the other hand, proposed 4ch ABC suppresses overshoot and position error well. These results show that proposed novel position control is more stable than conventional position control.

8.4.2 Contact motion

The experimental results of contact motion with hard environment are shown in Fig. 8-16 and Fig. 8-17. Both controllers realize stable contact motions. In conventional 4ch ABC, shown as Fig. 3-8, position controller C_p makes minor negative feedback loop, and it improves the stability as spring and damping injection. On the other hand, in proposed novel 4ch ABC, the negative feedback loop by FDD improves the stability shown as Fig. 8-3.

8.4.3 Push motion with each other

Fig. 8-18 shows the result of push motion between two operator as an example of haptic communication under time delay. A stable push motion is realized with proposed 4ch ABC even under time delay. Proposed 4ch ABC realizes stable haptic communication under time delay.

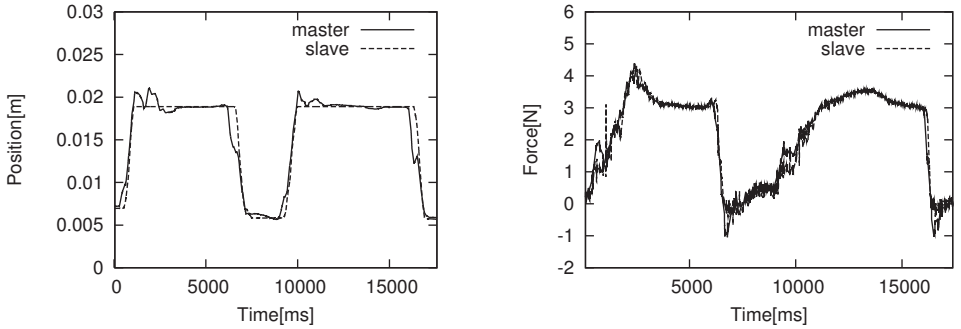

(a) Position response (b) Force response

Fig. 8-16: Contact motion with hard environment (conventional 4ch ABC)

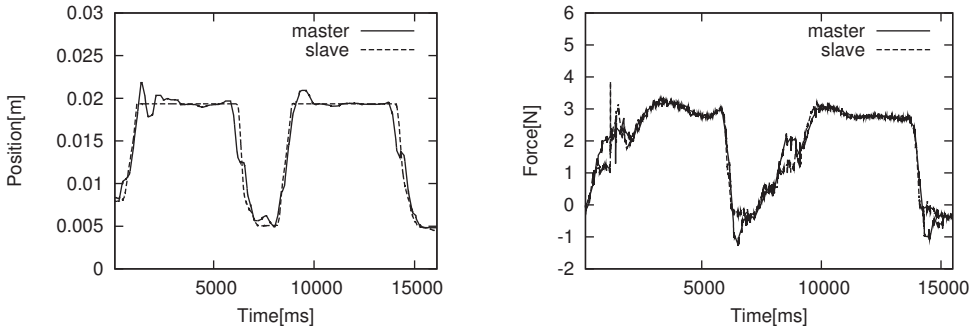

(a) Position response (b) Force response

Fig. 8-17: Contact motion with hard environment (proposed novel 4ch ABC)

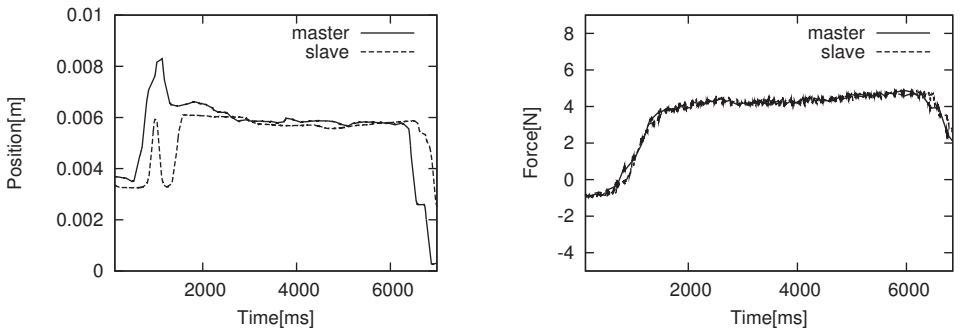

(a) Position response (b) Force response

Fig. 8-18: Push motion with each other (proposed novel 4ch ABC)

8.5 Summary

This chapter proposed a novel four-channel ABC architecture for haptic communication under time delay. In proposed 4ch ABC, the difference of position was controlled to be zero by P-D control(differential proactive PD control), and the sum of force was controlled to be zero by P control with damping injection. Proposed 4ch ABC improved the stability of each modal space, and suppressed overshoot between master and slave robot. The validity of the proposed control system was confirmed by some experimental results.

Chapter 9

New Design of CDOB for Haptic Communication under Time Delay

9.1 Introduction

In addition to novel 4ch ABC system in chapter 8, This chapter proposes a new design of communication disturbance observer (CDOB) for haptic communication with bilateral control. Proposed new CDOB works time delay compensation only in high frequency area. Furthermore, proposed ABC system with new CDOB works time delay compensation on both master and slave robot. Proposed ABC system realizes much further stable and high-performance haptic communication even under time delay. The validity of proposed system is demonstrated experimentally.

9.2 New Design of CDOB Based on Frequency-domain ND Characteristic

This section proposes a new design of CDOB based on frequency-domain ND characteristic.

9.2.1 Frequency-domain characteristic of ND

CDOB regards the effect of time delay on communication line as ND in force dimension. The concept of ND is shown as Fig. 9-1. ND in steady state is described as (9.1) on the assumption that F^{ref} is constant value.

$$\lim_{s \to 0} F^{ref}(1 - e^{-Ts}) = 0 \tag{9.1}$$

(9.1) shows that the effect of ND is very little in low frequency area. Furthermore, the property of time delay element is described as follows.

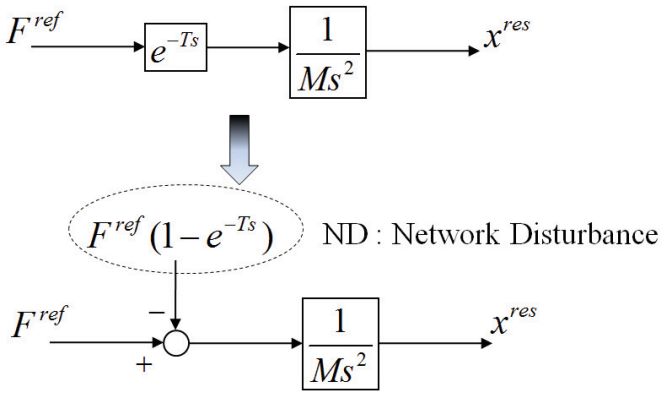

Fig. 9-1: Concept of network disturbance (ND

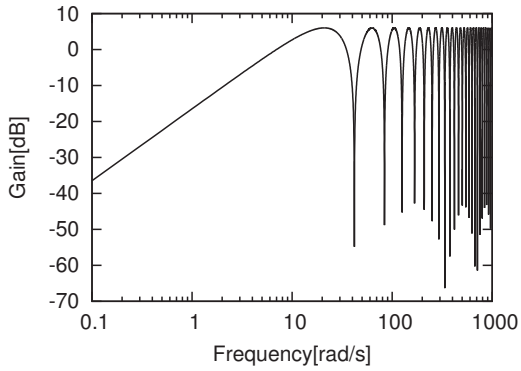

Fig. 9-2: Frequency-domain characteristic of ND

$$|e^{-j\omega T}| = 1 \tag{9.2}$$

$$\angle e^{-j\omega T} = -\omega T \tag{9.3}$$

Phase delay caused by e^{-Ts} is proportional to frequency value ω. Bode diagram of ND is shown as Fig. 9-2 on the assumption that F^{ref} is constant value (=1.0). ND becomes large as frequency value gets large. On the other hand, ND is almost nothing in low frequency area.

9.2.2 New design of CDOB

Based on the frequency-domain characteristic of ND, this section proposes a new design of CDOB. Fig. 9-3 is the block diagram of new design of CDOB using loop-shaping HPF. Input values are force reference and time-delayed velocity response. LPF is utilized to cut the sensing noise. ND is extracted through loop-shaping HPF. G_{HPF} means the transfer function of loop-shaping HPF in new CDOB. Time delay compensation is worked only in high frequency area to realize both good performance and stability.

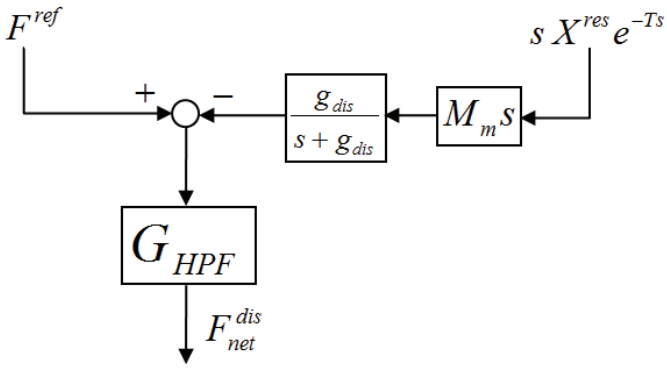

Fig. 9-3: New design of CDOB using shaping HPF

9.3 4ch ABC with Proposed New CDOB

This section explains the structure of 4ch ABC with new CDOB. Proposed ABC system works time delay compensation on both master and slave robot as Fig. 9-4. In this section, posititon P controller $C_p'(= K_p)$ is utilized to reduce overshoot compared with position PD controller $C_p(= K_p + sK_v)$

9.3.1 Structure of new CDOB in ABC system

Structure of new CDOB in 4ch ABC is shown as Fig. 9-5. Acceleration reference of master and slave robot in 4ch ABC with new CDOB are as follows.

$$s^2X_m^{ref} = s^2X_m^{res} = C_p'(X_se^{-T_2s} - X_m + X_s^{cmp}) - C_f(\hat{F}_m + \hat{F}_se^{-T_2s}) \tag{9.4}$$

$$s^2X_s^{ref} = s^2X_s^{res} = C_p'(X_me^{-T_1s} - X_s + X_m^{cmp}) - C_f(\hat{F}_me^{-T_1s} + \hat{F}_s) \tag{9.5}$$

Estimated ND in master side is described as follows.

$$\hat{D}_{net} = G_{HPF}(M_ns^2X_{sm} - \frac{g_{dis}}{s+g_{dis}}M_ns^2X_s^{res}e^{-T_2s}) \tag{9.6}$$

If the cutoff frequency of LPF g_{dis} is large enough, (9.6) is changed as follows.

$$\hat{D}_{net} = G_{HPF}(M_ns^2X_{sm} - M_ns^2X_s^{res}e^{-T_2s}) \tag{9.7}$$

Then compensation value is shown as follows.

$$\begin{aligned} X_s^{cmp} &= \frac{1}{M_ns^2}\hat{D}_{net} \\ &= G_{HPF}(X_{sm} - X_se^{-T_2s}) \end{aligned} \tag{9.8}$$

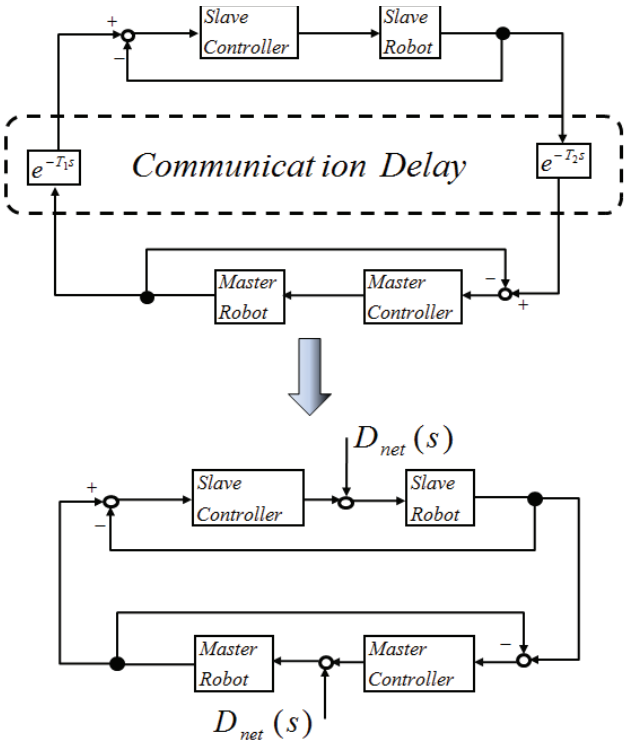

Fig. 9-4: Time delay compensation in the proposed 4ch ABC system

The acceleration reference value of master robot with compensation is shown as follows.

$$\begin{aligned} s^2 X_m^{ref} = s^2 X_m^{res} &= C_p'(X_s e^{-T_2 s} + X_s^{cmp} - X_m) - C_f(\hat{F}_m + \hat{F}_s e^{-T_2 s}) \\ &= C_p'\{(1 - G_{HPF}) X_s e^{-T_2 s} + G_{HPF} X_{sm} - X_m\} \\ &- C_f(\hat{F}_m + \hat{F}_s e^{-T_2 s}) \end{aligned} \tag{9.9}$$

The acceleration response value of slave model is shown as follows.

$$s^2 X_{sm}^{res} = C_p'(X_m - X_{sm}) \tag{9.10}$$

(9.10) is changed to as follows.

$$\begin{aligned} X_{sm} &= \frac{C_p'}{C_p' + s^2} X_m \\ &\cong X_m \end{aligned} \tag{9.11}$$

If (9.11) is substituted to (9.9), (9.9) is changed to as follows.

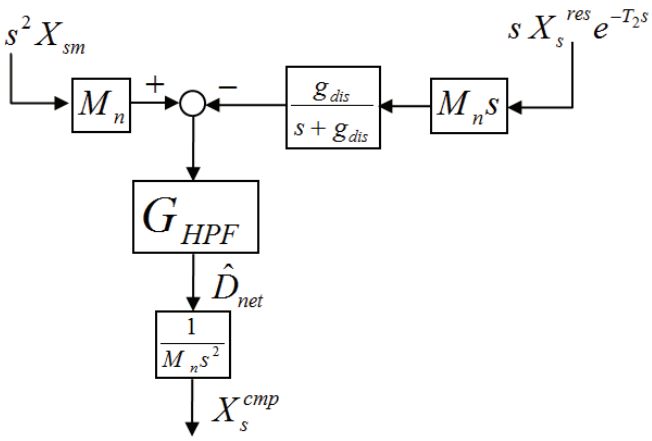

Fig. 9-5: Structure of new CDOB in 4ch ABC system

$$s^2 X_m^{ref} = s^2 X_m^{res} = C_p' \underbrace{(1 - G_{HPF})}_{G_{LPF}} (X_s e^{-T_2 s} - X_m) - C_f(\hat{F}_m + \hat{F}_s e^{-T_2 s}) \tag{9.12}$$

(9.12) shows that position control works only in low frequency area by time delay compensation in high frequency area due to the proposed new CDOB. Here, the transfer function of loop-shaping LPF was defined as follows.

$$G_{LPF} = 1 - G_{HPF} \tag{9.13}$$

By the similar procedure of compensation, The acceleration response value of slave robot is shown as follows.

$$s^2 X_s^{res} = C_p' \underbrace{(1 - G_{HPF})}_{G_{LPF}} (X_m e^{-T_1 s} - X_s) - C_f(\hat{F}_s + \hat{F}_m e^{-T_1 s}) \tag{9.14}$$

9.3.2 Design of loop-shaping HPF based on robust stability of differential modal space

By the difference of (9.12) and (9.14), the acceleration response of position control in differential modal space is described as follows.

$$s^2 (X_m - X_s)^{res} = -C_p'(X_m - X_s)(1 - G_{HPF})(1 + e^{-Ts}) - C_f(1 - e^{-Ts})(\hat{F}_m - \hat{F}_s) \tag{9.15}$$

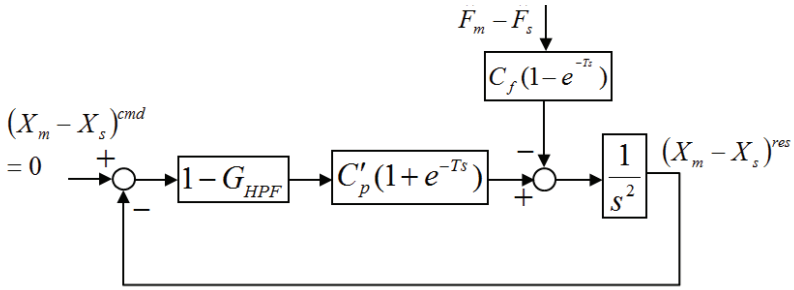

Fig. 9-6: Position control in differential modal space (4ch ABC + New CDOB)

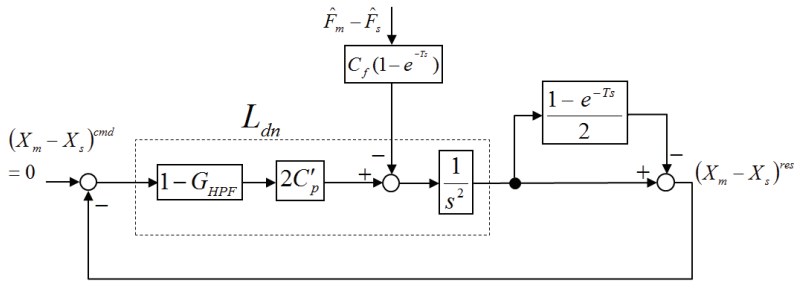

Fig. 9-7: Multiplicative representation of time delay effect in differential modal space

The block diagram of (9.15) is shown as Fig. 9-6. The multiplicative representation of Fig. 9-6 is shown as Fig. 9-7. The dotted part is regarded as the nominal open-loop transfer function of differential modal space L_{dn}. Parameter values are shown as Table 9-1. The multiplicative uncertainty of time delay is represented by the weighting function $W(s)$ as follows , where $\Delta(s)$ shows uncertainty.

$$\frac{1-e^{-Ts}}{2} = W(s)\Delta(s), \quad |\Delta(j\omega)| < 1, \ \forall\omega \tag{9.16}$$

Weighting function $W(s)$ is shown as follows. Bode diagram is shown as Fig. 9-8.

$$W(s) = \frac{11s(s+36)(s+17)}{10(s^2+36s+400)(s+20)} \tag{9.17}$$

The time delay uncertainty under 150 ms is tightly-covered with the weighting function in all frequency area. Furthermore, Fig. 9-7 is equivalently transformed into Fig. 9-9. The design objective is to minimize the weighted complementary sensitivity function (nominal closed-loop transfer function) $T_d = L_{dn}/(1+L_{dn})$. The robust stability condition is as follows.

$$\begin{aligned} ||W(s)T_d(s)||_\infty &< 1 \\ \Leftrightarrow |W(j\omega)T_d(j\omega)| &< 1, \ \forall\omega \end{aligned} \tag{9.18}$$

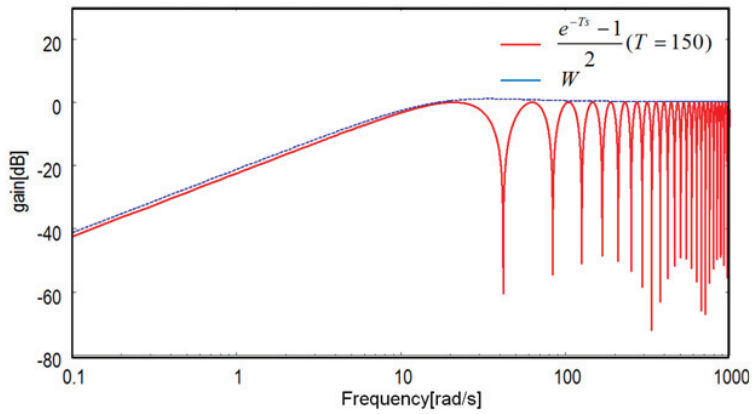

Fig. 9-8: Bode diagram of weighting function

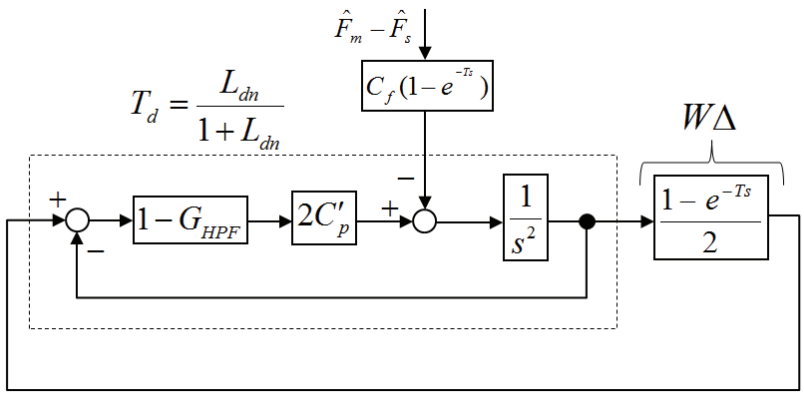

Fig. 9-9: Robust stability condition of position control in differential modal space

In addition, according to the performance condition, the gain-crossover frequency of open-loop transfer function ω_{gc_d} should be larger than 12.56 rad/s (= 2.0Hz). ω_{gc_d} means position control bandwidth. 12.56 rad/s (= 2.0Hz) means the usual frequency of human manipulation.

$$\omega_{gc\_d} \geq 12.56[rad/s] \tag{9.19}$$

To satisfy (9.18) and (9.19), position P gain K_p is set at 400. On the other hand, the transfer function of loop-shaping HPF is determined from the inverse calculation of the transfer function of loop-shaping LPF. the transfer function of loop-shaping LPF is described as follows.

Table 9-1: Parameters in analysis and experiment

Parameter	Meaning	Value
T	Time delay(one way)	50 $\sim$ 150[ms]
K_p	Position gain	400
K_v	Velocity gain	40
K_f	Force gain	1.0
g_{dis}	Cutoff frequency of DOB(RFOB)	1000[rad/s]
M_n	Nominal mass of motor	0.5[kg]
K_{tn}	Nominal Force coefficient	22.0[N/A]
st	Sampling time	0.1[ms]
Z_e	Impedance of environment	10000+10s
Z_h	Impedance of human	1000+100s
M_n	Nominal inertia of motor	0.5[kg]
K_{tn}	Thrust coefficient	22.0[Nm/A]
st	Sampling time	0.1[ms]
g_{fdd}	Cutoff frequency of FDD	11[rad/s]
K_{fdd}	Damping gain of FDD	250
g_{net}	Cutoff frequency of New CDOB	100[rad/s]

$$G_{LPF} = 1 - G_{HPF} = \underbrace{\frac{g_{net}}{s + g_{net}}}_{1st\ LPF} \underbrace{\frac{1 + \frac{1}{15}s}{1 + \frac{1}{5}s}}_{phase\ lag} \tag{9.20}$$

(9.20) shows that proposed loop-shaping LPF consists of 1st order LPF and phase lag compensator. The cutoff frequency of 1st order LPF g_{net} determines the position control bandwidth. On the other hand, phase lag compensator reduces the gain value in high frequency area, and the stability is improved. Bode diagram of phase lag compensator is shown as Fig. 9-10. Fig. 9-10 shows that gain values decreases in high frequency area above 5.0 rad/s. The gain value becomes 0.5 times at 10.0 rad/s, and becomes 0.3 times at 15.0 rad/s, so the weakend frequency area around 10 rad/s which tends to become unstable is stabilized by phase lag compensator. On the other hand, g_{net} of 1st-order LPF determines position control bandwidth and robust stability, and set at 100 rad/s. Parameter values of loop-shaping LPF are determined experimentally and regardless of time delay value. Bode diagram of the proposed loop-shaping LPF compared with conventional 1st order LPF is shown as Fig. 9-11. The gain value of proposed loop-shaping LPF becomes small from 5.0 rad/s slowly. The transfer function of loop-shaping HPF is inversely calculted as follows.

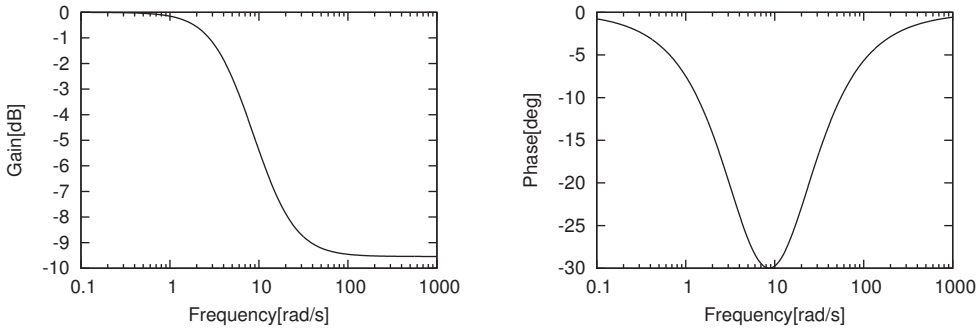

(a) Gain (b) Phase

Fig. 9-10: Bode diagram of phase lag compensator

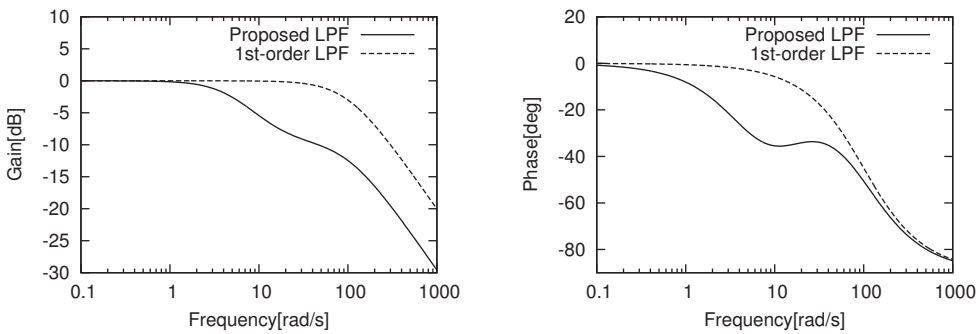

(a) Gain (b) Phase

Fig. 9-11: Bode diagram of proposed loop-shaping LPF

$$
\begin{aligned}
G_{HPF} &= 1 - G_{LPF} = 1 - \frac{g_{net}}{s + g_{net}} \frac{1 + \frac{1}{15}s}{1 + \frac{1}{5}s} \\
&= \frac{s(3s + 2g_{net} + 15)}{3(s+5)(s+g_{net})}
\end{aligned}
\tag{9.21}
$$

Bode diagram of proposed loop-shaping HPF compared with conventional 1st-order HPF is shown as Fig.9-12. Fig. 9-12 shows that phase lead of proposed HPF is mitigated better than that of conventional 1st order HPF, and the cutoff frequency is 5.0 rad/s.

Fig. 9-13 shows the H_∞ norm of position control in differential modal space. The H_∞ norm of 4ch ABC with new CDOB makes high frequency gain small, so the robust stability is improved by time delay compensation by new CDOB. In addition, Fig. 9-14 shows Bode diagram of the open-loop transfer function of 4ch ABC + New CDOB system. gain-crossover frequency ω_{gc_d} is larger than 12.56 rad/s, so 4ch ABC with new CDOB system satisfies the target position control bandwidth.

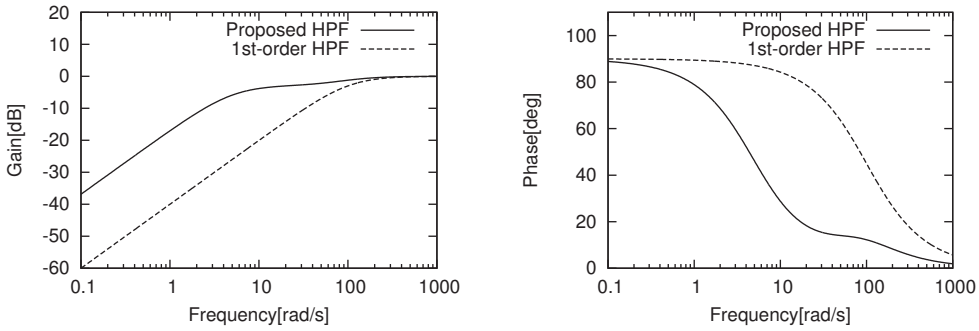

(a) Gain (b) Phase

Fig. 9-12: Bode diagram of proposed loop-shaping HPF

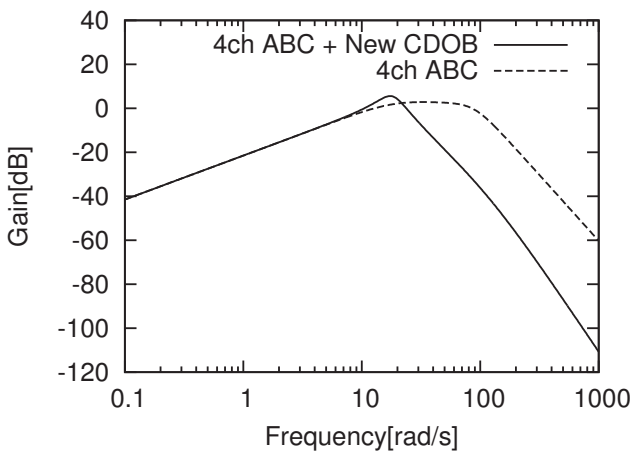

Fig. 9-13: H_∞ norm of differential modal space (4ch ABC + New CDOB)

9.4 Frequency-domain Damping Design (FDD)

Time delay compensation by new CDOB stabilizes the positon control in differential modal space. However, another solution method is essential to improve the stability of force control. This section proposes frequency-domain damping design (FDD) to satisfy robust stability of force control in common modal space while retaining good reproducibility and operationality in the low frequency area.

9.4.1 Concept of FDD

Damping controller C_{dm} is shown as follows. K_{fdd} is the gain of FDD. G_{hpf} is the transfer function of HPF in FDD.

$$C_{dm} = K_{fdd} G_{hpf} \tag{9.22}$$

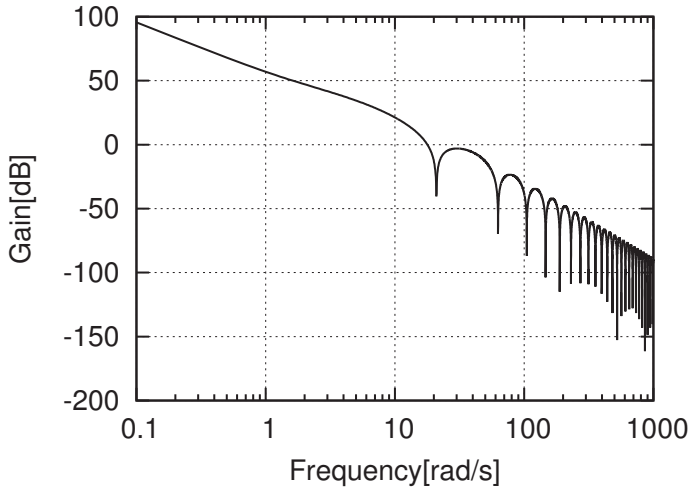

Fig. 9-14: Bode diagram of Open-loop transfer function

The acceleration response values of proposed ABC system (4ch ABC + New CDOB + FDD) are given by the following equations.

$$s^2 X_m^{ref} = s^2 X_m^{res} = C_p \underbrace{(1 - G_{HPF})}_{G_{LPF}} (X_s e^{-T_2 s} - X_m) - C_f(\hat{F}_m + \hat{F}_s e^{-T_2 s}) - C_{dm} s X_m \quad (9.23)$$

$$s^2 X_s^{ref} = s^2 X_s^{res} = C_p \underbrace{(1 - G_{HPF})}_{G_{LPF}} (X_m e^{-T_1 s} - X_s) - C_f(\hat{F}_m e^{-T_1 s} + \hat{F}_s) - C_{dm} s X_s \quad (9.24)$$

The characteristic of time delay element e^{-Ts} in the frequency domain is described as follows.

$$|e^{-j\omega T}| = 1 \quad (9.25)$$

$$\angle e^{-j\omega T} = -\omega T \quad (9.26)$$

Time delay element e^{-Ts} delays the phase of any control system in proportion to frequency value ω. This means that the control system which has time delay element e^{-Ts} tends to become unstable in high frequency area. From this reason, this section proposes high damping injection only in high frequency area using loop-shaping HPF to suppress only the high frequency oscillations in contact motion. FDD realizes a high-performance and stable bilateral teleoperation system under time delay. The block diagram of proposed system is shown as Fig. 9-16. Force control in common modal space is given by adding (9.23) and (9.24) as follows.

$$s^2(X_m + X_s)^{res} = -(1 - G_{HPF}) C_p'(X_m + X_s)(1 - e^{-Ts}) - C_f(1 + e^{-Ts})(\hat{F_m} + \hat{F_s}) \\ -C_{dm}(sX_m + sX_s) \quad (9.27)$$

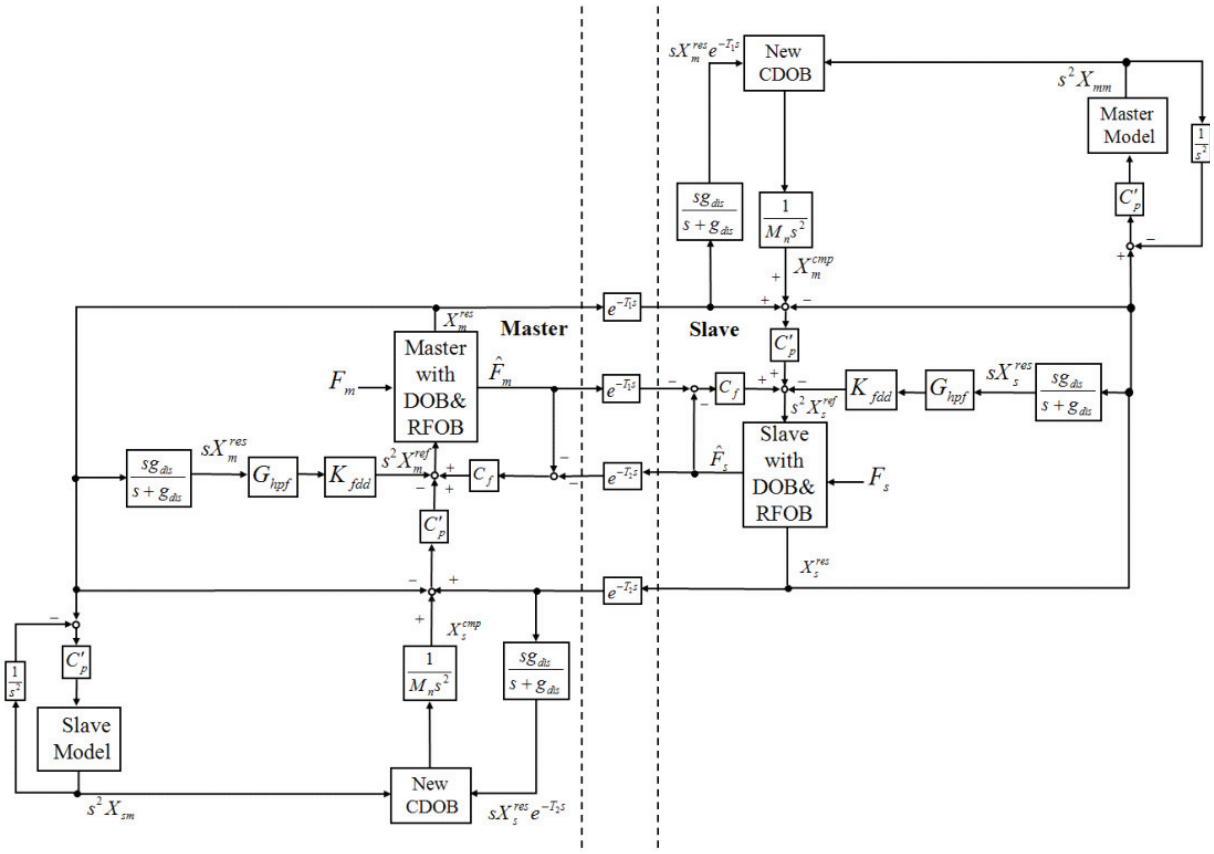

Fig. 9-15: Block diagram of proposed ABC system (4ch ABC + New CDOB + FDD)

Fig. 9-16 shows the block diagram of force control in common modal space. Velocity damping loop is injected to the force control in common modal space. Damping injection improves the stability of force control. The stability of force control is also improved. Then the minor feedback-loop by position controller C'_p increases the stability of force control. However, in order to simplify the robust stability condition, the minor feedback-loop by C'_p should be disregarded. Fig. 9-16 is transformed into Fig. 9-17 equivalently. Fig. 9-17 is multiplicative representation of time delay effect on common modal space. The dotted part is regarded as the nominal open-loop transfer function of common modal space L_{cn}. By using $W(s)$, Fig. 9-17 is transformed into Fig. 9-18. Furthermore, Fig. 9-18 is equivalently transformed into Fig. 9-19. The design objective is to minimize the weighted complementary sensitivity function (nominal closed-loop transfer function) $T_c = L_{cn}/(1 + L_{cn})$. The robust stability condition is as follows.

$$\begin{aligned} ||W(s)T_c(s)||_\infty &< 1 \\ \Leftrightarrow |W(j\omega)T_c(j\omega)| &< 1, \ \forall\omega \end{aligned} \tag{9.28}$$

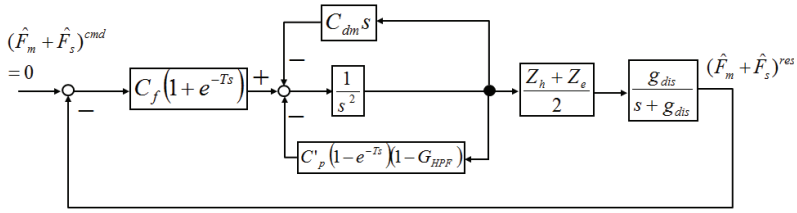

Fig. 9-16: Block diagram of common modal space (4ch ABC + New CDOB + FDD)

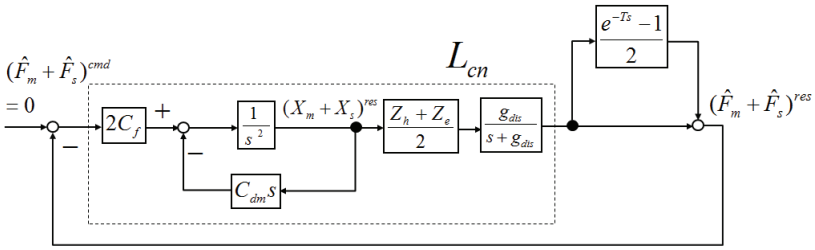

Fig. 9-17: Multiplicative representation of time delay effect on common modal space (4ch ABC + New CDOB + FDD)

9.4.2 Design of loop-shaping HPF

To satisfy (9.18) and (9.28), Damping gain K_{fdd} is set at 250, and a 3rd order loop-shaping HPF is designed as follows.

$$G_{hpf} = \frac{s^2(s+29)}{(s^2+15s+11^2)(s+11)} \tag{9.29}$$

Then the H_∞ norm of each modal space is shown as Fig. 9-20. Each H_∞ norm is smaller than 1(=0[dB]), so that the robust stability of the whole ABC system is achieved in proposed ABC system. However, if the maximum delay time is set at more than 150 ms, the cutoff frequency g_h should be redesigned to be smaller than 11 rad/s, and the other parameters might need some adjustment to satisfy the robust stability condition. Table 9-2 shows corresponding parameter values of g_h and K_{dm} to other time delay cases. T_{max} means the maximum delay time.

Furthermore, Fig. 9-21 shows Bode diagram of reproducibility and operationality in proposed ABC system(4ch ABC + New CDOB + FDD) and conventional 4ch ABC system. Reproducibility and operationality of proposed ABC system retains same such as conventional 4ch ABC.

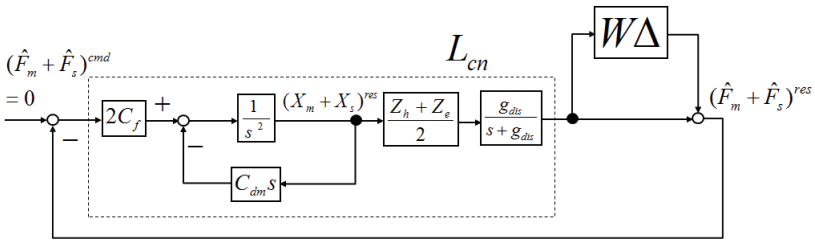

Fig. 9-18: Multiplicative representation of time delay effect using weighting function (4ch ABC + New CDOB + FDD)

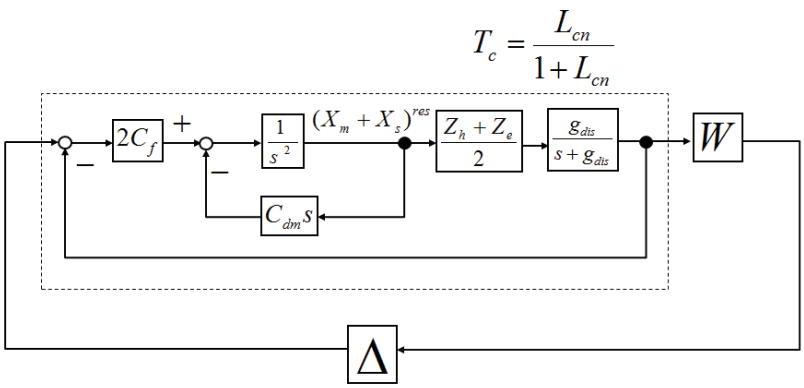

Fig. 9-19: Block diagram of robust stability condition in common modal space (4ch ABC + New CDOB + FDD)

9.5 Experiments

Fig. 9-22 shows the experimental system. The master and slave system consists of 1-DOF robots. The robots consist of linear motors and position encoders. The proposed ABC system (4ch ABC + New CDOB + FDD) and conventional 4ch ABC are compared. Time delay is varying from 100 ms to 150 ms. Other experimental parameters are set as Table 9-1.

9.5.1 Free motion

Experiments in free motion is implemented. The operator handles the master robot with back-and-forth motion. The experimental results of free motion are shown in Fig. 9-23 and Fig. 9-24. Overshoot and position error in go back moment is outstanding with conventional 4ch ABC. On the other hand, the proposed ABC system (4ch ABC + New CDOB + FDD) suppresses overshoot and position error well. These results show that proposed position control is more stable than conventional position control.

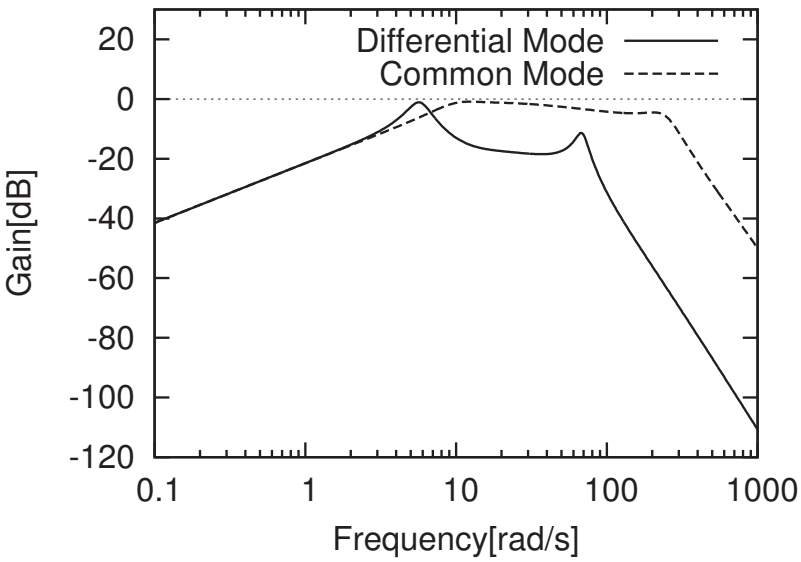

Fig. 9-20: H_∞ norm of each modal space (4ch ABC + New CDOB + FDD)

Table 9-2: Corresponding parameters to other time delay cases

T_{max}[ms]	g_h[rad/s]	K_{fdd}
150	11	250
200	8.0	255
250	6.0	260
300	3.0	270

9.5.2 Contact motion

The experimental results of contact motion with hard environment are shown in Fig. 9-25 and Fig. 9-26. With conventional 4ch ABC, there are some oscillations in contact motion. This is because force control tends to be unstable. On the other hand, with proposed ABC system (4ch ABC + New CDOB + FDD), oscillation in contact motion is suppressed, so the stability of force control in common modal space is well improved in proposed ABC system.

9.5.3 Push motion with each other

Fig. 9-27 shows the result of push motion between two operator as an example of haptic communication under time delay. A stable push motion is realized with the proposed ABC system (4ch ABC + new CDOB + FDD) even under time delay. The proposed ABC system realizes stable haptic communication under time delay.

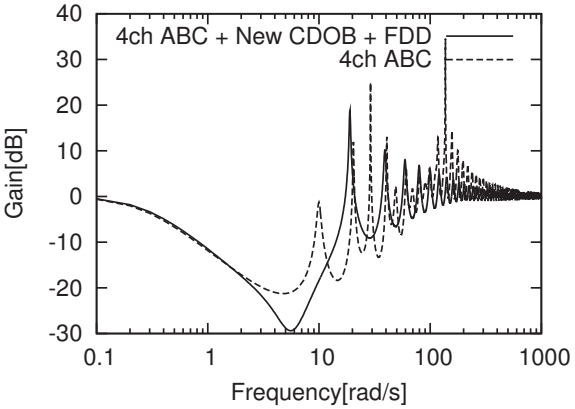

(a) Reproducibility

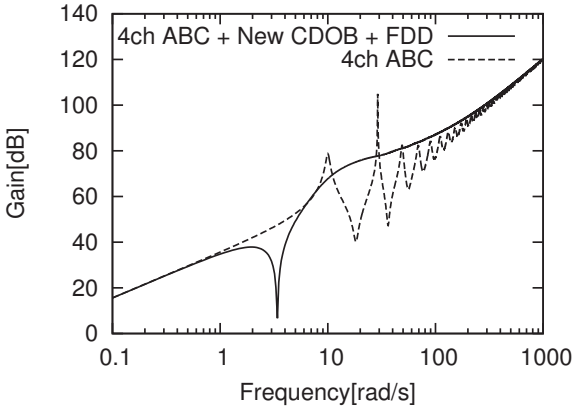

(b) Operationality

Fig. 9-21: Reproducibility and Operationality of 4ch ABC + new CDOB

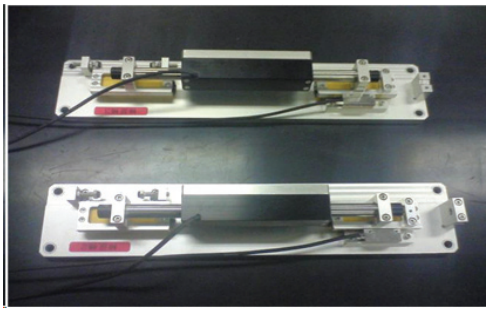

(a) two linear motors

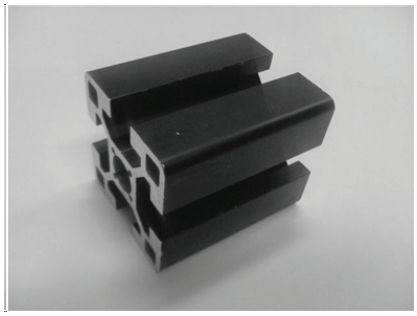

(b) environment(aluminum)

Fig. 9-22: Experimental system

9.6 Summary

This chapter proposed a new design of communication disturbance observer (CDOB) for haptic communication with ABC. New CDOB worked time delay compensation only in high frequency area both on master and slave robot. Proposed ABC system realized stable and high-performance haptic communication even under time delay. The validity of proposed system was demonstrated experimentally.

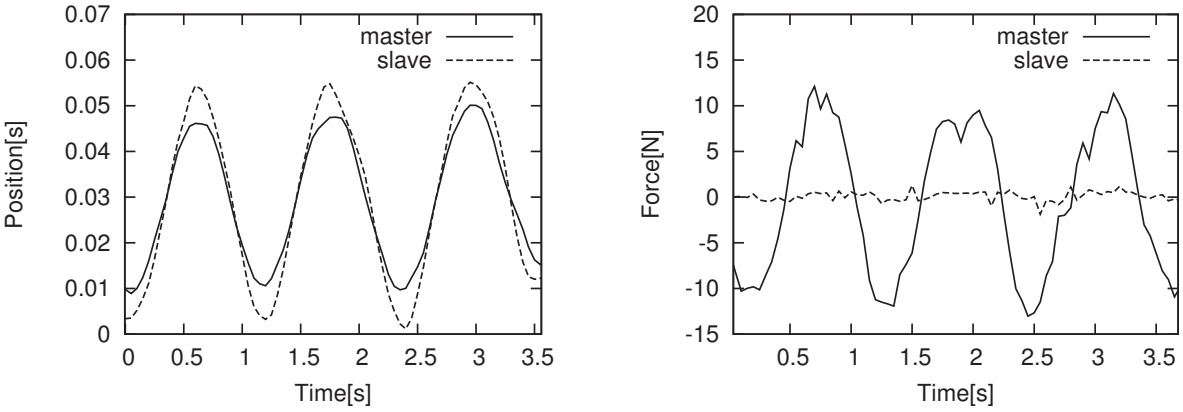

(a) Position response (b) Force response

Fig. 9-23: Free motion of conventional 4ch ABC

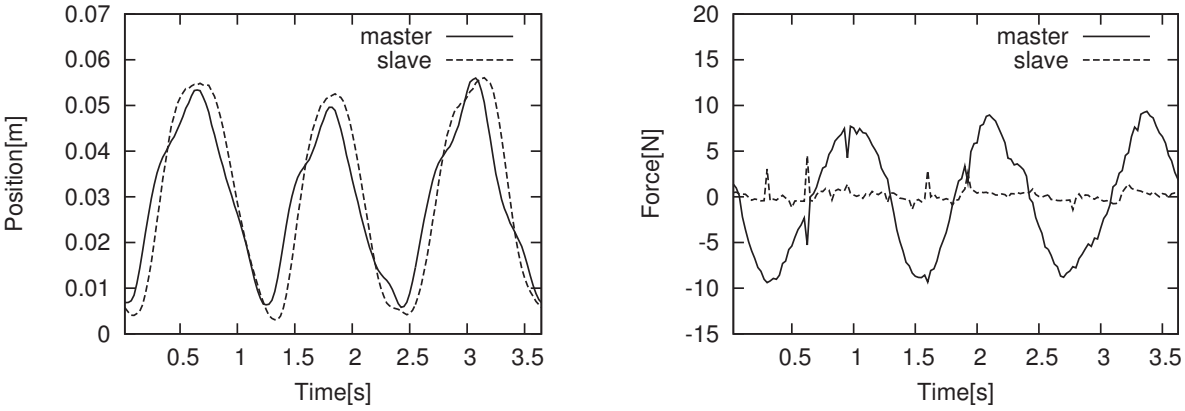

(a) Position response (b) Force response

Fig. 9-24: Free motion of Proposed system (4ch ABC + New CDOB + FDD)

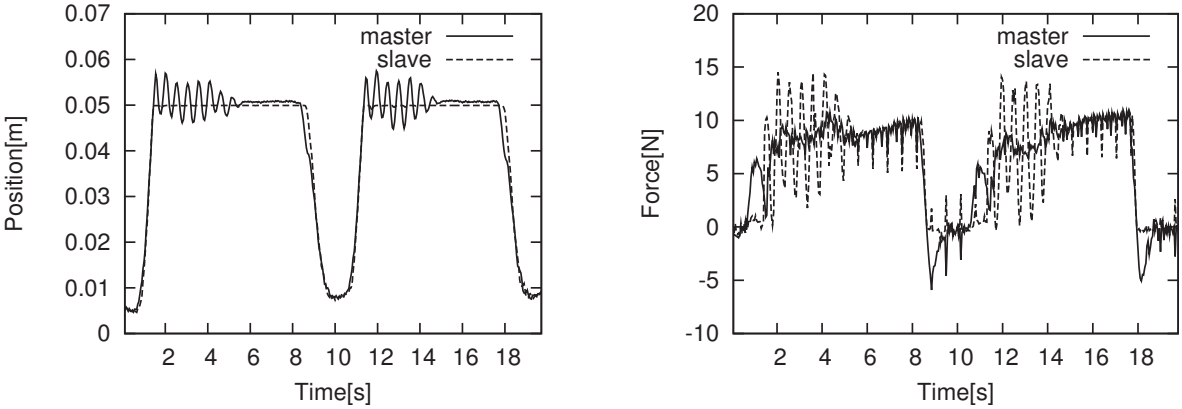

(a) Position response (b) Force response

Fig. 9-25: Contact motion of conventional 4ch ABC

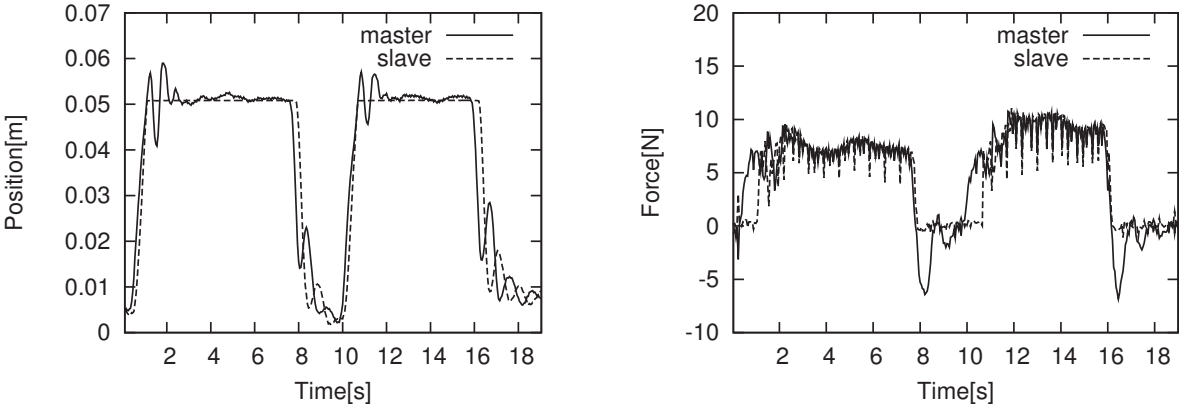

(a) Position response (b) Force response

Fig. 9-26: Contact motion of proposed system (4ch ABC + New CDOB + FDD)

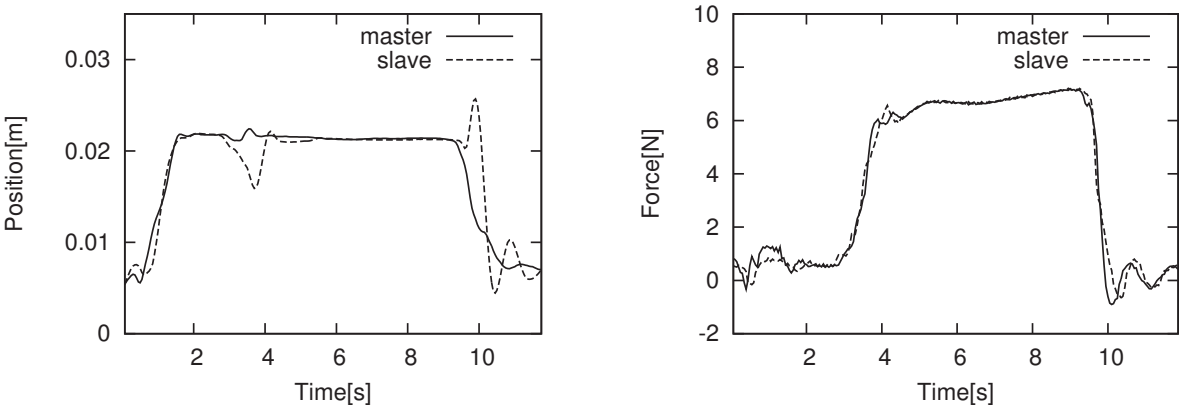

(a) Position response (b) Force response

Fig. 9-27: Push motion with each other (4ch ABC + New CDOB + FDD)

Chapter 10

Adaptive Performance Tuning of ABC by Using CDOB

10.1 Introduction

Chapter 10 introduces a method for adaptive performance tuning of time-delayed 4ch ABC by using communication disturbance observer (CDOB). Time delay compensation by CDOB is explained in chapter 5. Chapter 10 analyzes the effect of time delay compensation by CDOB on reproducibility and operationality. Time delay compensation by CDOB improves operationality, but simultaneously deteriorates reproducibility. From the analysis, chapter 10 proposes scaling down compensation value of CDOB only in contact motion with environment to realize both good reproducibility and operationality. Reproducibility is improved in all frequency area by scaling down compensation value from 0 to 1.0. The validity of the proposal is verified by experimental results.

10.2 Reproducibility and Operationality of 4ch ABC with CDOB System

Hybrid parameters are defined as (4.1). Hybrid parameters of 4ch ABC with CDOB are shown as follows.

$$H_{11} = -\frac{C_p^2(-1+e^{-2Ts})s + s^2(g_{net}+s)(2C_p+s^2)}{C_f\{s^2 g_{net} + s^3 + C_p(g_{net}+s+se^{-2Ts})\}} \tag{10.1}$$

$$H_{12} = \frac{e^{-Ts}\{s^2 g_{net} + s^3 + C_p(g_{net}+2s)\}}{C_f\{s^2 g_{net} + s^3 + C_p(g_{net}+s+se^{-2Ts})\}} \tag{10.2}$$

$$H_{21} = -\frac{e^{-Ts}\{s^2(s+g_{net})(3C_p+s^2) + C_p^2(g_{net}+2s)\}}{(C_p+s^2)\{s^2(g_{net}+s) + C_p(g_{net}+s+e^{-2Ts}s\}} \tag{10.3}$$

$$H_{22} = \frac{e^{-Ts}\{s^2 g_{net} + s^3 + C_p(g_{net}+2s)}{C_f\{s^2 g_{net} + s^3 + C_p(g_{net}+s+se^{-2Ts})\}} \tag{10.4}$$

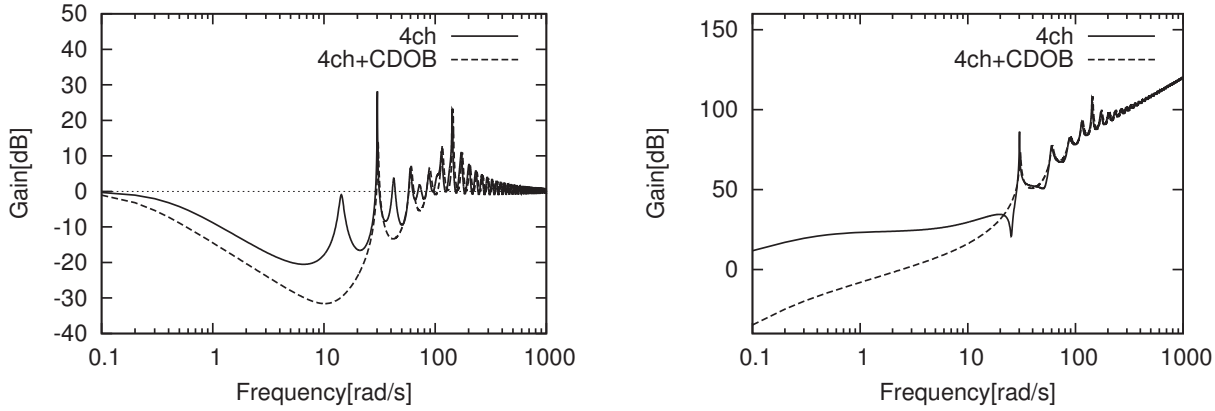

(a) Reproducibility (b) Operationality

Fig. 10-1: Bode diagram of reproducibility and operationality

Table 10-1: Parameters in analysis of reproducibility and operationality

Parameter	Meaning	Value
T	Time delay(one way)	100[ms]
K_p	Position gain	900
K_v	Velocity gain	60
K_f	Force gain	1.0
g_{dis}	Cutoff frequency of DOB	800[rad/s]
g_{net}	Cutoff frequency of DOB	800[rad/s]
Z_e	Impedance of environment	7000+20s

By using them, reproducibility P_r and operationality P_o are described as (4.6) and (4.7). The gain characteristic of P_r and P_o are shown in Fig. 10-1. Parameters are listed in Table. 10-1. Fig. 10-1 indicates that time delay compensation by CDOB improves operationality. However, reproducibility is deteriorated.

10.3 Performance Tuning by Scaling down Compensation Value

This chapter 10 proposes scaling down compensation value produced by CDOB to achieve high operationality and reproducibility.

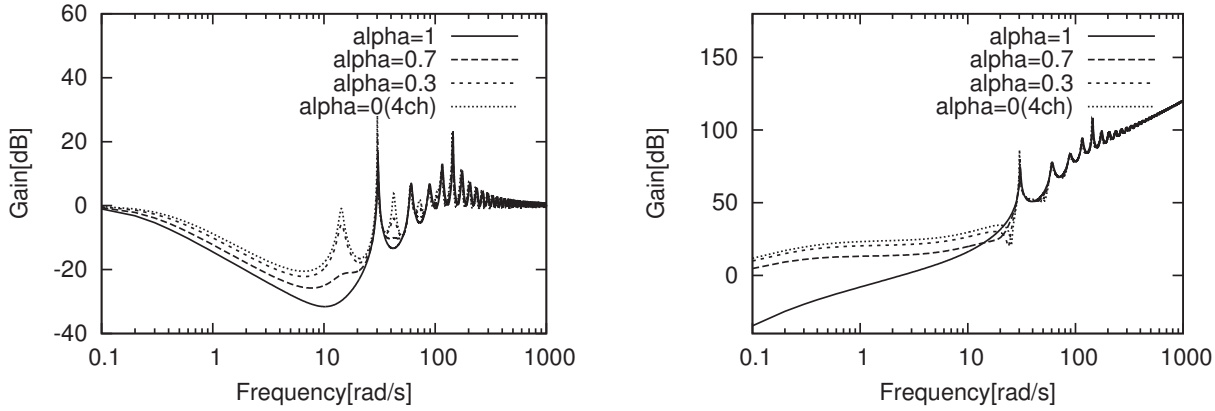

(a) Reproducibility (b) Operationality

Fig. 10-2: Bode diagram of reproducibility and operationality(Adaptive performance tuning of 4ch ABC)

10.3.1 Change of P_r and P_o induced by scaling down compensation value

Reproducibility is improved in all frequency area by scaling down compensation value from 0 to 1.0. Scaling factor α is injected to compensation value X^{cmp}. As a result, compensation value is changed to αX^{cmp}. Hybrid parameters of proposed system are calculated as follows.

$$H_{11} = -\frac{C_p^2(-1+e^{-2Ts})(-g_{net}+\alpha g_{net}-s)+s^2(g_{net}+s)(2C_p+s^2)}{C_f\{s^2 g_{net}+s^3+C_p(g_{net}+g_{net}e^{-2Ts}+\alpha g_{net}e^{-2Ts}+s+se^{-2Ts})\}} \tag{10.5}$$

$$H_{12} = \frac{e^{-Ts}\{s^2 g_{net}+s^3+C_p(2g_{net}-\alpha g_{net}+2s)\}}{C_f\{s^2 g_{net}+s^3+C_p(g_{net}+g_{net}e^{-2Ts}+\alpha g_{net}e^{-2Ts}+s+se^{-2Ts})\}} \tag{10.6}$$

$$H_{21} = -\frac{e^{-Ts}\{s^2(s+g_{net})(3C_p+s^2)+C_p^2(g_{net}\{2-\alpha\}+2s)\}}{(C_p+s^2)\{s^2(g_{net}+s)+C_p(g_{net}+e^{-2Ts}g_{net}-\alpha e^{-2Ts}g_{net}s+e^{-2Ts}s\}} \tag{10.7}$$

$$H_{22} = \frac{e^{-Ts}\{s^2 g_{net}+s^3+C_p(g_{net}+2s)}{C_f\{s^2 g_{net}+s^3+C_p(g_{net}+e^{-2Ts}g_{net}-\alpha e^{-2Ts}g_{net}+s+se^{-2Ts})\}} \tag{10.8}$$

Fig. 10-2 shows the result of reproducibility and operationality of the proposed system. By scaling down compensation value, reproducibility in the low frequency area under 100 rad/s is improved. In the moment of contact with the environment, the law of action and reaction is not achieved due to time delay. Therefore, in the steady state of the contact motion, reproducibility in low frequency area is important.

10.3.2 Scaling down compensation value only in contact motion

In order to realize both good reproducibility and operationality, this chapter proposes scaling down compensation value only in contact motion with environments. Scaling factor α is determined depending

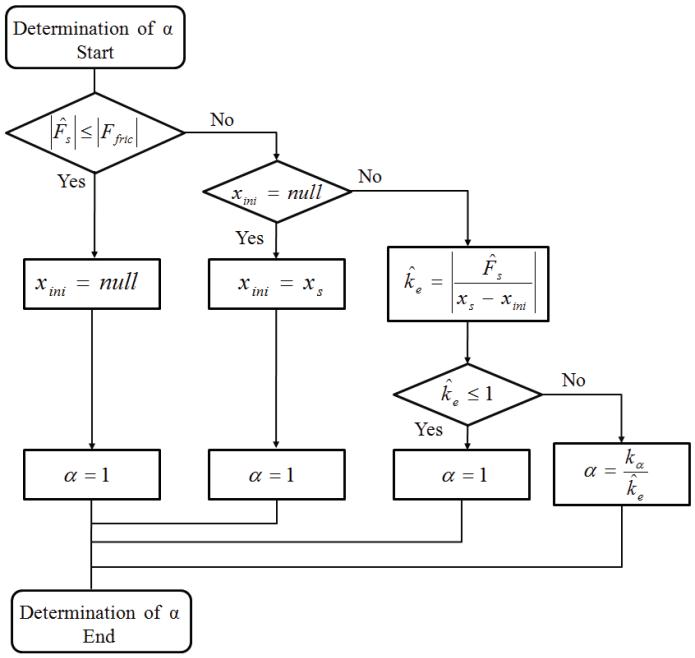

Fig. 10-3: Flow chart of α

on the value of the reaction force $\hat{F}_s$ and the environmental stiffness $\hat{k}_e$ such as Fig. 10-3. To avoid the effect of the friction force which the RFOB cannot separate from the reaction force, compensation value is scaled down only when $\hat{F}_s$ is bigger than the friction force F_{fric}. The value of F_{fric} is fixed at the maximum value of the friction force of the slave robot. The moment $\hat{F}_s$ becomes bigger than F_{fric}, the slave position is memorized as initial position x_{ini}. Environmental stiffness $\hat{k}_e$ is given by the following equation.

$$\hat{k}_e = \frac{1}{\alpha} = |\frac{\hat{F}_s}{x_s - x_{ini}}| \tag{10.9}$$

By using $\hat{k}_e$, α is defined as follows.

$$\alpha = \frac{k_\alpha}{\hat{k}_e} \tag{10.10}$$

Where $k_\alpha[m/N]$ is the coefficient factor for adjustment of α. α is proportional to the inverse of $\hat{k}_e$. If the environment is hard, α is equal to zero. As a result, reproducibility is enhanced only in contact with hard environment. On the other hand, if $\hat{k}_e$ is smaller than 1.0, α is fixed at 1.0 as the countermeasure of contact with soft environments.

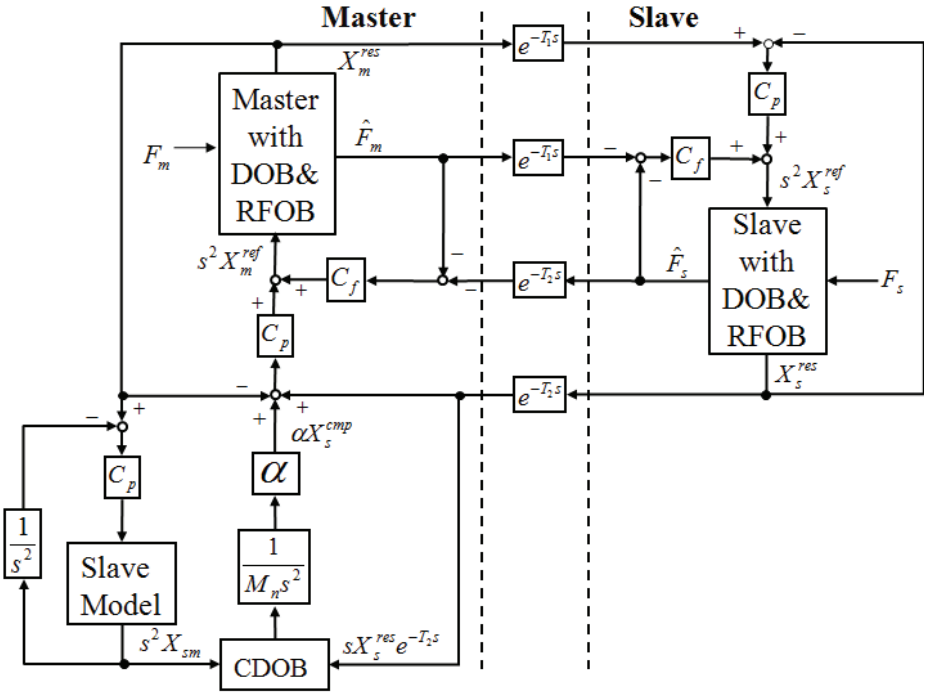

Fig. 10-4: Block diagram of proposed system (Adaptive performance tuning of 4ch ABC)

10.3.3 Stability analysis

The stability of conventional 4ch ABC ($\alpha = 0$) and that of 4ch ABC with CDOB ($\alpha = 1$) are compared. In contact motion, the stability of force control is predominant. The block diagrams of force control in common modal space are shown as Fig. 3-8 and Fig. 5-6. Used parameters in this analysis are listed in Table 10-2. Nyquist plots of L_c are shown in Fig. 10-5. The locus of 4ch ABC with CDOB ($\alpha = 1$) goes around (-1, 0). On the other hand, the locus of 4ch ABC ($\alpha = 0$) goes through the right of (-1, 0). Compared Fig. 3-8 with Fig. 5-6, in conventional 4ch ABC ($\alpha = 0$), position controller C_p makes a feedback loop in common modal space, and it improves the stability as spring and damping injection. C_p fixes each robot in the same position because the position response of the other robot is not attained due to time delay. From this analysis, scaling down compensation value in contact motion also improves the stability of force control.

10.4 Simulations

Fig. 10-6 and Fig. 10-7 show the simulation results of contact motion. Parameters are set as Table 10-3. With conventional 4ch ABC + CDOB, there are oscillations after contact with the environment. On the other hand, proposed system suppresses vibrations well. Proposed adaptive performance tuning method

Table 10-2: Parameters in stability analysis of force control in common modal space

Parameter	Meaning	Value
T	Time delay(one way)	80[ms]
K_p	Position gain	900
K_v	Velocity gain	60
K_f	Force gain	1.0
g_{dis}	Cutoff frequency of DOB	800[rad/s]
g_{net}	Cutoff frequency of DOB	800[rad/s]
Z_e	Impedance of environment	7000+20s
Z_h	Impedance of environment	1000+20s

Table 10-3: Parameters in simulation and experiment

Parameter	Meaning	Value
T	Time delay(one way)	100 $\sim$ 120[ms]
K_p	Position gain	900
K_v	Velocity gain	60
K_f	Force gain	1.0
g_{dis}	Cutoff frequency of DOB	800[rad/s]
g_{net}	Cutoff frequency of DOB	800[rad/s]
F_{fric}	friction force	1.5[N]
k_α	coefficient factor	1.0[m/N]
M_n	Nominal mass of motor	0.5[kg]
K_{tn}	Nominal Force coefficient	22.0[N/A]
st	Sampling time	0.1[ms]

improves the stability of force control.

10.5 Experiments

Fig. 10-8 shows the experimental system. The master system and the slave system consist of 1–Dof robot, respectively. The robots consist of linear motors and position encoders. The environment with which slave robot conacts is aluminum. 4ch ABC with CDOB and proposed controller (adaptive performance tuning of 4ch ABC) are compared. Experimental parameters are set as Table 10-3.

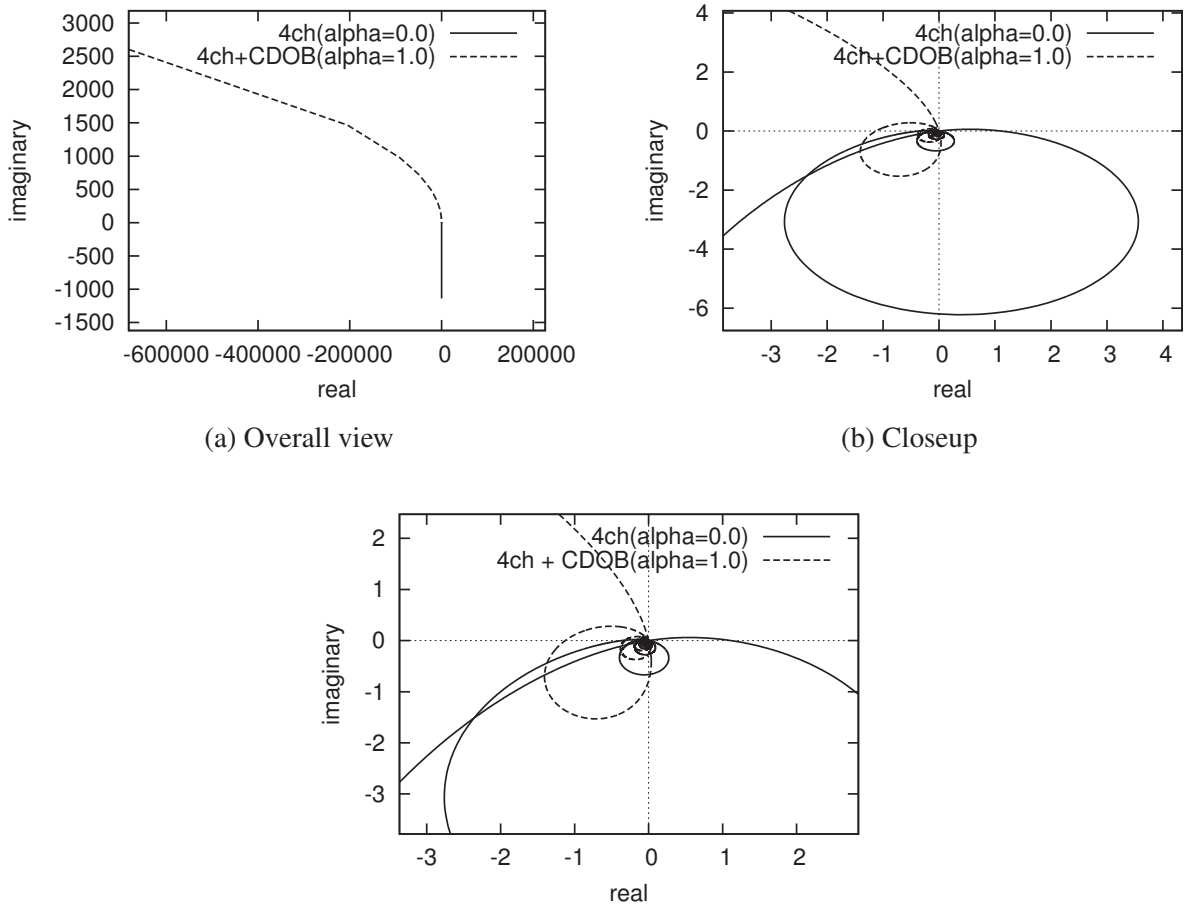

(a) Overall view

(b) Closeup

(c) Super closeup

Fig. 10-5: Nyquist plot of force control in common modal space (conventional 4ch ABC and 4ch ABC + CDOB)

10.5.1 Free motion

The experimental results of free motion are shown in Fig. 10-9 and Fig. 10-10. Both controllers have good operationality, so that there are small operational force. Slave robots follow the position of their master robots precisely.

10.5.2 Contact motion

The experimental results of contact motion with environment are shown in Fig. 10-11 and Fig. 10-12. With 4ch ABC with CDOB, there are vibrations in contact with environment. Due to the vibrations, human can not feel good touch sense. On the other hand, with proposed controller (adaptive performance tuning of 4ch ABC), vibrations are suppressed well, and reproducibility is progressed. Then human operator can feel sharp touch sense of hard aluminum naturally. In addition, proposed method improves

the stability of contact motion.

10.6 Summary

This chapter analyzed the effect of the time delay compensation by CDOB on reproducibility and operationality in bilateral teleoperation. Time delay compensation by CDOB improved the operationality, but simultaneously deteriorated reproducibility. From the analysis, this chapter 10 proposed scaling down compensation value produced by CDOB to achieve high reproducibility and operationality. Reproducibility was improved by scaling down compensation value from 0 to 1.0. Scaling compensation value in contact motion also improved the stability of force control in common modal space. Furthermore, this chapter 10 proposed scaling down compensation value only in contact motion with environment to realize both good reproducibility and operationality. The validity was verified by experimental results.

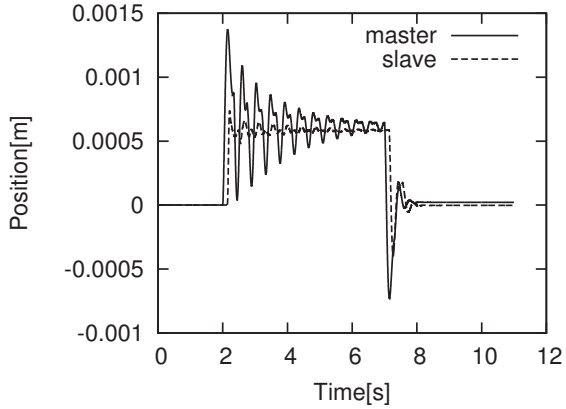

(a) Position response

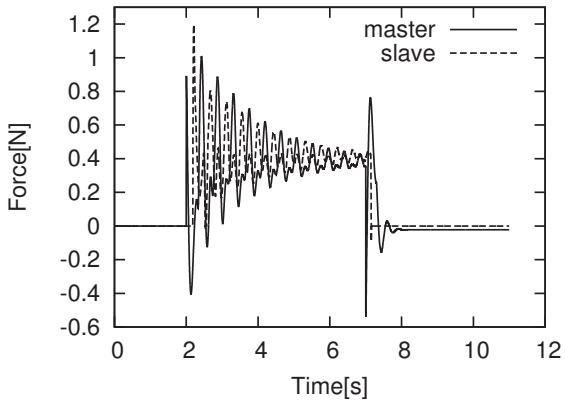

(b) Force response

Fig. 10-6: Contact motion of 4ch + CDOB (simulation result)

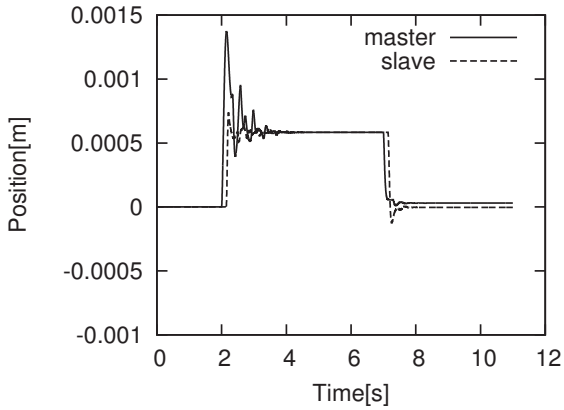

(a) Position response

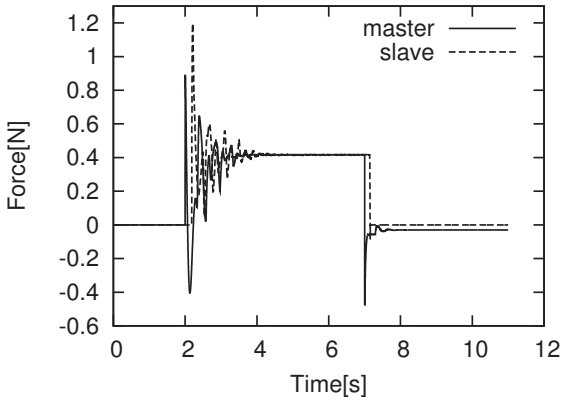

(b) Force response

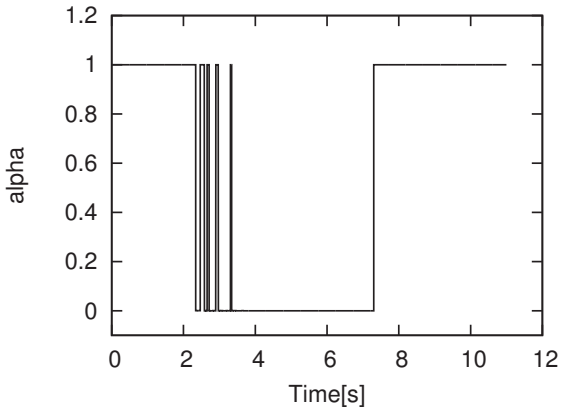

(c) Value of α

Fig. 10-7: Contact notion of proposed system (Adaptive performance tuning of 4ch ABC)

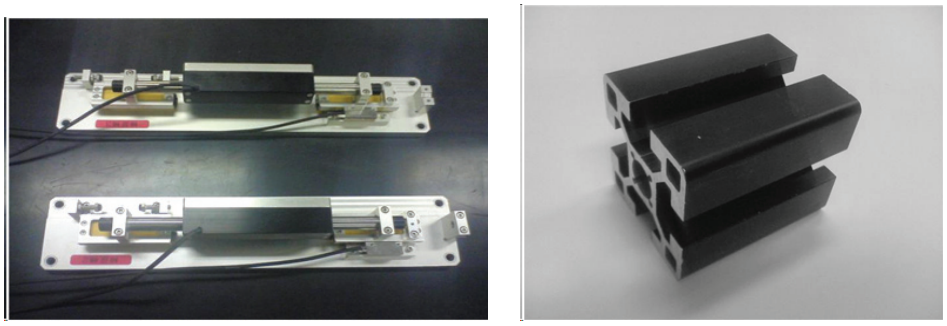

(a) two linear motors (b) environment(aluminum)

Fig. 10-8: Experimental system

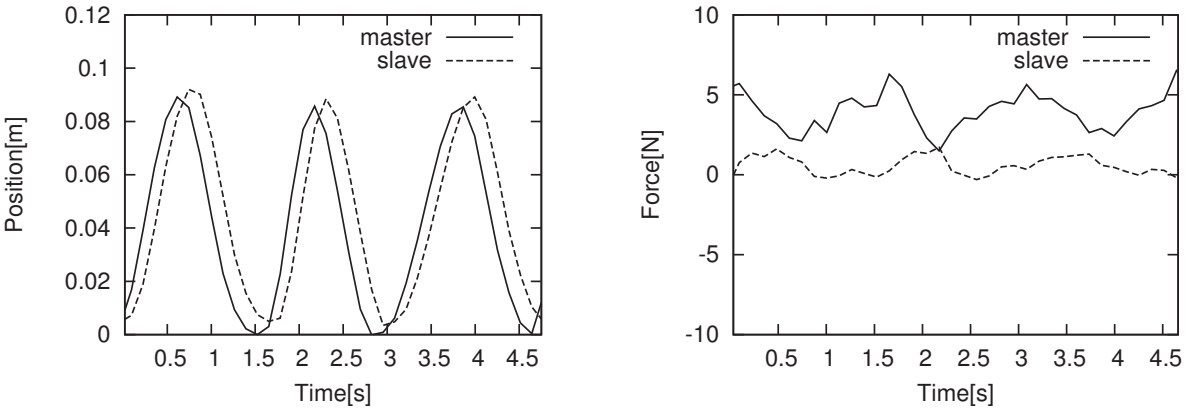

(a) Position response (b) Force response

Fig. 10-9: Free motion(4ch ABC with CDOB)

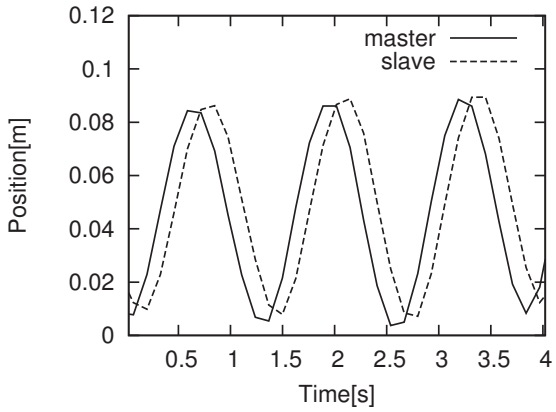

(a) Position response

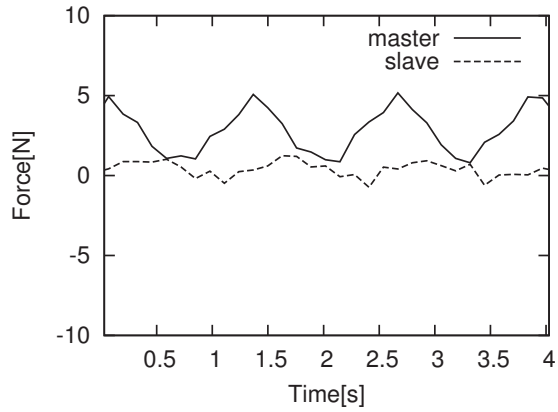

(b) Force response

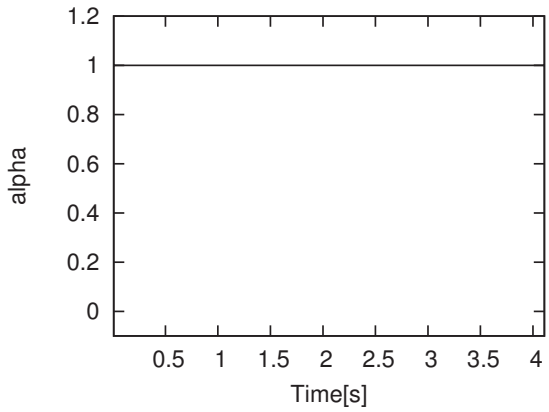

(c) Value of α

Fig. 10-10: Free motion (Adaptive performance tuning of 4ch ABC)

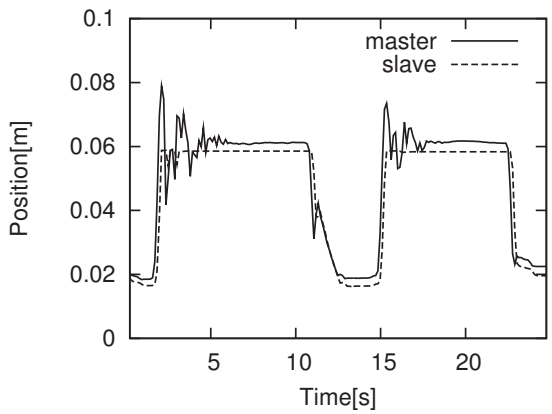

(a) Position response

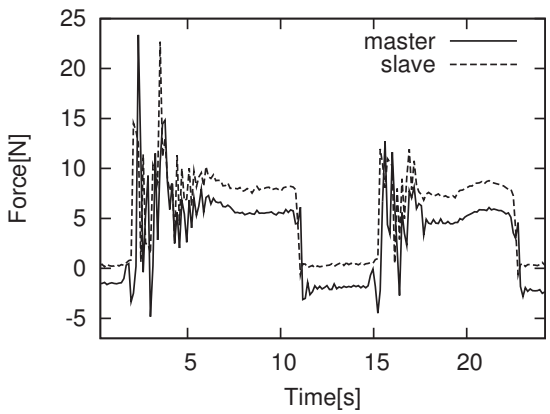

(b) Force response

Fig. 10-11: Contact motion(4ch ABC with CDOB)

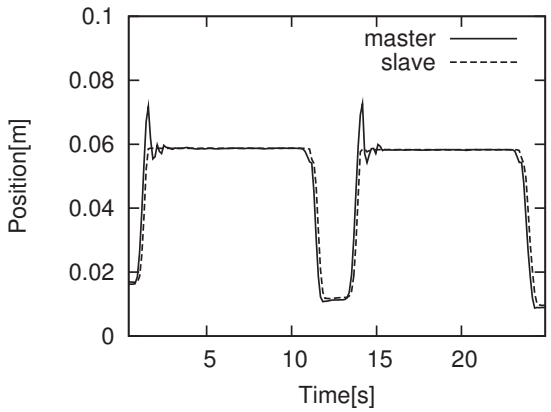

(a) Position response

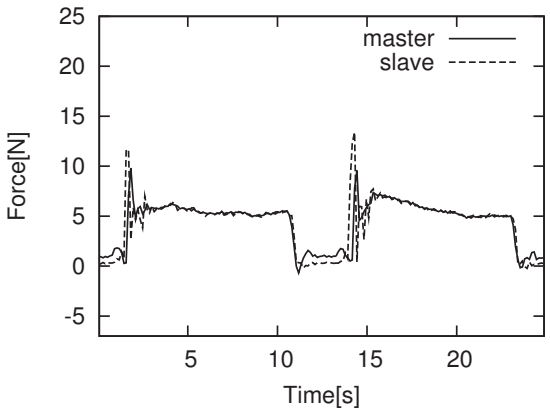

(b) Force response

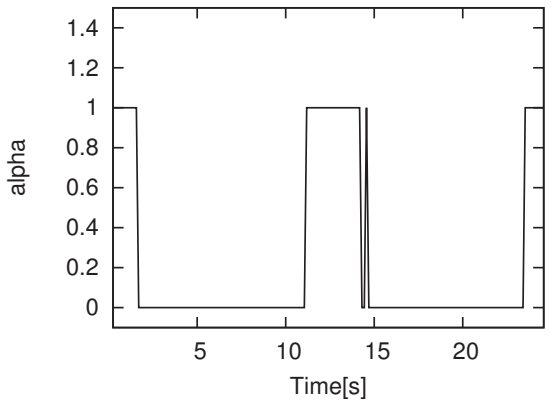

(c) Value of α

Fig. 10-12: Contact motion (Adaptive performance tuning of 4ch ABC)

Chapter 11

Velocity Difference Damping for ABC

11.1 Introduction

This Chapter 11 introduces an event-based damping design for time-delayed ABC. Damping injection by local velocity feedback is a major solution to improve the stability of force control. However, it causes small deterioration of operationality. If operationality is worse, the operator needs extra force to manipulate master robot, and cannot feel environmental impedance precisely. This Chapter 11 proposes a method of velocity difference damping that utilizes the velocity difference between the robot and the robot model. this method improves the performance and the stability of force control in the common modal space without deteriorating the performance of position control.

11.2 3ch ABC under Time Delay

Chapter 11 utilizes three-channel acceleration-based bilateral control (3ch ABC) under time delay[68]. Three-channel means master/slave force and master position. Fig. 11-1 shows the block diagram of 3ch ABC under time delay. The acceleration reference values of 3ch ABC under time delay are given as follows.

$$s^2 X_m^{ref} = s^2 X_m^{res} = -C_f(\hat{F}_m + \hat{F}_s e^{-Ts}) \tag{11.1}$$

$$s^2 X_s^{ref} = s^2 X_s^{res} = C_p(X_m e^{-Ts} - X_s) - C_f(\hat{F}_s + \hat{F}_m e^{-Ts}) \tag{11.2}$$

11.2.1 Position control (3ch ABC)

The block diagram of (11.2) is shown in Fig. 11-2. This is a servo-type control system that the slave position serves the master position. There is no time delay e^{-Ts} in closed-loop, so that the position control of 3ch ABC system is stable.

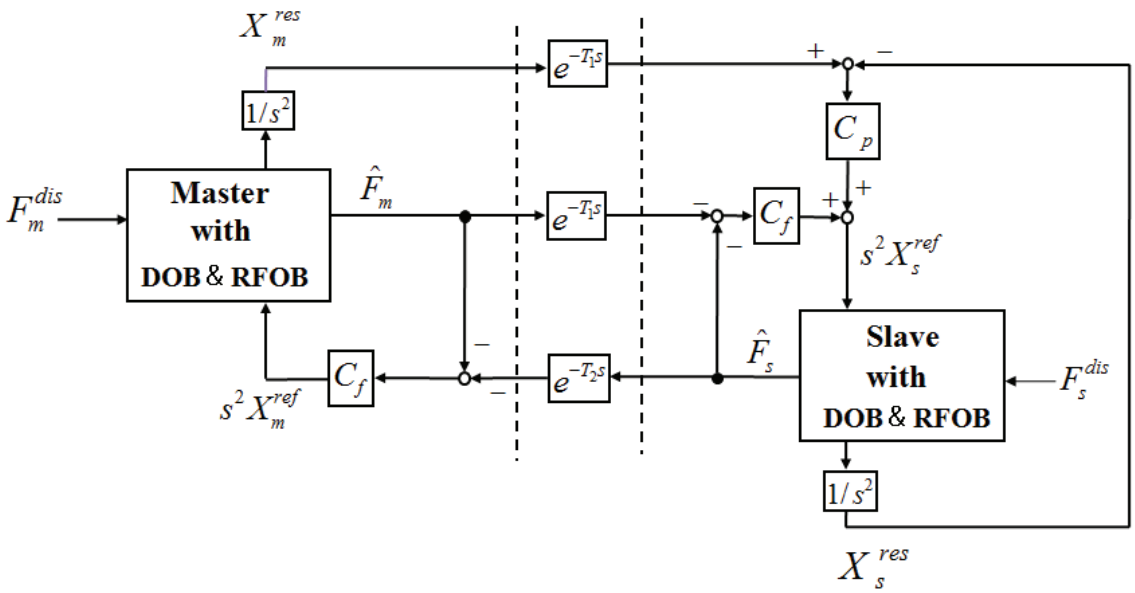

Fig. 11-1: Block diagram of 3ch ABC system under time delay

11.2.2 Force control (3ch ABC)

Force control in common modal space of 3ch ABC is given by adding (11.1) and (11.2) as follows.

$$s^2(X_m + X_s)^{res} = -C_f(1 + e^{-Ts})(\hat{F}_m + \hat{F}_s) + C_p(X_m e^{-Ts} - X_s) \tag{11.3}$$

Fig. 11-3 shows the block diagram of force control of 3ch ABC in common modal space. Time delay still exists in feedback loop of force control in common modal space. Position control of 3ch ABC is stable. However, another solution is necessary to improve the stability of force control in common modal space.

11.3 Proposed Velocity Difference Damping

11.3.1 Inprovement of stability by proposed method

In this section, proposed velocity difference damping is introduced which utilizes the velocity difference caused by contact with environment between slave robot and slave model. This method assumes a slave model which follows the master robot without contact with environment like Fig. 11-5. The acceleration reference values of slave model and slave robot are shown in (11.4) and (11.5).

$$s^2 X_{sm}^{ref} = s^2 X_{sm}^{res} = C_p(X_m e^{-Ts} - X_{sm}) - C_f(\hat{F}_m e^{-Ts}) \tag{11.4}$$

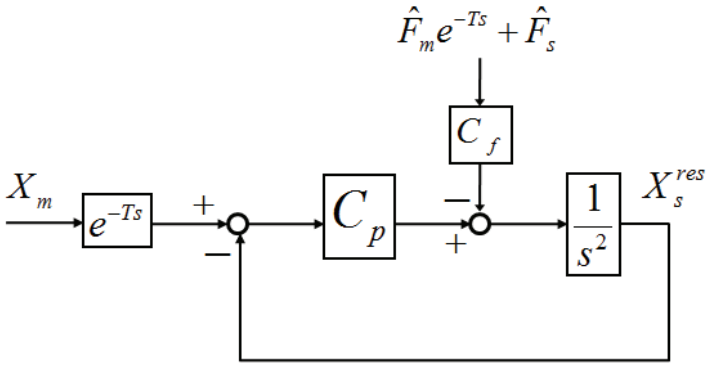

Fig. 11-2: Position control (3ch ABC)

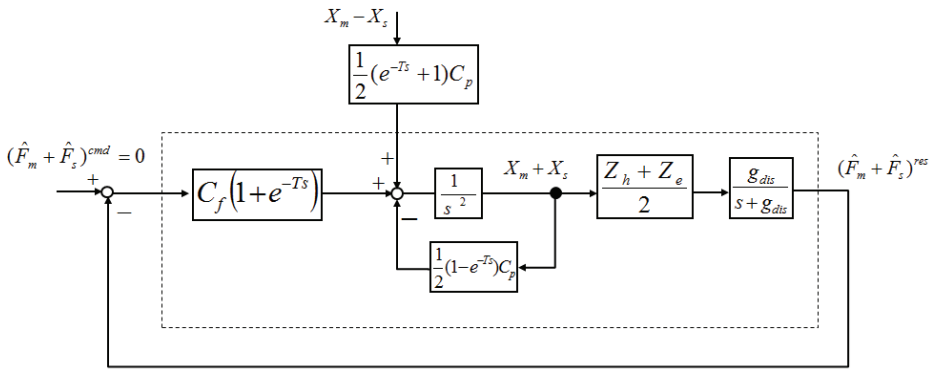

Fig. 11-3: Force control in common modal space (3ch ABC)

$$s^2 X_s^{ref} = s^2 X_s^{res} = C_p(X_m e^{-Ts} - X_s) - C_f(\hat{F}_s + \hat{F}_m e^{-Ts}) \tag{11.5}$$

The difference of (11.4) and (11.5) is shown as follows.

$$s^2(X_{sm} - X_s)^{res} = -C_p(X_{sm} - X_s) + C_f \hat{F}_s \tag{11.6}$$

From (11.6), the velocity difference is calculated as follows.

$$s(X_{sm} - X_s) = \frac{sC_f \hat{F}_s}{s^2 + C_p} \tag{11.7}$$

(11-7) shows that the velocity difference is a stable 2nd order system, and proportional to the reaction force of environment $\hat{F}_s$. The velocity difference is sent to master side for damping master robot only when the slave robot contacts with the envirinment. At the same time, in master side, another velocity difference should be developed, which is proportional to operational force $\hat{F}_m$. Two master models are

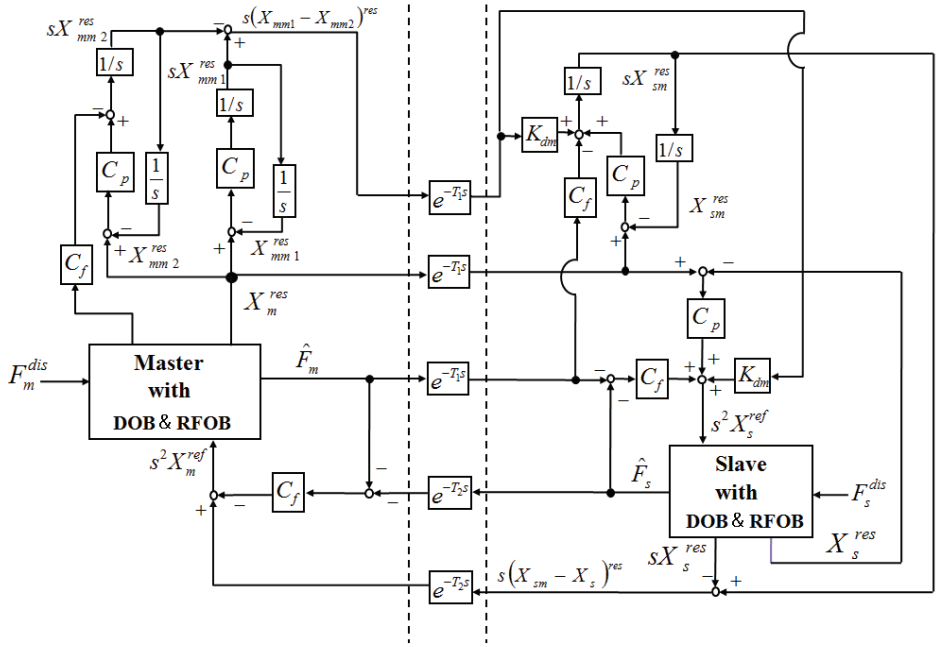

Fig. 11-4: Block diagram of proposed system (3ch ABC with velocity difference damping)

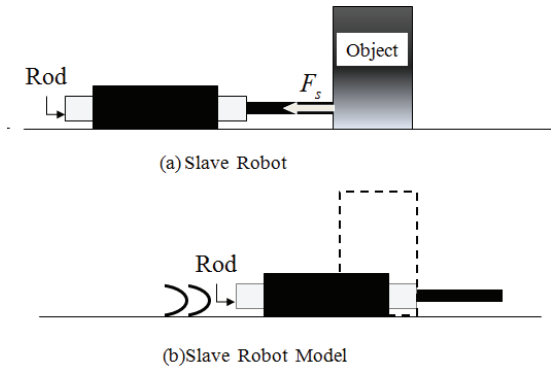

Fig. 11-5: Slave robot and slave model

prepared which follow the position of the master robot like Fig. 11-6 because master robot is not position controlled in 3ch ABC. The acceleration reference value of master robot is shown as (11-8), and those of two master models are shown as (11-9) and (11-10).

$$s^2 X_m^{res} = -C_f(\hat{F}_m + \hat{F}_s e^{-Ts}) + K_{dm} s(X_{sm} - X_s)e^{-Ts} \tag{11.8}$$

$$s^2 X_{mm1}^{res} = C_p(X_m - X_{mm1}) \tag{11.9}$$

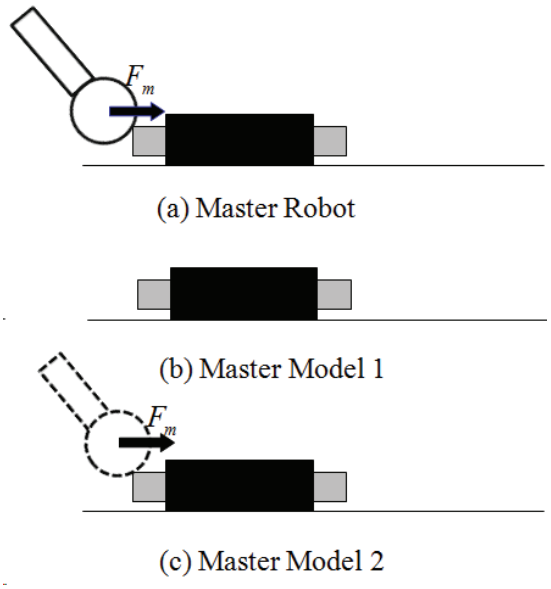

Fig. 11-6: Master robot and master models

$$s^2 X_{mm2}^{res} = C_p(X_m - X_{mm2}) - C_f \hat{F}_m \tag{11.10}$$

From (11.9) and (11.10), The difference between two models is calculated as (11.11).

$$s(X_{mm1} - X_{mm2}) = \frac{sC_f \hat{F}_m}{s^2 + C_p} \tag{11.11}$$

This velocity difference is sent to slave side for damping slave motion. The ultimate acceleration reference values of master and slave robot are shown as (11.12) and (11.13). K_{dm} denotes damping gain.

$$s^2 X_m^{res} = -C_f(\hat{F}_m + \hat{F}_s e^{-Ts}) + K_{dm} s(X_{sm} - X_s)e^{-Ts} \tag{11.12}$$

$$s^2 X_s^{res} = C_p(X_m e^{-Ts} - X_s) - C_f(\hat{F}_s + \hat{F}_m e^{-Ts}) + K_{dm} s(X_{mm1} - X_{mm2})e^{-Ts} \tag{11.13}$$

(11.12) and (11.13) are transformed as follows by substituting (11.7) and (11.11).

$$s^2 X_m^{res} = -C_f\{\hat{F}_m + \hat{F}_s e^{-Ts}(1 - \frac{sK_{dm}}{s^2 + C_p})\} \tag{11.14}$$

$$s^2 X_s^{res} = -C_f\{\hat{F}_s + \hat{F}_m e^{-Ts}(1 - \frac{sK_{dm}}{s^2 + C_p})\} + C_p(x_m e^{-Ts} - x_s) \tag{11.15}$$

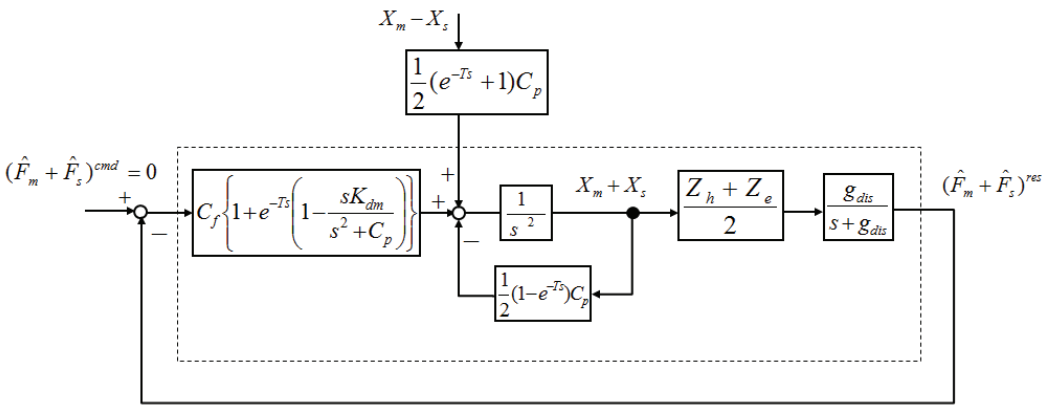

Fig. 11-7: Common modal space of proposed system (3ch ABC with velocity difference damping)

Table 11-1: Parameters in analysis(proposed system)

Parameter	Meaning	Value	unit
T	Time delay(one way)	0.1	s
K_p	Position gain	900	
K_v	Velocity gain	60	
K_f	Force gain	1.0	
K_{dm}	Damping gain	70.0	
g_{dis}	Cutoff frequency of DOB & RFOB	500	rad/s
Z_h	Impedance of human	1000+10s	N/m
Z_e	Impedance of environment	10000+10s	N/m

Acceleration reference value of common modal space is given by adding (11.14) and (11.15) as follows.

$$s^2(X_m + X_s)^{res} = -C_f(\hat{F}_m + \hat{F}_s)\{1 + e^{-Ts}(1 - \frac{sK_{dm}}{s^2 + C_p})\} + C_p(x_m e^{-Ts} - x_s) \qquad (11.16)$$

The block diagram of (11.16) is shown in Fig. 11-7. Fig. 11-7 shows that the proposed velocity difference damping reduces the effect of time delay in feedback loop. Bode diagram of L_c is shown as Fig. 11-8. Fig. 11-8 shows that the proposed method increases the value of gain-crossover frequency, and reduces phase delay. Nyquist plot is shown as Fig. 11-9. Parameters are same as Table 11-1. As the damping gain (K_{dm}) becomes large, the stability of common modal space is improved. On the other hand, the block diagram of (11.15) is shown as Fig. 11-10. Compared with Fig. 11-2, there is no change in feedback loop. From these analyses, proposed method improves the stability of force control without deteriorating the performance of position control.

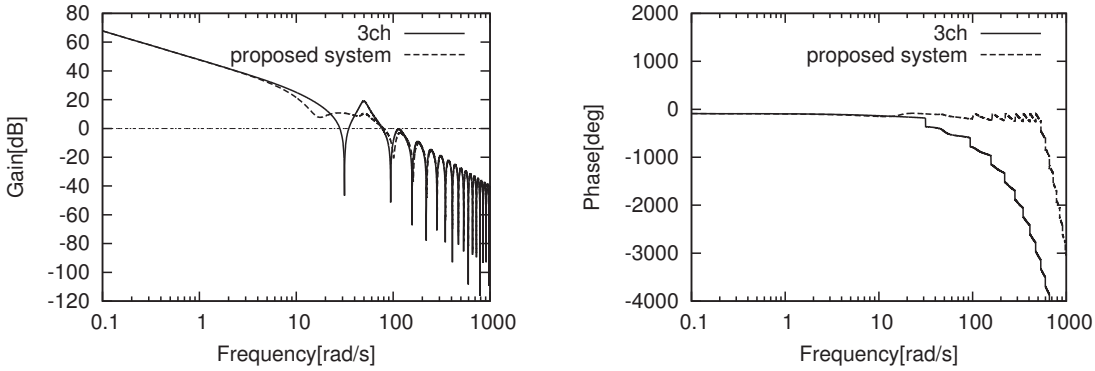

(a) Gain characteristics of L_c (b) Phase characteristics of L_c

Fig. 11-8: Bode diagram of L_c (3ch ABC + velocity difference damping)

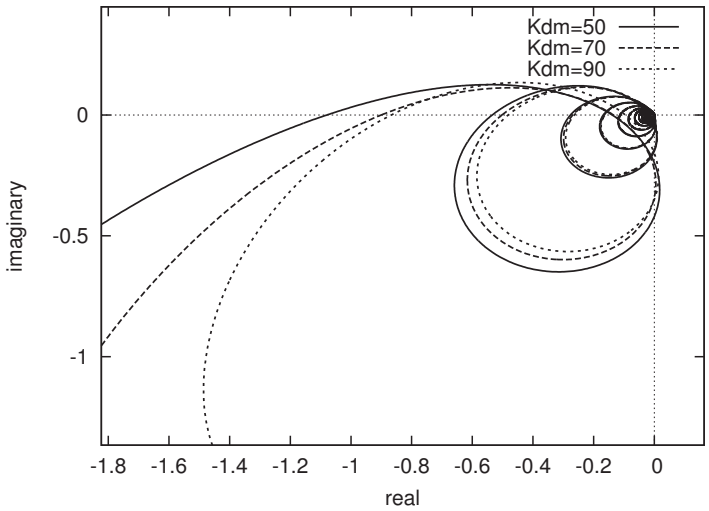

Fig. 11-9: Nyquist plot of common modal space of proposed system (3ch ABC + velocity difference damping)

11.3.2 Reproducibility and operationality of proposed method

Hybrid parameters of proposed system are calculated as follows.

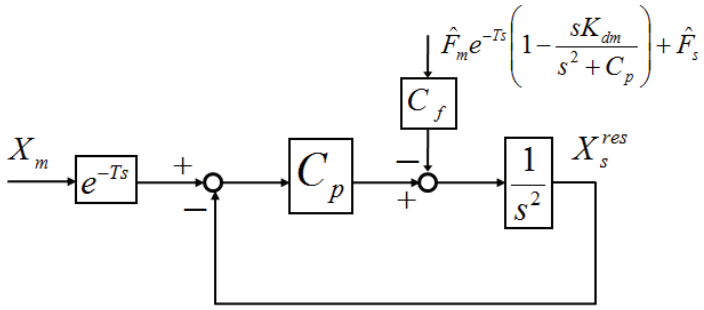

Fig. 11-10: Position control (proposed system: 3ch ABC + velocity difference damping)

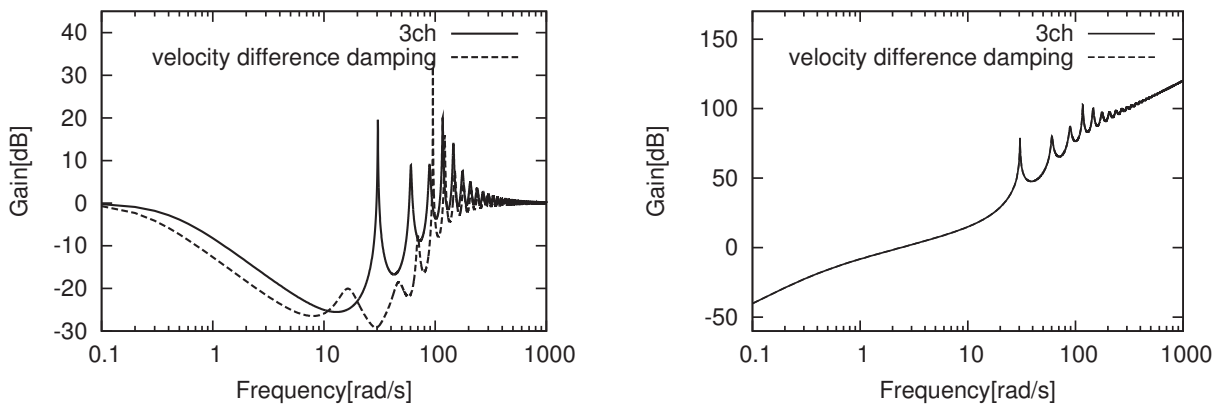

(a) Reproducibility (b) Operationality

Fig. 11-11: Bode diagram of operationality and reproducibility of the proposed system 3ch ABC + velocity difference damping

$$\left.\begin{aligned} H_{11} &= -\frac{s^2}{C_f} \\ H_{12} &= e^{-Ts}(1-\frac{sK_{dm}}{s^2+C_p}) \\ H_{21} &= \frac{e^{-Ts}\{K_{dm}s^3-(C_p+s^2)^2\}}{(C_p+s^2)^2} \\ H_{22} &= \frac{(e^{-Ts}-1)(C_p+s^2)^2-2e^{-2Ts}sK_{dm}(C_p+s^2)+e^{-2Ts}K_{dm}^2s^2}{(C_p+s^2)^2(\frac{C_p}{C_f}+\frac{s^2}{C_f})} \end{aligned}\right\} \tag{11.17}$$

Gain characteristic of reproducibility and operationality are shown as Fig. 11-11. Proposed method has almost no influence on the operationality. However, it deteriorates reproducibility.

Table 11-2: Parameters in simulation

Parameter	Meaning	Value	unit
T	Time delay(one way)	0.1	s
K_p	Position gain	900	
K_v	Velocity gain	60	
K_f	Force gain	1.0	
K_{dm}	Damping gain	70.0	
g_{dis}	Cutoff frequency of DOB & RFOB	500	rad/s
Z_h	Impedance of human	1000+10s	N/m
Z_e	Impedance of environment	10000+10s	N/m
M_n	Nominal inertia of motor	0.5	kg
K_{tn}	Torque coefficient	22.0	N/A
st	Sampling time	0.1	ms

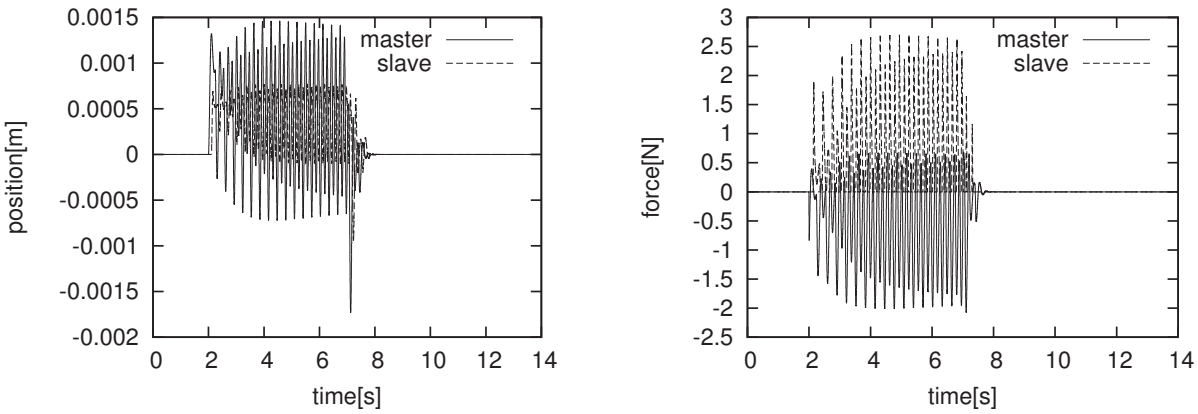

(a) Position response (b) Force response

Fig. 11-12: simulation result of contact motion (3ch ABC)

11.4 Simulations

This section shows the simulation results of contact motion in Fig. 11-12 and Fig. 11-13. Parameters are shown as Table 11-2. With conventional 3ch ABC, there are heavy oscillations in contact with the environment. On the other hand, proposed system suppresses oscillations well, so that the stable contact motion is achieved by proposed method.

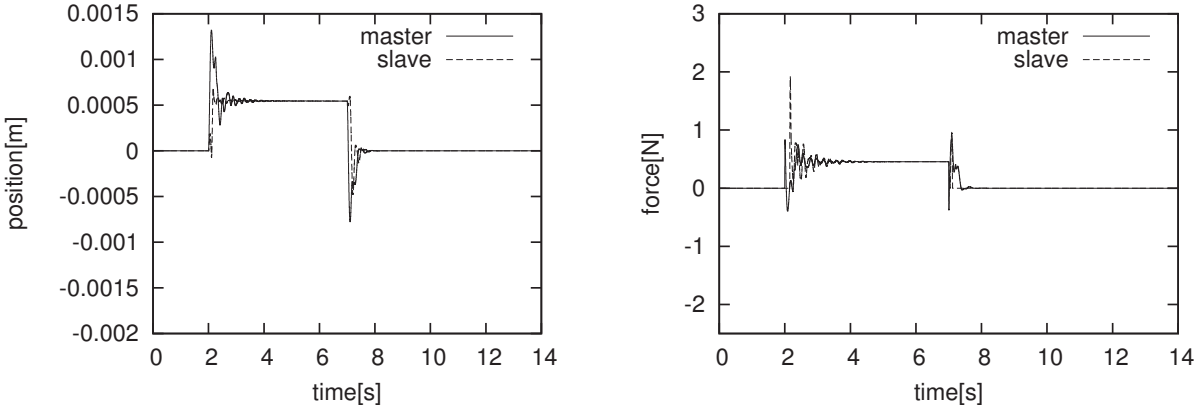

(a) Position response (b) Force response

Fig. 11-13: Simulation result of contact motion (3ch ABC + velocity difference damping)

11.5 Experiments

Fig. 11-14 and Fig. 11-15 are the experimental system. The master system and slave system consist of 1-Dof robots. The robots consist of linear motors and position encoders. 3ch ABC and proposed controller (3ch ABC + velocity difference damping) are compared. Experimental parameters are set as Table 11-2, and $K_{dm} = 70$.

11.5.1 Free motion

The experimental results of free motion are shown in Fig. 11-16 and Fig. 11-17. Both controllers have good operationality, so that there are no operational force. Each slave robot follows the position of the master robot precisely.

11.5.2 Contact motion

The experimental results of contact motion with soft environment are shown in Fig. 11-18 and Fig. 11-19. With 3ch ABC, there are oscillations after contact with the environment. On the other hand, with proposed controller (3ch ABC + velocity difference damping) oscillations are suppressed well. Fig. 11-20 shows the contact with the hard environment using proposed controller. From these experimental results, it is ascertained that proposed velocity difference damping improves stability without deterioration of operationality.

11.6 Summary

This chapter 11 proposed a method of velocity difference damping. With the experimental and analytical results, proposed method improved the stability of contact motion with unknown environments,

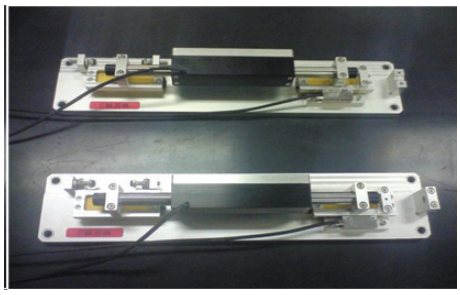

Fig. 11-14: Experiment using two linear motors

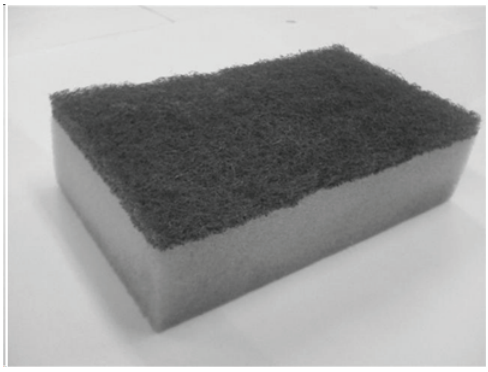

(a) Soft environment

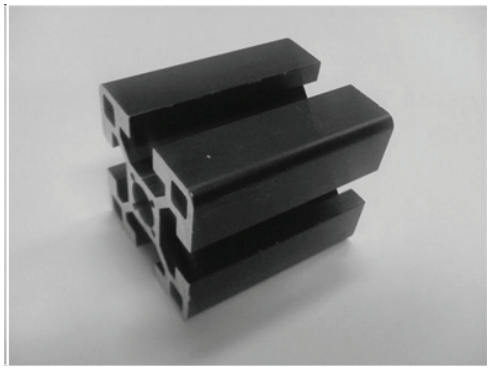

(b) Hard environment

Fig. 11-15: Environments for contact motion

maintaining good operationality. However, there was a trade-off relation between the stability and the reproducibility with the damping gain K_{dm}. The validity of the proposed control system was confirmed by several experimental results.

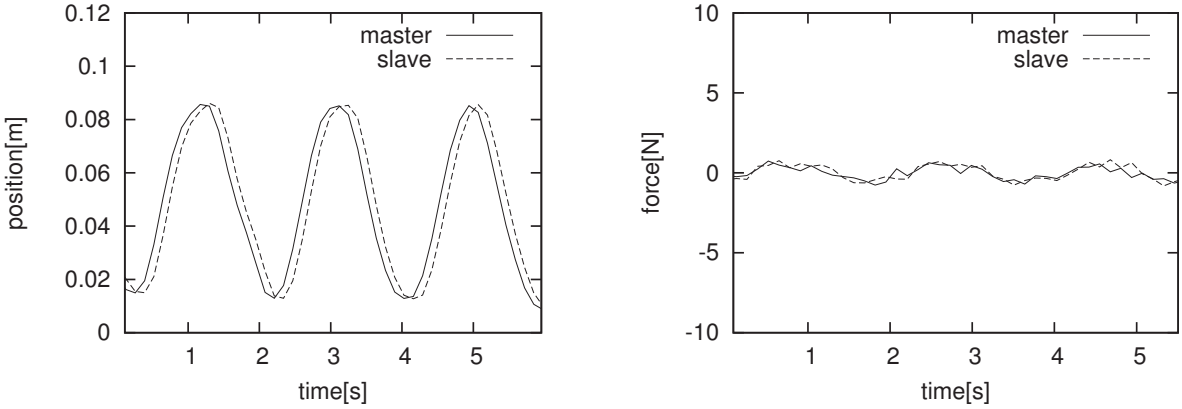

(a) Position response (b) Force response

Fig. 11-16: Free motion (conventional 3ch ABC)

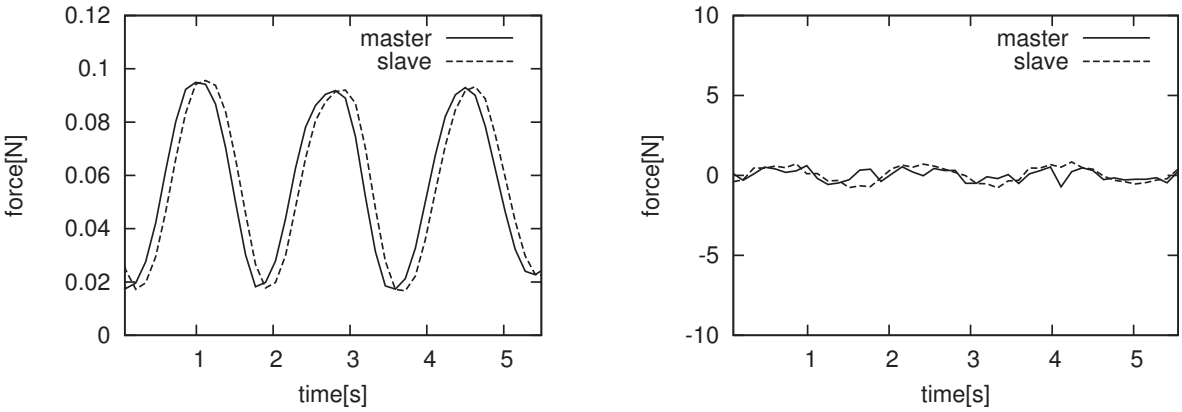

(a) Position response (b) Force response

Fig. 11-17: Free motion (3ch ABC + velocity difference damping)

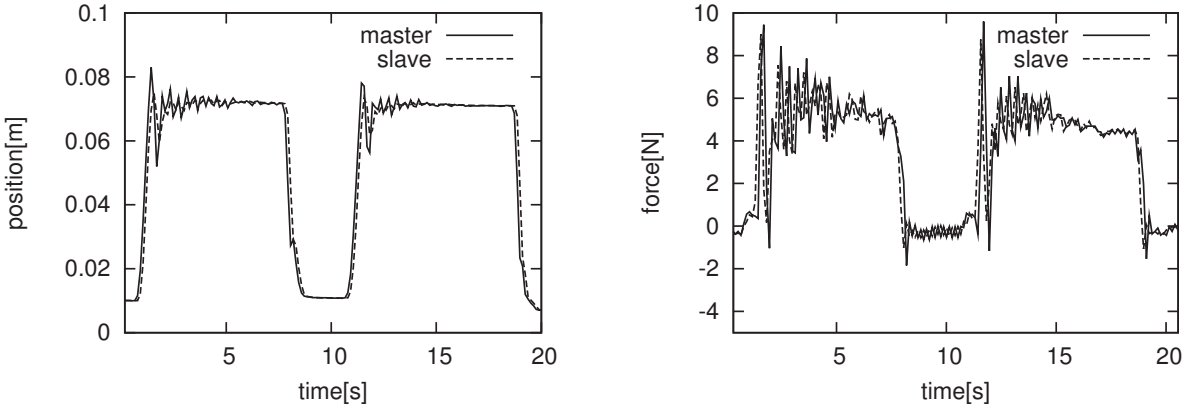

(a) Position response (b) Force response

Fig. 11-18: Contact motion with soft environment (conventional 3ch ABC)

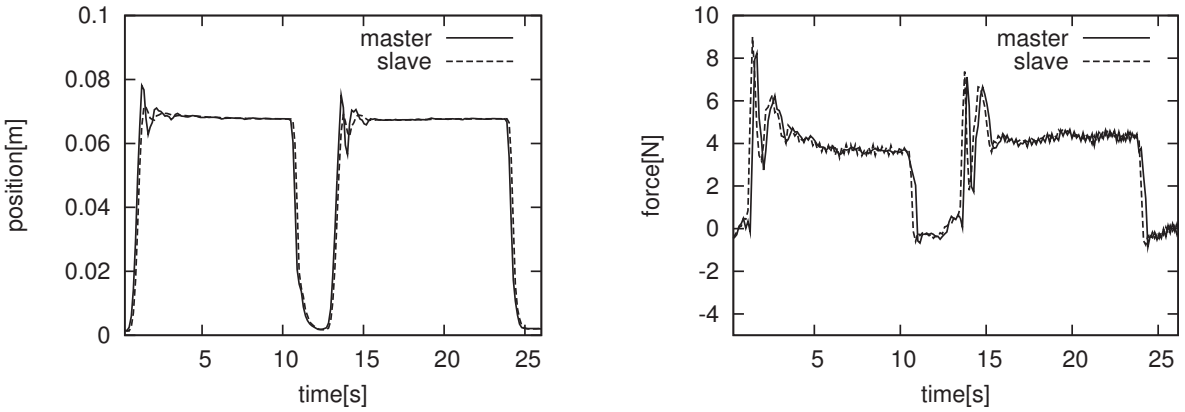

(a) Position response (b) Force response

Fig. 11-19: Contact motion with soft environment (3ch ABC + velocity difference damping)

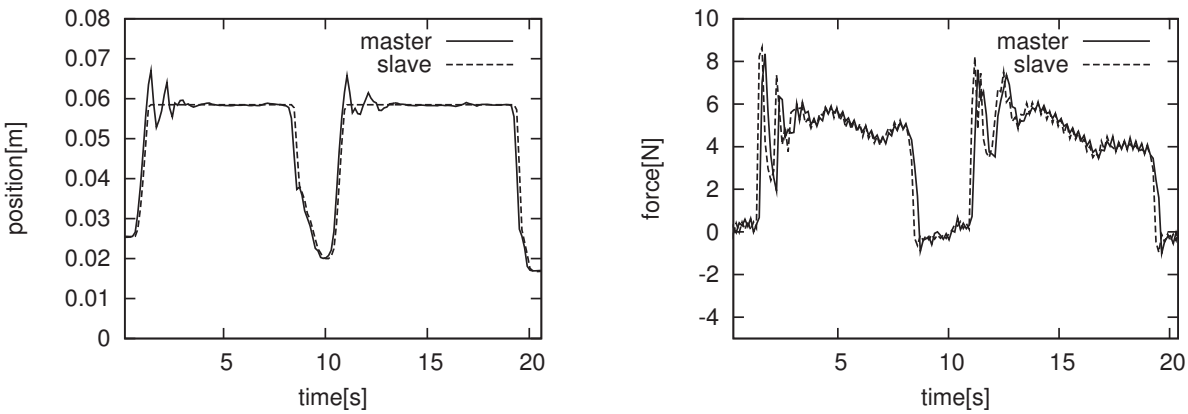

(a) Position response

(b) Force response

Fig. 11-20: Contact motion with hard environment (3ch ABC + velocity difference damping)

Chapter 12

Conclusions

This dissertation proposed some solutions for time-delayed ABC based on modal space analysis. Chapter 5 and 6 introduced conventional solutions. Chapter 5 explained time delay compensation by CDOB. Chapter 6 analyzed the effect of damping injection on ABC.

Chapter 7 proposed frequency-domain damping design (FDD) for 4ch ABC with CDOB system. FDD changed the strength of damping injection depending on frequency area in order to realize good operationality and stability. Time delay element delays the phase of feedback systems. As a result, systems which have time delay element tend to become unstable in high frequency area. FDD worked high damping injection only in high frequency area using loop-shaping HPF. The design of loop-shaping HPF was based on robust H_∞ stability condition.

Chapter 8 proposed a novel 4ch ABC design for haptic communication under time delay. In conventional 4ch ABC, the difference of position was controlled to be zero by PD control, and the sum of force was controlled to be zero by force P control. On the other hand, in proposed 4ch ABC, the difference of position was controlled to be zero by P-D control (differential proactive PD control), and the sum of force was controlled to be zero by damping-injected force P control. Furthermore, the damping controller was designed based on FDD.

Chapter 9 proposed a new design of communication disturbance observer (CDOB) for haptic communication with bilateral control. The proposed new CDOB worked time delay compensation only in high frequency area. Furthermore, the proposed ABC system with new CDOB improved time delay compensation on both master and slave robot. The proposed ABC system realized much further stable and high-performance haptic communication even under time delay.

Chapter 10 and 11 introduced event-based approaches only in contact motion. Chapter 10 explained an adaptive performance tuning method of time-delayed ABC by using CDOB. Time delay compensation by CDOB improved operationality, but simultaneously deteriorated reproducibility. Therefore, chapter 10 proposed scaling down compensation value of CDOB only in contact motion with the environment. Reproducibility was improved in all frequency area by scaling down compensation value from 0 to 1.0.

Chapter 11 introduced an event-based damping method only in contact motion. Chapter 11 proposed

a method of velocity difference damping that utilized the velocity difference between the robot and the robot model. This method improved the performance and the stability of force control in common modal space without deteriorating the performance of position control.

Among these solution methods, especially, the proposed FDD method drastically improved the performance of operationality under time delay. In conventional stabilization method such as wave variables, stability was the most important, and should be above everything else. As a result, other performance such as operationality was critically deteriorated. On the other hand, the proposed FDD method ensured comfortable operationality to the extent possible in the satisfaction of robust stability. The proposed FDD method is easily implementable and adjustable by the design of H_∞ norm if the maximum delay time value including jitter delay is known in advance.

In summing up above descriptions, this dissertation clarifies the follows.

1. Time delay deteriorates the stability of each modal space in ABC system.

2. The stability of each modal space means the whole ABC system stability.

3. Appropriate loop-shaping of each modal space realizes high-performance and stable ABC system.

appendix A

Improvement in Steady-State Accuracy of CDOB by Low-Frequency Model Error Feedback

A.1 Introduction

This chapter proposes a method to improve the steady state accuracy of time delayed control systems with communication disturbance observer (CDOB) by low frequency model error feedback. The feature of time delay compensation by CDOB is that it can be utilized without delay time model. However, CDOB needs a model of controlled system (plant model), and the model error occurs steady state error. Until now, some solution method are proposed to remove steady state error of CDOB[69–71]. However all methods deteriorate the stability in exchange for steady state accuracy, and detailed papameter tuning procedure are not shown. Sabanovic proposed a method to remove steady state error without deteriorating stability by spring and damping injection[66]. However, initial position of spring is essential, and this may cause critical performance deterioration. Considering this background, this chapter proposes a novel solution method to improve steady state accuracy of time delayed control system with CDOB, retaining high robust stability.

A.2 Position PD Control under Time Delay

This section explains position PD control under time delay.

A.2.1 Position PD control under time delay

Block diagram of position PD control under time delay is shown in Fig. A-1. $C_p(= K_p + sK_v)$ is position PD controller. Plant consists of double integration and inertia, and this is realized by DOB[63]. Closed-loop transfer function $G_a(s)$ is described as follows.

Table A-1: Parameters in analysis and experiment

Parameter	Meaning	Value
T	Time delay(one way)	300[ms]
K_p	Position gain	900
K_v	Velocity gain	60
g_{dis}	Cutoff frequency of DOB	1000[rad/s]
g_{net}	Cutoff frequency of CDOB	1000[rad/s]
g_{error}	Cutoff frequency of model error feedback	5[rad/s]
M_n	Nominal mass of motor	0.5[kg]
M_m	Model mass of motor	0.35[kg]
K_{tn}	Nominal Force coefficient	22.0[N/A]
st	Sampling time	0.1[ms]

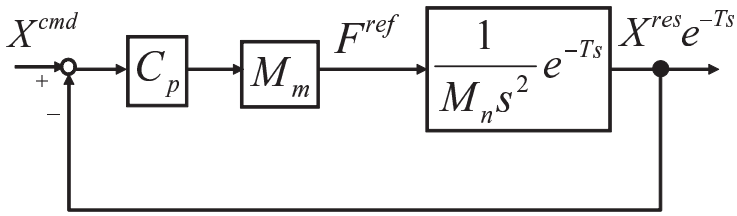

Fig. A-1: Time delayed position PD control

$$G_a(s) = \frac{C_p M_m e^{-Ts}}{M_n s^2 + C_p M_m e^{-Ts}} \tag{A.1}$$

From (A.1), there is time delay element in characteristic polynominal of denominator, so position control is destabilized by time delay.

A.2.2 Time delay compensation by CDOB

Block diagram of position control with CDOB is shown Fig. A-2. Internal structure of CDOB is shown in Fig. A-3. CDOB regards time delay effect as network disturbance($F^{net-dis}$) in force dimension. CDOB calculates compensation value X^{cmp} from $F^{net-dis}$ and M_m. Closed-loop transfer function $G_b(s)$ is shown as follows on the assumption that cutoff frequency g_{net} is large enough.

$$G_b(s) = \frac{C_p M_m e^{-Ts}}{M_n (s^2 + C_p)} \tag{A.2}$$

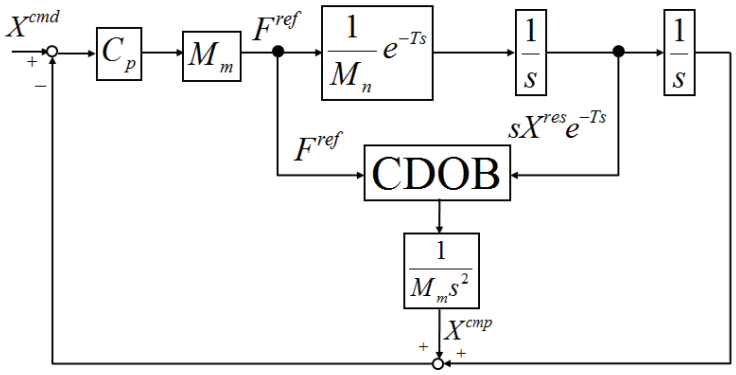

Fig. A-2: Position PD control + CDOB

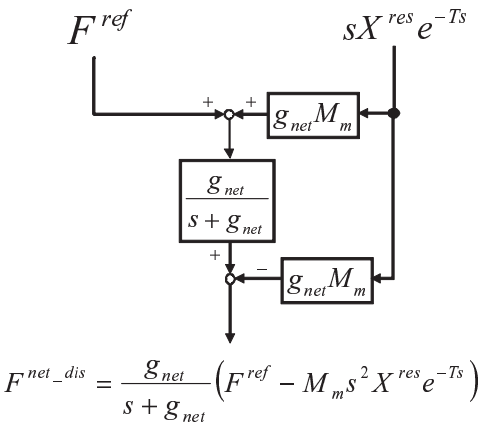

Fig. A-3: Structure of CDOB

(A.2) shows that time delay element is removed from the characteristic polynominal by time delay compensation.

A.2.3 Steady state error caused by plant model error

This part analyzes existence or non-existence of steady state error caused by plant model error. Difference $E_a(s)$ between X^{cmd} and $X^{res}e^{-Ts}$ is described as follows.

$$E_a(s) = (1 - \frac{C_p M_m e^{-Ts}}{M_n(s^2 + C_p)})X^{cmd} \tag{A.3}$$

Steady state error to step input is described as follows using final-value theorem.

$$\lim_{s \to 0} sE_a(s)\frac{1}{s} \to 1 - \frac{M_m}{M_n} \tag{A.4}$$

(A.4) shows that stady state error exits depending on the ratio of M_m/M_n.

A.3 Improvement Steady State Accuracy by Low Frequency Model Error Feedback

This section proposes a method to improve the steady state accuracy by low frequency model error feedback.

A.3.1 Structure of low frequency model error feedback

Block diagram of the proposed system is shown in Fig. A-4. Position model X_m is calculated from F^{ref} and M_m. model error is defined as the difference between position response $X^{res}e^{-Ts}$ and position model without time delay X_m. X_m should be delayed to close to the phase of $X^{res}e^{-Ts}$. However, to do so, it requires delay time model, and this eliminate the advantage that CDOB requires no delay model. In addition, in steady state, the frequency value is close to zero, so time delay effect is almost nothing ($\because \lim_{s \to 0} e^{-Ts} \to 1$). As a result, the same phase model error is feedbacked to controller in steady state. Furthermore, to suppress the deterioration of stability, model error passes through LPF (Low pass filter). The cutoff frequency of LPF is defined as g_{error}.

A.3.2 Improvement steady state accuracy by model error feedback

Closed-loop transfer function $G_c(s)$ on the assumption that g_{net} is large enough is described as follows.

$$\begin{aligned} & G_c(s) \\ = & \frac{C_p M_m (s + g_{error}) e^{-Ts}}{C_p M_m g_{error} e^{-Ts} + M_n (s^3 + s^2 g_{error} + C_p s)} \end{aligned} \tag{A.5}$$

Difference $E_b(s)$ between X^{cmd} and $X^{res}e^{-Ts}$ in Fig. A-4 is described as follows.

$$E_b(s) = (1 - G(s))X^{cmd} \tag{A.6}$$

Steady state error to step input is described as follows using final-value theorem.

$$\lim_{s \to 0} sE(s)\frac{1}{s} \to 1 - \frac{g_{error}}{g_{error}} = 0 \tag{A.7}$$

(A.7) shows that steady state error is removed if g_{error} is larger than 0.

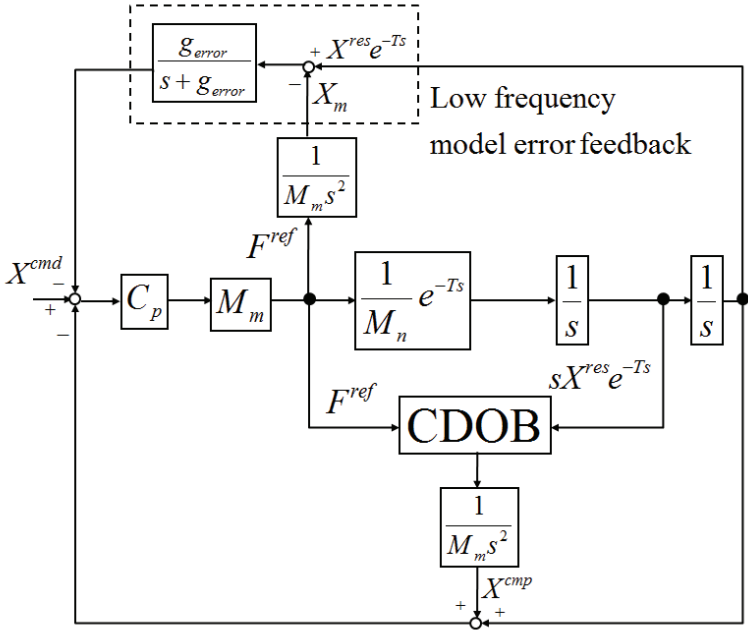

Fig. A-4: Position PD control + CDOB + Low frequency model error feedback (proposed system)

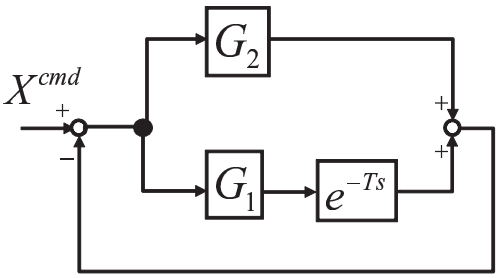

Fig. A-5: Block diagram of $L_a(s)$ using G_1 and G_2

A.3.3 Change of stability caused by low frequency model error feedback

The previous part shows that the proposed low frequency model error feedback removes steady state error. However, by model error feedback, time delay element is also feedbacked to controller. The advantage of delay independent stability is broken. This part analyzes the stability change depending on g_{error}. Open-loop transfer function $L_a(s)$ in Fig. A-4 is described as follows.

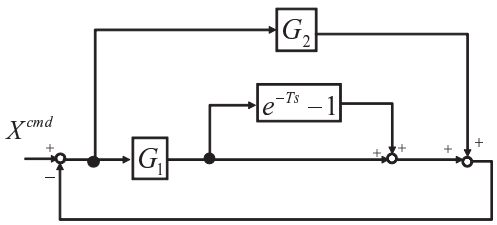

Fig. A-6: Multiplicative representation of time delay effect

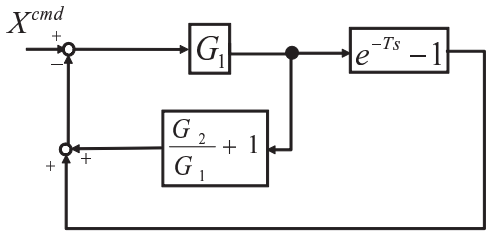

Fig. A-7: Equivalent transformation of Fig. A-6

$$
\begin{aligned}
L_a(s) &= \underbrace{\left(\frac{C_p M_m e^{-Ts}}{M_n s^2} - \frac{C_p M_m}{s^2 M_m}\right)\frac{g_{error}}{s+g_{error}}}_{Low\,frequency\,model\,error\,feedback} + \underbrace{\frac{C_p M_m}{M_m s^2}}_{CDOB} \\
&= \underbrace{\frac{C_p M_m e^{-Ts}}{M_n s^2}\frac{g_{error}}{s+g_{error}}}_{low-frequency\,area} + \underbrace{\frac{C_p M_m}{M_m s^2}\frac{s}{s+g_{error}}}_{high-frequency\,area} \qquad \text{(A.8)}
\end{aligned}
$$

(A.8) shows that system is switched at $\omega = g_{error}$. In high frequency area, the model response is feedbacked, and in low frequency area, the delayed response value is feedbacked. The characteristic of e^{-Ts} is described as follows.

$$
|e^{-j\omega T}| = 1 \qquad \text{(A.9)}
$$

$$
\angle e^{-j\omega T} = -\omega T \qquad \text{(A.10)}
$$

(A.10) shows that phase delay is proportion to frequency value ω. So time-delayed system tends to become unstable in high frequency area. In other word, it does not become unstable in low frequency area. Based on this property, This section feedbacks model error only in low frequency area. This idea is closely similar to frequency-domain loop-shaping in H_∞. In (A.8), $G_1(s)$ and $G_2(s)$ are defined as follows.

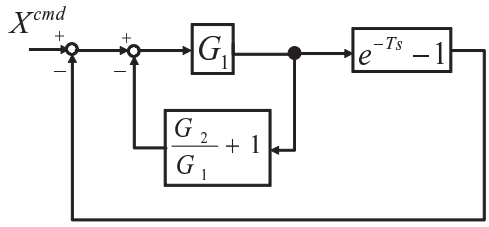

Fig. A-8: Equivalent transformation of Fig. A-7

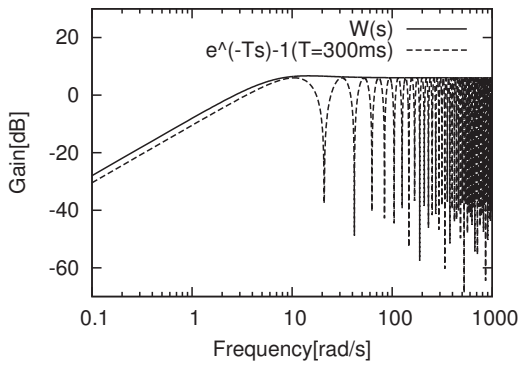

Fig. A-9: Bode diagram of weighting function (T=300ms)

$$G_1(s) = \frac{C_p M_m}{M_n s^2} \frac{g_{error}}{s + g_{error}} \tag{A.11}$$

$$G_2(s) = \frac{C_p M_m}{M_m s^2} \frac{s}{s + g_{error}} \tag{A.12}$$

Block diagram of $L_a(s)$ is shown in Fig. A-5 using $G_1(s)$ and $G_2(s)$. The multiplicative uncertainty representation of Fig. A-5 is shown in Fig. A-6. Fig. A-6 is equivalently transformed into Fig. A-7. Multiplicative uncertainty by time delay is expressed as follows using weighting function $W(s)$. $\Delta(s)$ means uncertainty.

$$e^{-Ts} - 1 = W(s)\Delta(s), \quad |\Delta(jw)| < 1, \ \forall w \tag{A.13}$$

Open-loop transfer function $L_b(s)$ in Fig. A-8 is described as follows.

$$L_b(s) = \frac{G_1(s)}{1 + G_1(s) + G_2(s)} W(s)\Delta(s) \tag{A.14}$$

Robust stability condition is described as follows.

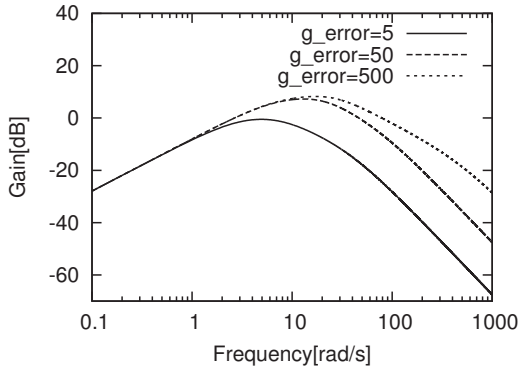

Fig. A-10: H_∞ norm in g_{error} variation (T=300[ms])

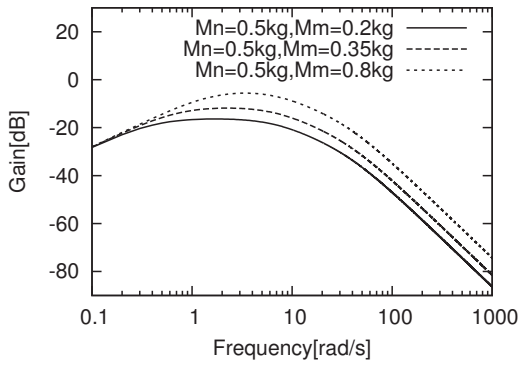

Fig. A-11: H_∞ norm in M_m variation (T=300[ms], g_{error}=1.0[rad/s])

$$
\begin{aligned}
||\frac{G_1(s)}{1+G_1(s)+G_2(s)}W(s)||_\infty &< 1 \\
\Leftrightarrow |\frac{G_1(j\omega)}{1+G_1(j\omega)+G_2(j\omega)}W(j\omega)| &< 1, \ \forall w
\end{aligned}
\tag{A.15}
$$

(A.15) shows that the maximum value of open-loop transfer function in all frequency area (H_∞ norm) should be smaller than 1(=0[dB]). This is the stabilization theory based on samall gain theorem. The gain bode diagram of multiplicative uncertainty at (T=300ms) is shown as Fig. A-9. $W(s)$ is shown as follows.

$$
W(s) = \frac{2s(s+16)}{(s+9)^2} \tag{A.16}
$$

Fig. A-9 shows that weighting function $W(s)$ tightly covers with the time delay uncertainty in all frequency area. This shows that $W(s)$ exceeds the upper bound of time delay uncertainty under T=300ms.

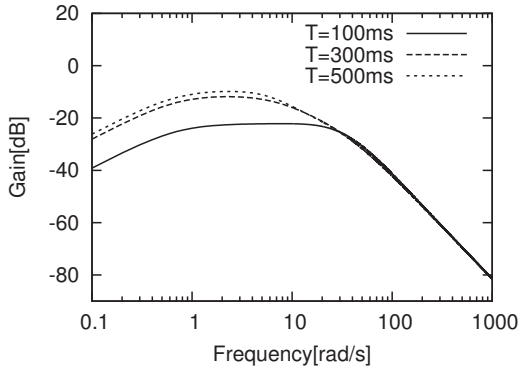

Fig. A-12: H_∞ norm in T variation (M_m=0.35[kg], g_{error}=1.0[rad/s])

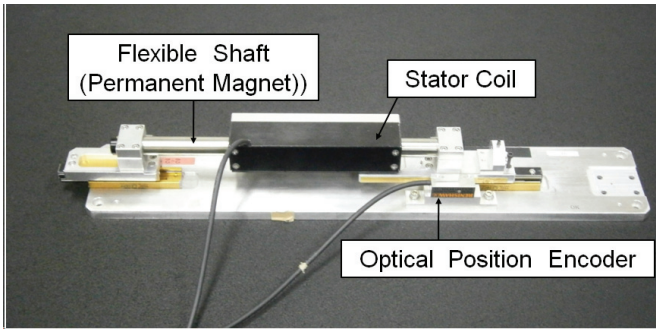

Fig. A-13: linear motor utilized in experiment

Fig. A-10 shows that the change of H_∞ norm in variation of g_{error}. Parameters are shown in Table A-1. With the decrease of g_{error}, H_∞ norm becomes smaller. In the case of $g_{error} = 5\ rad/s$, H_∞ norm becomes smaller than 0 dB, so the robust stability condition is achieved. With the decrease of g_{error}, the robust stability gets higher. Fig. A-11 and Fig. A-12 show the H_∞ norm in the variation of M_m and T. They show that the change of plant model error and time delay cause the change of the stability and H_∞ norm. However, if g_{error} is small enough, robust stability is retained in any case.

A.3.4 Tuning procedure of g_{error}

This part explains the tuning procedure of g_{error}. (A.7) shows that steady state error is removed if g_{error} is larger than 0. Furthermore, from Figs. A-10 $\sim$ Fig. A-12, if g_{error} is small enough, the robust stability is retained in any case. As the procedure, firstly, the gain value of C_p is designed from the target control bandwidth (rapidity). Secondly, the maximum value of time delay is roughly estimated, and g_{error} of stability limit is calculated. Thirdly, g_{error} is set at sufficiently-small value under the value of stability limit. If steady state error remains because of the lack of control quantity, g_{error} should be set at larger value by little and little in the range of the robust stability condition.

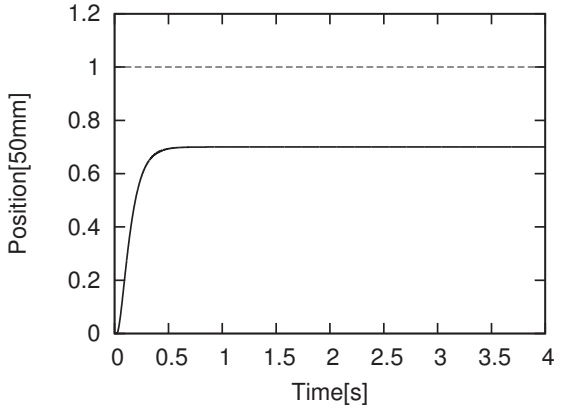

(a) CDOB

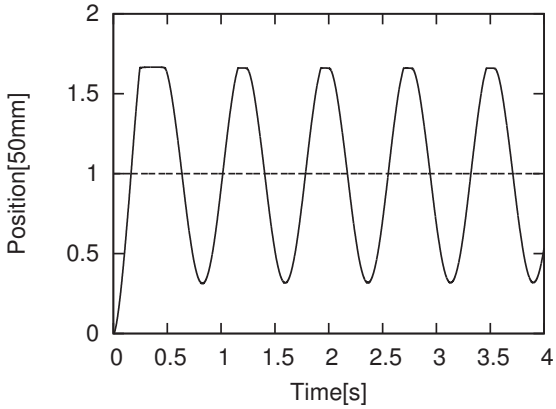

(b) CDOB + Model error feedback

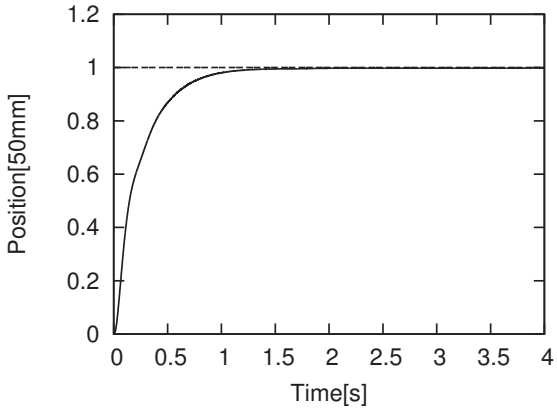

(c) CDOB + Low frequency model error feedback(proposed system)

Fig. A-14: Experimental results

A.4 Experiments

This section shows the validity of the proposed system by some experimental results. Linear motor utilized in experiment is shown in Fig. A-13. Parameters are shown as Table A-1. Three controllers are compared: Position PD control with CDOB (case a), Position PD control with CDOB + Model error feedback (case b), Position PD control with CDOB + Low frequency model error feedback (case c). Case b is the controller which is removed the LPF of the proposed system. The step response of each controller is compared. Time delay is 300ms. Experimental results are shown in Fig. A-14. From Fig. A-14(a), with case a, stable response is achieved. However, steady state error is left remained. From Fig. A-14(b), with case b, the response is unstable and vibrating. This is because model error feedback causes destabilization. On the other hand, from Fig. A-14(c), with case c, stable and accurate response is achieved. This is because model error is feedbacked slowly through LPF, and response value converges to target value stably. From experimental results, it is demonstrated that proposed low frequency model

error feedback realizes both high robust stability and steady state accuracy.

A.5 Summary

This section proposed a method to improve the steady state accuracy of time delayed control systems with CDOB by low frequency model error feedback. The validity of proposed method was demonstrated by some experimental results.

References

[1] P. Dario, E. Guglielmelli, B. Allotta, and M. C. Carrozza, "Robotics for Medical Applications," *IEEE Robotics and Automation Magazine*, pp. 44–56, 1996.

[2] J. Rosen and B. Hannaford, "Doc at a Distance," *IEEE Spectrum*, Vol. 43, No. 10 pp. 44–56, 1996.

[3] " Intuitive Surgical Inc. " (online), available from h http://www.intuitivesurgical.com i, (accessed 2007-02-02).

[4] J. Rosen, B. Hannaford, M. P. MacFarlane, and M. N. Sinanan, "Force controlled and teleoperated endoscopic grasper for minimally invasive surgery-experimental performance evaluation," *IEEE Transactions on Biomedical Engineering*, Vol. 46, No. 10 pp. 1212–1221, 1999.

[5] M. Tavakoli, R. V. Patel, and M. Moallem, "A Force-Reflective Master-Slave System for Minimally Invasive Surgery," *Proceedings of the IEEE/RSJ International Conference on Intelligent Robots and Systems*, Vol. 4, pp. 3077–3082, 2003.

[6] K. Ohnishi, S. Katsura, and W. Iida, "Medical Mechatronics - An Application to Haptic Forceps," *Proceedings of the 3rd IFAC Symposium on Mechatronic Systems*, pp. 365–370, 2004.

[7] P. F. Hokayem and M. W. Spong, "Bilateral Teleoperation: An History Survey," *Automatica*, Vol. 42, No. 12, pp. 2035–2057, 2006.

[8] Y. Yokokohji and T. Yoshikawa, "Bilateral Control of Master-Slave Manipulators for Ideal Kinesthetic Coupling - Formulation and Experiment," *IEEE Transaction on Robotics and Automation*, Vol. 10, No. 5, pp. 605–620, 1994.

[9] B. Hannaford, "A Design Framework for Teleoperators with Kinesthetic Feedback," *IEEE Transaction on Robotics and Automation*, Vol. 5, No. 4, pp. 426–434, 1989.

[10] D. A. Lawrence, "Stability and Transparency in Bilateral Teleoperation," *IEEE Transaction on Robotics and Automation*, Vol. 9, No. 5, 1993.

[11] K. Hashtrudi-Zaad and S. E. Salcudean, "Transparency in Time-Delayed Systems and the Effect of Local Force Feedback for Transparent Teleoperation," *IEEE Transactions on Robotics and Automation*, Vol. 18, No. 1, pp. 108–114, 2002.

[12] W. Iida and K. Ohnishi, "Reproductbility and Operationality in Bilateral Teleoperation," *Proceedings of the 8th IEEE international Workshop on Advanced Motion Control, AMC 2004*, Kawasaki, Japan, 25-28th, March, 2004.

[13] Y. Matsumoto, S. Katsura, and K. Ohnishi, "An Analysis and Design of Bilateral Control Based on Disturbance Observer," *Proceedings of the 10th IEEE international Conference on Industrial Technology*, pp. 802–807, 2003.

[14] T. Tsuji, K. Natori, H. Nishi, and K. Ohnishi, "Controller Design Method of Bilateral Control System," *European Power Electronics and Drives Journal*, Vol. 16, No. 2, pp. 22–28, 2006.

[15] T. Shimono, S. Katsura, and K. Ohnishi, "Abstraction and Reproduction of Force Sensation From Real Environment by Bilateral Control," *IEEE Transaction on Industrial Electronics*, Vol. 54, No. 2, pp. 907–918, 2007.

[16] S. Hyodo, and K. Ohnishi, "A Method for Motion Abstraction Based on Haptic Information Directionality and an Application to Haptic Motion Display System," *IEEE Transaction on Industrial Electronics*, Vol. 56, No. 5, pp. 1356–1363, 2009.

[17] Y. Yokokura, S. Katsura and K. Ohishi, "Stability Analysis and Experimental Validation of a Motion-Copying System," *IEEE Transaction on Industrial Electronics*, Vol. 56, No. 10, pp. 3906–3913, 2009.

[18] H. Kuwahara, T. Shimono, H. Tanaka, D. Yashiro, K. Ohnishi, "Abstraction of Action Components Unconstrained by Alignment of Haptic Sensing Points," *IEEE Transaction on Industrial Electronics*, Vol. 58, No. 8, pp. 3196–3204, 2011.

[19] N. Tsunashima, S. Katsura, "Spatiotemporal Coupler: Storage and Reproduction of Human Finger Motions," *IEEE Transaction on Industrial Electronics*, Vol. 59, No. 2, pp. 1074–1085, 2012.

[20] S. Katsura, K. Ohnishi, and K. Ohishi, "Transmission of Force Sensation by Environment Quarrier Based on Multilateral Control," *IEEE Transaction on Industrial Electronics*, Vol. 54, No. 2, pp. 898–906, 2007.

[21] R. Kubo, T. Shimono, and K. Ohnishi, "Flexible Controller Design of Bilateral Grasping Systems Based on a Multilateral Control Scheme," *IEEE Transaction on Industrial Electronics*, Vol. 56, No. 1, pp. 62–68, 2009.

[22] G. Liu, A. Zinober, and Y. B. Shtessel, "Second-Order SM Approach to SISO Time-Delay System Output Tracking," *IEEE Transaction on Industrial Electronics*, Vol. 56, No. 9, pp. 3638–3645, 2009.

[23] T. Nussbaumer, M. L. Heldwein, G. Gong, S. D. Round, and J. W. Kolar, "Comparison of Prediction Techniques to Compensate Time Delays Caused by Digital Control of a Three-Phase Buck-Type PWM Rectifier System," *IEEE Transaction on Industrial Electronics*, Vol. 55, No. 2, pp. 791–799, 2008.

[24] T. Ohta and T. Murakami, "A Stabilization Control of Bilateral System with Time Delay by Vibration Index - Application to Inverted Pendulum Control," *IEEE Transaction on Industrial Electronics*, Vol. 56, No. 5, pp. 1595–1603, 2009.

[25] C. Hua, P. X. Liu, and X. Guan, "Backstepping Control for Nonlinear Systems with Time Delays and Applications to Chemical Reactor Systems," *IEEE Transaction on Industrial Electronics*, Vol. 56, No. 9, pp. 3723–3732, 2009.

[26] Y. Xia, M. Fu, H. Yang, and G. Liu, "Robust Sliding-Mode Control for Uncertain Time-Delay Systems Based on Delta Operator," *IEEE Transaction on Industrial Electronics*, Vol. 56, No. 9, pp. 3646–3655, 2009.

[27] P. Cortes, J. Rodriguez, C. Silva, A. Flores, "Delay Compensation in Model Predictive Current Control of a Three-Phase Inverter," *IEEE Transaction on Industrial Electronics*, Vol. 59, No. 2, pp. 1323–1325, 2012.

[28] Bo Liu, Yuanqing Xia, "Fault Detection and Compensation for Linear Systems Over Networks With Random Delays and Clock Asynchronism," *IEEE Transaction on Industrial Electronics*, Vol. 58, No. 9, pp. 4396–4406, 2011.

[29] B. Addad, S. Amari, J.J. Lesage, "A Virtual-Queuing-Based Algorithm for Delay Evaluation in Networked Control Systems," *IEEE Transaction on Industrial Electronics*, Vol. 58, No. 9, pp. 4471–4479, 2011.

[30] Yanyan Yin, Peng Shi, Fei Liu, "Gain-Scheduled Robust Fault Detection on Time-Delay Stochastic Nonlinear Systems," *IEEE Transaction on Industrial Electronics*, Vol. 58, No. 10, pp. 4908–4916, 2011.

[31] Hui Zhang, Yang Shi, A.S. Mehr, "Robust Static Output Feedback Control and Remote PID Design for Networked Motor Systems," *IEEE Transaction on Industrial Electronics*, Vol. 58, No. 12, pp. 5396–5405, 2011.

[32] P. Ignaciuk, A. Bartoszewicz, "Discrete-Time Sliding-Mode Congestion Control in Multisource Communication Networks with Time-Varying Delay," *IEEE Transaction on Control Systems Technology*, Vol. PP, pp. 1–16, 2010.

[33] H. Cho, S. M. Fadali, "Nonlinear Network-Induced Time Delay Systems with Stochastic Learning," *IEEE Transaction on Control Systems Technology*, Vol. PP, pp. 1–9, 2010.

[34] S.-L. Dai, H. Lin, S. S. Ge, "Scheduling-and-Control Codesign for a Collection of Networked Control Systems with Uncertain Delays," *IEEE Transaction on Control Systems Technology*, Vol. 18, pp. 66–78, 2010.

[35] H. Li, M.-Y. Chow, Z. Sun, "Optimal Stabilizing Gain Selection for Networked Control Systems with Time Delays and Packet Losses," *IEEE Transaction on Control Systems Technology*, Vol. 17, pp. 1154–1162, 2009.

[36] G.R. Cho, P.H. Chang, S.H. Park, and M. Jin, "Robust Tracking Under Nonlinear Friction Using Time-Delay Control with Internet Model," *IEEE Transaction on Control Systems Technology*, Vol. 17, pp. 1406–1414, 2009.

[37] Y. Tipsuwan, and M. Y. Chow, "Control methodologies in networked control systems," *Control Engineering Practice*, Vol. 11, pp. 1099–1111, 2003.

[38] T. C. Yang, "Networked control system: a brief survey," *IEEE Proceedings of Control Theory and Applicatations*, Vol. 153, no 4, pp. 403–412, 2003.

[39] P. Antsaklis and J. Baillieul, "Special Issue on Technology of Networked Control Systems," *Proceedings of the IEEE*, Vol. 95, no. 1, pp. 5–8, 2007.

[40] J. Baillieul and P. Antsaklis, "Control and Communication Challenges in Networked Real-Time System," *Proceedings of the IEEE*, Vol. 95, no. 1, pp. 9–28, 2007.

[41] J. P. Hespanha, P. Naghshtabrizi, and Y. Xu, "A survey on Recent Results in Networked Control Systems," *Proceedings of the IEEE*, Vol. 95, no. 1, pp. 138–162, 2007.

[42] A. Aziminejad, M. Tavakoli, R. V. Patel, and M. Moallem, "Transparent Time-Delayed Bilateral Teleoperation Using Wave Variables," *IEEE Transaction on Control Systems Technology*, Vol. 16, No. 3, pp. 548–555, 2008.

[43] D. Lee and P. Y. Li, "Passive Bilateral Control and Tool Dynamics Rendering for Nonlinear Mechanical Teleoperators," *IEEE Transaction on Robotics*, Vol. 21, No. 5, pp. 936–951, 2005.

[44] G.M.H. Leung, B.A. Francis and J. Apkarian, "Bilateral controller for teleoperators with time delay via μ-synthesis," *IEEE Transaction on Robotics and Automation*, Vol. 11, No. 1, pp. 105–116, 1995.

[45] J. Yan, S.E. Salcudean, "Teleoperation controller design using H_∞-optimization with application to motion-scaling," *IEEE Transaction on Control Systems Technology*, Vol. 4, pp. 244–258, 1996.

[46] M. Boukhnifer, and A. Ferreira, "H_∞ Loop Shaping Bilateral Controller for a Two-Fingered Tele-Micromanipulation System," *IEEE Transaction on Control Systems Technology*, Vol. 15, pp. 891–905, 2007.

[47] A. Shahdi, S. Sirouspour, "Adaptive/Robust Control for Time-Delay Teleoperation," *IEEE Transaction on Robotics*, Vol. 25, pp. 196–205, 2009.

[48] T. Slama, A. Trevisani, D. Aubry, R. Oboe, and F. Kratz, "Experimental Analysis of an Internet-Based Bilateral Teleoperation System With Motion and Force scaling Using a Model Predictive Controller," *IEEE Transaction on Industrial Electronics*, Vol. 55, No. 9, pp. 3290–3299, 2008.

[49] Y. Pan, C. Canudas-de-Wit, and O. Sename, "A new predictive approach for bilateral teleoperation with applications to drive-by-wire systems," *IEEE Transaction on Robotics*, Vol. 22, No. 6, pp. 1146–1162, 2006.

[50] S. Munir and W. J. Book, "Internet-based teleoperation using wave variables with prediction," *IEEE/ASME Transaction on Mechatronics*, Vol. 7, No. 2, pp. 124–133, 2002.

[51] S. Sirouspour and A. Shahdi, "Model Predictive Control for Transparent Teleoperation under Communication Time Delay," *IEEE Transaction on Robotics*, Vol. 22, No. 6, pp. 1131–1145, 2006.

[52] Y. Pan, C. Canudas-de-Wit, and O. Sename, "A New Predictive Approach for Bilateral Teleoperation with Application to Drive-by-Wire System," *IEEE Transaction on Robotics*, Vol. 22, No. 6, pp. 1146–1162, 2006.

[53] R. Oboe and P. Fiorini, "A Design and Control Environment for Internet-Based Telerobotics," *International Journal of Robotics Research*, Vol. 17, No. 4, pp. 43–449, 1998.

[54] R. Oboe, "Force-Reflecting Teleoperation Over the Internet: The JBIT Project," *Proceedings of the IEEE*, Vol. 91, No. 3, pp. 449–462, 2003.

[55] R. Oboe, "Web-Interfaced, Force-Reflecting Teleoperation Systems," *IEEE Transaction on Industrial Electronics*, Vol. 48, No. 6, pp. 1257–1265, 2001.

[56] Y. Uchimura and T. Yakoh, "Bilateral Robot System on the Real-Time Network Structure," *IEEE Transaction on Industrial Electronics*, Vol. 51, No. 5, pp. 940–946, 2004.

[57] D. Yashiro and K. Ohnishi, "Performance Analysis of Bilateral Control System With Communication Bandwidth Constraint," *IEEE Transaction on Industrial Electronics*, Vol. 58, No. 2, pp. 436–443, 2011.

[58] E. Kamrani, H. R. Momeni, and A. R. Sharafat, "Modeling Internet Delay Dynamics for Teleoperation," *Proceedings of the 2005 IEEE Conference on Control Applications, OCA'05*, Toronto, Canada, pp. 1528–1533, 28-31th August 2005.

[59] C. Y. Kao and B. Lincoln, "Simple Stability Criteria for Systems with time-varying delay," *Automatica*, Vol. 40, pp. 1429–1434, 2004.

[60] K. Natori and K. Ohnishi, "A Design Method of Communication Disturbance Observer for Time-Delay Compensation, Taking the Dynamic Property of Network Disturbance into Account," *IEEE Transaction on Industrial Electronics*, Vol. 55, No. 5, pp. 2152–2168, May, 2008.

[61] K. Natori, T. Tsuji, and K. Ohnishi, "Time-Delay Compensation by Communication Disturbance Observer for Bilateral Teleoperation under Time-Varying Delay," *IEEE Transaction on Industrial Electronics*, Vol. 57, No. 3, pp. 1050–1062, 2010.

[62] K. Natori, R. Kubo, and K. Ohnishi, "Transparency of Time Delayed Bilateral Teleoperation Systems with Communication Disturbance Observer," *Proceedings of the IEEE 4th International Conference on Mechatronics*, Kumamoto, Japan, WA1-A-3, May 2007.

[63] K. Ohnishi, M. Shibata, and T. Murakami, "Motion Control for Advanced Mechatronics," *IEEE/ASME Transactions on Mechatronics*, Vol. 1, No. 1, pp. 56–67, 1996.

[64] T. Murakami, F. Yu, and K. Ohnishi, "Torque Sensorless Control in Multidegree-of-Freedom Manipulator," *IEEE Transaction on Industrial Electronics*, Vol. 40, No. 2, pp. 259–265, 1993.

[65] O. Khatib and J. Burdick, "Motion and Force Control of Robot Manipulation," *Proceedings of the IEEE International Conference on Robotics and Automation*, Vol. 3, pp. 1381–1386, 1986

[66] A. Sabanovic, K. Ohnishi, D. Yashiro, and N. Sabanovic, "Motion control systems with network delay," *Proceedings of the 35th Annual Conference of the IEEE Industrial Electronics Society, IECON 2009*, pp. 1779-1783, July, 2010.

[67] U. Tumerdem and K. Ohnishi, "Robust four channel teleoperation under time delay by damping injection," *Proceedings of the IEEE International Conference on Mechatronics, ICM 2009*, April, 2009.

[68] R. Kubo, N. Iiyama, K. Natori, and K. Ohnishi, "Analysis of a Three Channel Control Architecture for Bilateral Teleoperation with Time Delay," *IEEJ Transactions on Industry Applications*, Vol. 127-D, No. 12, pp. 1224–1230, December, 2007.

[69] K. Natori and K. Ohnishi, "A Modified Structure for Robustness Enhancement of Time-Delay Systems with Communication Disturbance Observer," *Proceedings of the 35th Annual Conference of the IEEE Industrial Electronics Society, IECON 2009*, pp. 2983-2988, November 10-13, 2009.

[70] D. Yashiro and K. Ohnishi, "A Communication Disturbance Observer with a Band-pass Fileter for Delay Time Compensation," *Proceeding of The IEEE International Symposium on Industrial Electronics 2010, ISIE 2010*, pp. 3585-3589, Bari, Italy, 4-7th July 2010.

[71] A.A. Rahman, Kenji Natori, Kouhei Ohnishi, "Motion Control Systems with Network Delay," *Proceedings of the IEEE International Conference on Industrial Technology 2009, ICIT 2009*, pp. 1-6, February 10-13, 2009.

List of Achievements

Journals

[1] Atsushi Suzuki and Kouhei Ohnishi, "Stability Improvement of Bilateral Teleoperation with Time Delay by Velocity Difference Damping Based on Performance Analysis in Modal Space," *IEEJ Transactions on Industry Applications*, Vol. 130-D, No. 2, pp. 243–250, February 2010. (in Japanese)

[2] Atsushi Suzuki and Kouhei Ohnishi, "A Method for Adaptive Performance Tuning of Time-Delayed Bilateral Teleoperation Using Communication Disturbance Observer," *IEEJ Transactions on Industry Applications*, Vol. 131-D, No. 3, pp. 244–251, March 2011. (in Japanese)

[3] Atsushi Suzuki and Kouhei Ohnishi, "Frequency-Domain Damping Design for Time-Delayed Bilateral Teleoperation System Based on Modal Space Analysis," *IEEE Transactions on Industrial Electronics*, Vol. 60, No. 1, pp. 177–190, January 2013.

[4] Atsushi Suzuki and Kouhei Ohnishi, "Novel Four-Channel Bilateral Control Design for Haptic Communication Under Time Delay Based on Modal Space Analysis," *IEEE Transactions on Control Systems Technology*, Vol. 21, No. 3, pp. 882–890, May 2013.

[5] Atsushi Suzuki and Kouhei Ohnishi, "Reproducibility and Operationality in Bilateral Teleoperation under Time Delay," *IEEJ Transactions on Industry Applications*, Vol. 133-D, No. 7, July 2013. (in Japanese)(accepted)

[6] Atsushi Suzuki and Kouhei Ohnishi, "Improvement in Steady-State Accuracy of Time-Delayed Control Systems with Communication Disturbance Observer by Low-Frequency Model Error Feedback," *IEEJ Transactions on Industry Applications*, Vol. 133-D, No. 9, July 2013. (in Japanese) (accepted)

International Conferences

[1] Atsushi Suzuki and Kouhei Ohnishi, "Performance Conditioning of Time Delayed Bilateral Teleoperation System by Scaling Down Compensation Value of Communication Disturbance Observer," *Proceedings of the 11th IEEE International Workshop on Advanced Motion Control, AMC '10, Nagaoka, Japan*, pp. 524–529, March 21–24, 2010.

[2] Atsushi Suzuki and Kouhei Ohnishi, "A Constitution Method of Bilateral Teleoperation under Time Delay Based on Stablity Analysis of Modal Space," *Proceedings of the 19th IEEE International Symposium on Industrial Electronics 2010, ISIE '10, Bari, Italy*, pp. 1779–1783, July 4–7, 2010.

[3] Atsushi Suzuki, Takahiro Mizoguchi, and Kouhei Ohnishi, "Appropriate Controller Gain Design of Acceleration-based Bilateral Teleoperation under Time Delay," *Proceedings of the 22nd IEEE International Symposium on Industrial Electronics 2013, ISIE '13, Taipei, Taiwan*, May 28–31, 2013.

Domestic Conferences

[1] Atsushi suzuki, Kazuya Kitamura, Daisuke Yashiro, Akira Yamaguchi, Kenji natori and Kouhei Ohnishi, "A Design Method of Four-Channel Bilateral Control System under Time Delay Based on Stability Analysis in Modal Space," *Papers of the IEEJ Technical Meeting on Industrial Instrumentation and Control*, IIC-09-58, pp. 1–6, March 9–10, 2009. (in Japanese)

[2] Atsushi suzuki, Daisuke Yashiro and Kouhei Ohnishi, "Stability Improvement of Bilateral Teleoperation with Time Delay by Velocity Difference Damping," *Proceedings of the 2009 Annual Conference of the IEEJ Industry Applications Society, JIASC '09*, Vol. 2009, no. 2, pp. II 523–528, August 31th - September 2nd, 2009. (in Japanese)

[3] Atsushi suzuki and Kouhei Ohnishi, "Adaptive Performance Tuning Method of Time Delayed Bilateral Teleoperation System Using Communication Disturbance Observer," *Papers of the IEEJ Technical Meeting on Industrial Instrumentation and Control*, IIC-10-67, pp. 25–30, March 8–9, 2010. (in Japanese)

[4] Atsushi suzuki and Kouhei Ohnishi, "A Design Method of Time-Delayed Bilateral Teleoperation System using P-D Control for Haptic Communication," *Proceedings of the 2009 Annual Conference of the IEEJ Industry Applications Society, JIASC '10*, Vol. 2010, no. 2, pp. II 347–352, August 24-26th, 2010. (in Japanese)